(1) PERIODICAL
Oceanographical Magazine

歐文海洋報告

第7巻 第1号

THE OCEANOGRAPHICAL MAGAZINE

Vol. 7 No. 1

CONTENTS

Page

K. Hishida: On the Coastal Water and its Relation to the Oceanic Water (2) (Second report: Statistical study on the specific gravity of sea waters in the monthly interval) 1

K. Hishida: On the Coastal Water and its Relation to the Oceanic water (3) (Third report: Analytical study on the annual variation of coastal surface water temperature) 5

M. Miyazaki: Storm Surges at the Kobe Harbour (Part 1) 11

J. Sugiura: On the Transport in the Eastern Sea of Honshu (Part 2. Conditions during 1946~48) 21

J. Masuzawa: An Outline of the Kuroshio in the Eastern Sea of Japan (Currents and water masses of the Kuroshio System. IV) 29

T. Ichiye: A Short Note on the Vertical Current in the Ocean 49

T. Ichiye: On the Friction in the Tidal Current 55

T. Ichiye: A Note on the Coagulation of Small Particles in the Electrolytes 79

Published by the Central Meteorological Observatory of Japan, Tokyo.

JUNE 1955

551.464

On the Coastal Water and Its Relation to the Oceanic Water (2)

(Second report: Statistical study on the specific gravity of sea waters in the monthly interval)

Kozo Hishida

(*Maizuru Marine Observatory*)

1. *Introduction*

The treatment of the specific gravity of coastal sea waters was made statistically by taking the frequency distributions of daily values in the interval of a year on the basis of the data of coastal observations for some twelve meteorological stations, which could be classified into three groups, say A, B, and C, specified by the histogram in the first report by the author. (K. Hishida 1950)

However, it seemed that the changes of specific gravity take place due to the meteorological and oceanographical conditions during the year. In this paper, therefore, it is intended to enter upon the character of the frequency distributions of the specific gravity σ_{15} of coastal waters in the interval of month, or season, with the same method as done in the previous paper, and then to give the scope of the seasonal variation on this character, relating to the amount of precipitation.

2. *Frequency distributions of specific gravity in the monthly interval.*

From the material of coastal oceanic observations carried out by various meteorological stations located along the coast of Japan, the daily values of standard specific gravity during 5 years are adopted as the sample for 4 stations, that is, Okinawa, Izuhara, Shionomisaki, and Wajima. Based on these about 150 samples in each monthly interval, the distribution diagrams or histograms for each intervals of $\Delta\sigma=1$ are first obtained for these stations. Among these histogram, examples in January and August are shown in Fig. 1, where it is easy to see the differences of the character of histogram between stations, as well as the seasonal change.

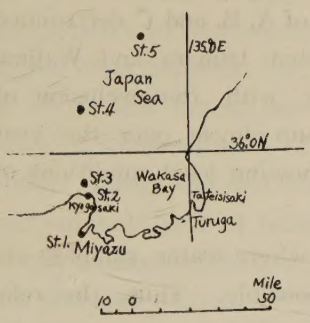

Fig. 1. Showing the location of five stations near Miyazu in Japan Sea.

Next, the following two quantities are obtained from samples adopted in each month.

1) mean value $M=\Sigma f_i x_i/\Sigma f_i$

2) standard deviaton $\sigma=\sqrt{\Sigma f_i(x_i-M)^2/\Sigma f_i}$

where f_i is the frequency in percentage and x_i is the value of standard specific gravity σ_{15}. The results will be indicated by plotting to-gether the value of the mean value M and standard deviation σ of specific gravity of each month in the diagram as in Fig. 2, where it may be considered to show some facts as follows.

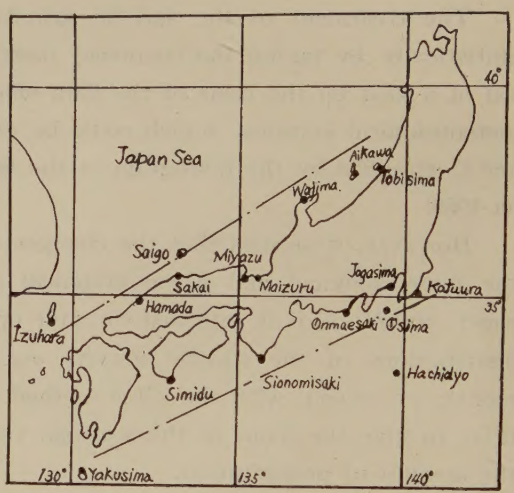

Fig. 2. Showing the location of various stations along the coast of Japan.

At first, fluctuations of mean values in the monthly interval is smaller throughout the year at Wajima, while it higher at the other three stations, where the minimum value occurs in warmer seasons. Next, the features of variations of standard deviation in each station appear almost similar to those of the mean value, except that the sense of increase or decrease is inverted between two. This is in good coincidence with that in the first report, and thus the classification of groups can be carried out by the computation either of two quantities, as mentioned before. Furthermore, according to circumstances, the groups of A, B, and C determined in the interval of the year may be alternated, such that Izuhara and Wajima belong to A-group showing the oceanic character, with the exclusion of several months, while Okinawa belongs still to B-group almost over the year and Shionomisaki is also considered as C-group, showing local conditions of inland bay itself, except in a few months of winter.

Now, this classification is related to the location where water samples are taken, and then the rainfall may be remarkably responsible. Thus, the relations between standard deviation of specific gravity and the average of the monthly amount of precipitation over the same five years are brought out in the diagram, as in Fig. 3, which shows clearly the marked correlation

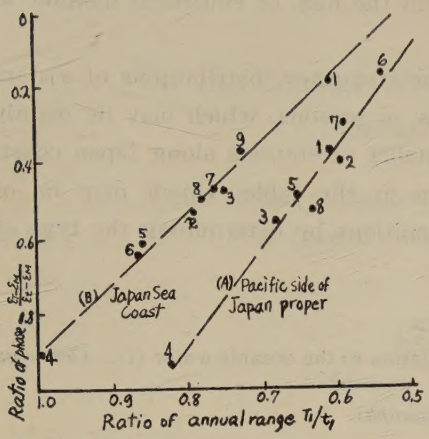

Fig. 3. Showing the relation between the ratio of phase angle and that of annual range.

between the two quantities. It is not within the scope of this study to enter upon this relation, though intended only to show that the ratio of precipitation amount to standard deviation indicates the some change with stations, as well as with seasons, as in the figure. Namely, this ratio takes a higher value at Wazima, especially in winter, while it takes a lower value at Okinawa, and also to a certain extent, the plotted points in the figure seem to concentrate over a certain interval of time at every stations. This tendency may be mainly abscribed to the character of the type of precipitation, relating to the location of the station observed.

3. Frequency distributions of specific gravity in the seasonal interval.

The procedure in the previous section is so troublesome to make for a number of stations that for simplicity, the method of taking the frequency for the interval of specific gravity σ_{15} 0 to 24 being denoted by n in percentage, as stated in the first report will be adopted, and also, as the based interval, the season will be chosen, deviding a year in four, such as, (1) January to March, (2) April to June, (3) July to September and (4) October to December.

Then, the quantity n are derived for four intervals of about 40 stations and tabulated in Table, where the quantity over the whole year is also involved for reference. It may be seen from this table that some of these stations are possible to be classified into groups by the value of n over the year, while in the other stations, the marked changes with seasons are fairly noticed. It is noted that the maximum value of n occur in the warmer seasons in almost cases of southern parts of Japan coast along Pacific ocean, while it seems to appear during the first half of the year in Japan sea coast, Okhotsk sea coast, and northern part of Japan along Pacific ocean. This may be mainly abscribed to the meteorological conditions such as the type of rainfall, as illustrated in the previous section.

4. Summery.

The present paper was treated with annual or seasonal variations of standard specific gravity σ_{15} of coastal sea waters, based on the data of observations

carried by some meteorological stations, with the help of statistical method in the same manner as in the first report.

It was shown that the features of the frequency distributions of σ_{15} are fairly marked in each stations as well as in seasons, which may by mainly abscribed to the type of rainfall. For a number of stations along Japan coast, the simpler treatments are made, as shown in the table, which may be of some use as guides to the study of sea conditions by determining the type of groups for stations, asociated with seasons.

References

Hisida, K, 1950: On the coastal water and its relation to the oceanic water (i). *Oceanogr. Mag.* Vol. 2 No. 3.

Kobe Marine Observatory: *The Journal of Oceanography.*

Table Frequency in percentage for the range 0 to 24 of specific gravity in the interval of the season at various stations.

Station	Season				Year
	1	2	3	4	
Japan Sea coast					
Izuhara	0	13	66	3	21
Saigo	31	12	49	5	24
Maizuru	100	100	95	94	97
Turuga	68	36	55	61	55
Wazima	15	7	11	18	13
Husiki	37	50	51	30	42
Aikawa	10	12	0	0	6
Sakata	94	44	33	76	62
Tobisima	87	47	33	44	53
Esasi	6	22	14	8	12
Sutu	28	30	4	26	22
Rumoe	47	63	6	5	35
Pacific Ocean coast					
Yakusima	6	17	28	24	19
Murotomisaki	0	0	16	16	8
Sionomisaki	8	26	46	12	24
Owase	13	70	93	49	57
Omaesaki	1	31	33	84	37
Niisima	0	2	26	4	9
Hachijo	0	0	00	0	0
Osima	0	1	0	0	0
Tomisaki	1	3	4	11	5
Katuura	6	15	15	11	12
Tyoshi	20	31	67	73	48
Miyako (Takohama)	0	8	20	0	7
Hachinoe	97	96	86	66	86
Hakodate	0	8	3	1	4
Aomori	22	45	19	26	28
Muroran	10	30	7	1	12
Urakawa	72	91	39	7	52
Kusiro	96	92	34	14	59
Okhotsk Sea coast					
Wakkanai	2	2	0	0	1
Kitamiesasi	72	67	3	25	43
Ontake	93	89	21	53	64
Abasiri	77	93	58	72	75
Nemuro	99	100	64	49	78

551.464

On the Coastal Water and Its Relation to the Oceanic Water (3)

(Third Report: Analytical study on the annual variation of coastal surface water temperature)

By

Kozo HISHIDA

(*Maizuru Marine Observatory*)

1. *Introduction*

The geographical and seasonal variations of sea-surface water temperature in the ocean were treated by the author, such as in the region of the western part of Pacific Ocean and also in the current region of Kurosio and Tusima current. (K. Hishida, 1953 and 1955) Among a number of factors responsible for the variation of sea water temperature, the amount of solar radiation, surface meteorological conditions and the heat content of the current are predominant in the ocean, while the mixing due to the inflow of fresh water from land and the effects of land and sea-bottom temperature as well as that of air, may be added to those factors in the coastal region.

Some of the results on the coastal water temperatures were obtained by Z. Yasui (1941), as a function latitude along the coast of Japan in the Pacific Ocean. In this paper, however, the author intends to treat this problem in the close connection with the corresponding air temperature and oceanic water temperature, which may be indicated as the above factors responsible for coastal water temperatures in a great degree. Though some different ways may be considered for this purpose, the features of annual variation of temperatures will be first investigated in this paper, since the effects may be seen to appear in the annual variation averaged over the interval of a longer time. The data here adopted are based on the coastal observations carried out by the meteorological stations in Japan, with the restriction in the region located along Kuroshio and Tusima current, where the oceanic temperature variation is well known.

2. *Basic conceptions*

The annual variation of temperature can be represented by means of a series of harmonic terms for the coastal water temperature in the form,

$$T=T_0+T_1\sin(\sigma\tau+\varepsilon_{T_1})+T_2\sin(z\sigma\tau+\varepsilon_{T_2})+ \quad \ldots\ldots(1)$$

where the first term of right hand side corresponds to annual means, second term to annual variation, and third to semiannual variation. With similar expressions,

$$t=t_0+t_1\sin(\sigma\tau+\varepsilon_{t_1})+t_2\sin(z\sigma\tau+\varepsilon_{t_2})+ \quad \ldots\ldots(2)$$

$$M=M_0+M_1\sin(\sigma\tau+\varepsilon_{M_1})+M_2\sin(z\sigma\tau+\varepsilon_{M_2})+ \quad \ldots\ldots(3)$$

are given for the case of air temperature and oceanic water temperature respectively. In these equations, the first and second terms being predominantly effective, the other remaining terms may be practically considered negligible for the air and oceanic water, and also this may be found applicable for the coastal water. (T. Okada, 1930; K. Hishida 1953) Now, in order to verify in actual cases how the temperature variation shows the different features between in the case of air, oceanic waters, and coastal waters, an example will be introduced in the neighbouring stations located at Miyazu and off Kyogamisaki in Japan Sea as shown in Fig. 1. The results obtained by means of harmonic analysis are given in Table 1, where it may be found that annual ranges and phase angles in the sea water temperature variation decrease almost gradually with increasing distances from the coast, and also the annual means, besides these two elements differs seriously in water temperatures from that in air temperatures.

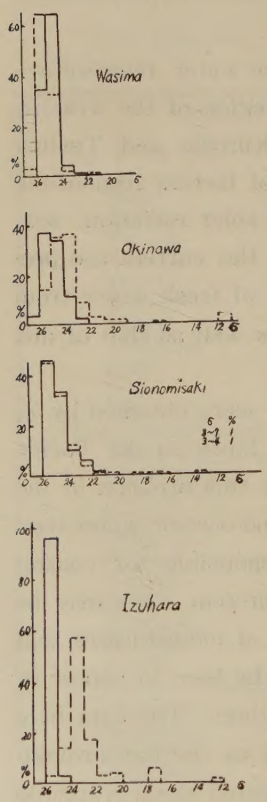

Fig. 1. Histogram of σ_{15} for four stations in the interval of January (full line) and August (broken line)

Table I. The results obtained by means of harmonic analysis at Miyazu and off Kyogamisaki

Stations	Annual means	Half annual ranges	Phase angles
Water temperature Miyazu (St. 1)	17.4	9.6	227
Kyogamisaki (St. 2)	16.7	8.1	222
2 miles off (St. 3)	18.2	8.3	216
30 miles off (St. 4)	17.8	7.9	211
50 miles off (St. 5)	17.4	7.8	205
Air temperature Miyazu (St. 1)	13.8	11.1	240

Then, the idea that the features of variation in the coastal water may be fairly treated in keen contact with that of the oceanic water as well as air, will be

extended to the further research, where it will be assumed that k times of second terms of right hand side in equation (2), added to l times of that in equation (3) equates to that in equation (1), as in the form

$$kt_1 \sin(\sigma\tau+\varepsilon_{t_1}) + lM_1 \sin(\sigma\tau+\varepsilon_{M_1}) = T_1 \sin(\sigma\tau+\varepsilon_{T_1})$$

Then, it follows that

$$\begin{cases} kt_1 \cos\varepsilon_{t_1} + lM_1 \cos\varepsilon_{M_1} = T_1 \cos\varepsilon_{T_1} \\ kt_1 \sin\varepsilon_{t_1} + lM_1 \sin\varepsilon_{M_1} = T_1 \sin\varepsilon_{T_1} \end{cases}$$

On eliminating the terms containing M_1 from both equations, there arises

$$kt_1 \sin(\varepsilon_{t_1} - \varepsilon_{M_1}) = T_1 \sin(\varepsilon_{T_1} - \varepsilon_{M_1})$$

Since the values of $(\varepsilon_{t_1}-\varepsilon_{M_1})$ and $(\varepsilon_{T_1}-\varepsilon_{M_1})$ are practically small, one obtains

$$k = k_1 k_2 \qquad \text{.....(4)}$$

to the first approximation, writing

$$k_1 = \frac{T_1}{t_1} \qquad k_2 = \frac{\varepsilon_{T_1}-\varepsilon_{M_1}}{\varepsilon_{t_1}-\varepsilon_{M_1}} \qquad (5)$$

This means that the rate of the effects on the coastal water due to the oceanic water and the air may be represented by the ratio of the annual ranges k_1 and the ratio of the phase angle differences k_2 to the rough approximation.

3. On the annual variation for coastal stations along Kurosio and Tusima current regions.

On the basis of the data of observations carried out by the meteorological stations along the coast of Japan in Kurosio and Tsusima current regions as shown in Fig. 2, the annual means, half amplitudes and phase angles are derived for coastal water temperature variation as well as for air temperature variation respectively. The results are summerized in Table 2, where those of oceanic water temperature variation are involved with respects to phase angles only, by taking the value at the nearest position to each station on the line as shown in this figure, as was studied before by the author. (K. Hishida 1953)

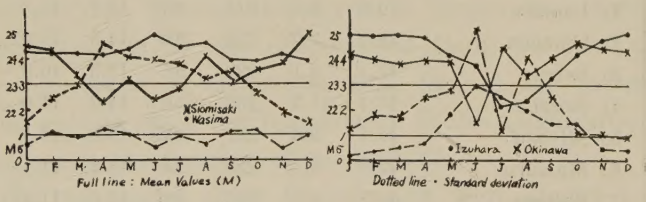

Fig. 2. Showing the annual variations of the monthly values of the mean (full line) and standard variation (broken line)

Here, it is only shown that the results for air temperature differ practically from that of the detailed study by T. Okada (1930) too little to enter upon

here in detail, and also that the annual means in air temperature variation takes the higher value than that in coastal water temperature variation in general as in the column of k_0 in the table. And then, much attention will be paid to the half annual ranges and phase angles, the values of which differ remarkably in the coastal water from that in the air and also change fairly with stations in the case of coastal water only. Thus, the quantities of k_1, k_2, and k shown in equations (4), (5) are evaluated for each stations, and indicated together in Table 2.

Table 2. The results obtained by means of harmonic analysis, and the derived quantities for various stations

Station	Water temperature				Air temperature			Quantity derived			
	T_0	T_1	ε_T	ε_M	t_0	t_1	ε_t	k_0	k_1	k_2	k
(A) Kurosio region											
1) Yakusima	23.0	5.0	225	216	18.9	8.3	239	1.22	0.60	0.39	0.24
2) Shimidu	20.8	5.8	224	214	16.5	9.8	239	1.26	0.59	0.40	0.24
3) Shionomisaki	20.7	6.3	226	211	16.4	9.3	238	1.26	0.68	0.55	0.38
4) Omaesaki	17.8	8.4	235	207	15.7	10.2	237	1.13	0.92	0.93	0.76
5) Jogasima	18.2	6.3	220	204	16.3	9.7	237	1.11	0.65	0.50	0.33
6) Osima	19.2	5.1	210	205	14.9	9.4	236	1.08	0.54	0.16	0.09
7) Hachijo	21.9	4.7	214	206	17.9	8.0	236	1.22	0.59	0.30	0.18
8) Katsuura	18.1	6.0	221	203	15.0	9.6	237	1.22	0.63	0.53	0.33
(B) Tsusima current region											
1) Izuhara	19.0	6.3	213	207	14.7	10.3	240	1.29	0.61	0.18	0.11
2) Hamada	18.3	7.9	224	207	14.5	10.0	239	1.26	0.79	0.53	0.42
3) Saigo	17.3	8.1	222	207	13.3	10.9	238	1.31	0.75	0.48	0.36
4) Sakai	16.1	11.0	235	207	14.2	11.0	238	1.14	1.00	0.90	0.90
5) Miyazu	17.4	9.6	227	206	13.8	11.1	240	1.26	0.86	0.62	0.53
6) Maizuru	17.7	9.5	228	206	13.8	11.1	241	1.28	0.86	0.63	0.54
7) Wajima	16.7	8.6	221	206	12.6	11.4	238	1.33	0.76	0.47	0.36
8) Aikawa	16.2	8.8	221	206	12.9	11.3	236	1.26	0.78	0.50	0.39
9) Tobishima	15.0	8.8	217	205	11.4	12.1	238	1.32	0.73	0.38	0.28

Remarks: $k_0=T_0/t_0$, $k_1=T_1/t_1$, $k_2=\varepsilon_T-\varepsilon_M/\varepsilon_t-\varepsilon_M$, $k=k_1k_2$

Now, stations may be roughly classified by the magnitude of k into three groups, such as A-group for $k<0.2$, B-group for $k=0.2\sim0.5$ and C-group for $k>0.5$. This classification may be seen in good coincidence with that which was determined by the specific gravity of coastal water studied in the first report, except a few exception. (K. Hishida 1950) The quantity k, therefore, may

be also seen to give a simple measure to the effects of factors responsible for coastal sea water conditions, similar to "oceanic factor" mentioned previously.

If one attempts to examine the relation between the quantity k_1 to k_2 by plotting each corresponding values in the diagram, it is seen that these points in Kurosio region and in Tsusima current region respectively, fall almost nearly on the each straight lines separately, as shown in Fig. 3. The good correlation thus obtained between these two in each regions may be led to the fact that either k_1 or k_2 is available as the measure, instead of k in each regions. In this case, however, it may be preferable to use k_1 for Kurosio region, and k_2 for Tsusima current region, since the changes of annual ranges with positions were practically negligible in the former region, whereas the changes of phase angles negligible in the latter. The result that the points fall on each lines corresponding to each regions may be interesting and, perhaps, it may be abscribed to oceanographical as well as meteorological conditions, such that the influence of current upon coastal waters may be more effective and that of air temperatures upon coastal waters may be more feeble in Kurosio region, compared with that in Tsusima current region.

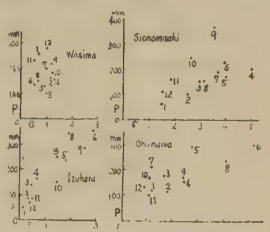

Fig. 3. Showing the relation between the standard deviation σ of specific gravity and the amount of precipitation p

4. Summary

By means of harmonic analysis, the features of annual temperature variation in the coastal waters obtained by the observations along the coast of Japan were quantitatively considered in connection with that in the corresponding air temperature as well as the water temperature in the neighbouring ocean region, without treating as the function of the latitude.

The various effects upon the coastal water temperatures were simply expressed by introducing the quantities such as the ratio of annual ranges k_1, the ratio of phase angle differences k_2 and the multiple of these two k at the stations along the Japan coast in the Kurosio region and Tsusima current region. This results appeared also to be almost similar to that obtained by the specific gravity of coastal waters in the first report.

References

Hishida, K., 1950: On the coastal water and its relation to the oceanic water (1). *Oceanogr. Mag.* Vol. 2, No. 3, p. 123.

Hishida, K., 1953: Annual variation of sea surface water temperature in the current region. *Records of Oceanogr. Works in Japan.* Vol. 1, No. 3, p. 7.

Hishida, K., 1955: Annual variation of sea surface water temperature and air temperature in the western part of North Pacific Ocean. *Records of Oceanogr. Works in Japan.* (In printing)

Okada, T., and Y. Yamada, 1930: On the influence of land and sea on the annual variation of air temperature. *Geo. Mag.* Vol. 3, No. 3, p. 101.

Yasui, Z., 1941: On the annual variation af coastal water temperature and specific gravity along the coast of Japan in the North Pacific Ocean. *Umi to Sora.* Vol. 21, No. 2. (in Japanese)

551.461.2

Storm Surges at the Kobe Harbour (Part 1)

By

Masamori MIYAZAKI

Kobe Marine Observatory

1. *Introduction*

The Kobe Harbour is often overtaken by destructive storm surges which are usually called by the Japanese name "Takashio". The dangerous sea-level, temporarily taken 50 cm above the mean high water level at springs, were marked 15 times by these storm surges during the period 1926–54. Especially, the surges on September 21, 1934, brought the highest sea-level 3.47 m (above the present datum line) and the largest sea-level anomaly 2.17 m in this harbour. The tidal record scaled out at that time, and these values were computed from the sea-water marks on the recording paper. The Typhoon Muroto came up the Cape Muroto in this early morning, and then struck the north coast of the Osaka Bay: the water came up in a great surge, and the highest sea-level was 2–4 m above normal at many localities along the Bay. The Typhoon Jane also brought severe surges in this district on September 3, 1950: the highest sea-level was 2.96 m above D.L. at Kobe, and a peak of the tidal curve clearly marked the level 3.16 m above D.L. at that time.

Tidal records were already collected and analysed by CMO and other authorities for these great surges, and the mechanism of their variations has been also discussed theoretically by using the actual meteorological data (Wadati 1938, Yamada 1950, and others). Owing to these studies, fairly cleared are the growth and decay of storm surges at Kobe and neighbouring area as long as the typhoon propagates northward along the main axis of the Osaka Bay. However, at least at the present time, their mechanisms are not clear when the typhoon or cyclone takes one of other routes. Most of the storm surges are rather caused by the typhoon cutting the Inland Sea from south to north. Although these surges do not include those of the largest scale, often observed are the anomalies of order 1 m accompanied with these storms. For instance, the Typhoon Makurazaki brought the maximum sea-level anomaly 1.48 m at this harbour on September 18, 1945.

In this paper, the author intends to pick up the storm surges from tidal

records of Kobe and discuss them from more synoptic view-points : or speaking in detail, to investigate (i) the statistical characteristics of surges, (ii) the correlations among surge profil, typhoon routes and features, and (iii) the experimental law predicting the maximum height of surges.

2. *Material used*

The Kobe Tidal Station was founded in 1899 for the sake of harbour work. The first record was obtained on May 29 of that year and the observation is continued to the present time. At first, the station was built near the south-eastern edge of the American Wharf, and was then removed to the south-western edge of the same wharf in 1939. The present datum line or "K.P." is taken 406.8 cm below the standard mark, 113.7 cm below the mean sea-level at Kobe (statistics of 1926–54), and 107.0 cm below the mean sea-level of the Tokyo Bay according to the results of the precise levelling carried out in 1951.

In the period May, 1899–November, 1925, we only have the statistical data of high and low waters.[1] The hourly records and those of high and low waters are given from the data December 1, 1925.[2] From the latter records we have picked up the surges which exceed the dangerous sea-level (50 cm above the mean high water level at springs, or 227.1 cm above D.L.), and the maxima of sea-level anomalies which are larger than 50 cm. They are shown in Table 1. When the predicted curves are available for us, the sea-level anomalies are easily given by adjusting the monthly mean values of observed and predicted curves. When the predicted curves are not available, we shall compute the anomalies by the following formula

$$\Delta h = h_0 - \frac{h_{-25}+h_{25}}{2} - \left(h_m - \frac{h_{-25}+h_{25}}{2}\right), \tag{1}$$

where Δh is the sea-level anomaly, h_0 is the observed sea-level at that time, h_{-25} and h_{25} are those 25 hours before and after that time, h_m is the monthly mean sea-level, and h_{-25} and h_{25} are the 25 hourly mean sea-levels from h_{-37} to h_{-13} and from h_{13} to h_{37}, respectively.

We have computed the anomalies in the period 1925–1949 by the second method, and those in the period 1950–1954 by the first method. Relative errors between two results given by these two methods will be at most 2 or 3 cm.

In Table 1, we also show the maxima of meteorological elements which act to heave the sea-level. In this meaning, we adopt the maximal pressure fall

from the monthly mean, and the maximum wind data in the directions of sea-level heaving.

3. *Frequency of surges*

It is very natural that the storm surges will be more serious when they take place in the period of higher water. However, it is also true that the astronomical tide changes are quite independent from the meteorological origins producing the storm surges. When we want to treat some problems on storm surges, those of the sea-level anomalies or the meteorological tides are to be discussed at first. The astronomical tides, which are superimposed to the meteorological ones, can be predicted easily and exactly as long at the harmonic constants are known and the tide-predictor is available for us.

In this paragraph, we shall estimate the frequency distribution of surges at Kobe from the data shown in Table 1. Objects of study are the maxima or sea-level anomalies larger than 50 cm.

We first pick up all maxima and minima from the time series of the sea-level anomaly at Kobe, and arrange them in order. An infinite series is thus obtained, and denoted by M'. When we further omit from M' all elements smaller than a finite value x_0 (+50 cm in this case), a new infinite series N is obtained. Our series (denoted by $\breve{N}$) is undoubtfully a sample of N.

It is here to be noted that the problem will be very simple if N and $\breve{N}$ are considered to be given from a stationary, independent and normal (mean 0, variance σ^2) mother series M.

M is not always equal to M'. These conditions are thought to hold in our case. The tests of the normality and stationariness are expressed in later sentences. The independence test can be made approximately by Anderson's method for subdivided samples of $\breve{N}$ in which the assumption of the normal distribution is not negated.

We can divide $\breve{N}$ into 4 sets including 4 or more elements and satisfying the last condition at the significance level of 5%. Computing the numerical values of

$$R=1-\Sigma (x_{i+1}-x_i)^2/2\Sigma (x_i-\bar{x})^2, \tag{2}$$

for these sets, we have 0.27, −0.06, 0.37 and −0.41 (n=4 to 9). These values are all within the significance level of 5%.

When three conditions are satisfied for M, the mean values of N will become

$$(3) \qquad m=\int_{x_0}^{\infty} xe^{-x^2/2\sigma^2}\,dx \Big/ \int_{x_0}^{\infty} e^{-x^2/2\sigma^2}\,dx=\frac{\sqrt{2}\,\sigma}{\sqrt{\pi}}\,\frac{e^{-x_0^2/2\sigma^2}}{\left[1-E\left(\frac{x_0}{\sqrt{2}\,\sigma}\right)\right]},$$

where

$$(4) \qquad E(\alpha)=\frac{2}{\sqrt{\pi}}\int_0^{\alpha} e^{-\eta^2}\,dy.$$

The 2nd-order moment of N around zero will be

$$(5) \qquad s^2=\int_{x_0}^{\infty} x^2e^{-x^2/2\sigma^2}\,dx \Big/ \int_{x_0}^{\infty} e^{-x^2/2\sigma^2}\,dx=\sigma^2+x_0m.$$

Now, the fiducial range of M's variance σ^2 is estimated from that of s^2, which is given from the distribution of

$$(6) \qquad f^2=\sum_{i=1}^{k} x_i^2/s^2.$$

In (6), x_i denotes the element of $N(x_1, x_2, \cdots\cdots, x_k)$. It is very difficult to compute the mathematical distribution of f^2 by rigorous method. However, we can estimate it in a sufficient approximation, when we compute the moments of its distribution curve from those of N around zero. The moments of f^2's distribution around zero are

$$(7) \qquad \begin{cases} \nu_1=k, \qquad \nu_2=k(k+2)-k\dfrac{mx_0^3}{s^4}, \\ \nu_3=k\left[(k+2)(k+4)-3(k-1)\dfrac{mx_0^3}{s^4}-\dfrac{mx_0^5}{s^6}\right], \quad \cdots\cdots \end{cases}$$

Therefore, the moments around the mean value $\nu_1=k$ are

$$(8) \qquad \begin{cases} \mu_2=k\left(2-\dfrac{mx_0^3}{s^4}\right), \\ \mu_3=k\left(8+\dfrac{3mx_0^3}{s^4}-\dfrac{mx_0^5}{s^6}\right), \\ \mu_4=k\left[12(k+4)-\dfrac{6mx_0^3}{s^4}(2k-1)+\dfrac{3m^2x_0^6}{s^8}(k-1)+\dfrac{4mx_0^5}{s^6}-\dfrac{mx_0^7}{s^8}\right], \quad \cdots\cdots \end{cases}$$

The distribution curve of f^2 is given by 4 elements ν_1, μ_2, μ_3 and μ_4 in a sufficient approximation.

Meanwhile, it is well-known that these moments are

$$(8) \qquad \nu_1=k, \quad \mu_2=2k, \quad \mu_3=8k \quad \text{and} \quad \mu_4=12k(k+4),$$

for the χ^2-distribution. Comparing (7) and (8), we easily find that the distribution of f^2 is approximated by χ^2-distribution if $k\gtrsim 20$ and $\dfrac{x_0}{\sqrt{2}\,\sigma}\lesssim 1$. The errors of this approximation are nearly within 2% in this case.

The fiducial range of s^2 is thus obtained from the numerical value of $\sum x_i^2$

Table 1. List of storm surges at Kobe (1925-54)

Data			Highest sea-level above present D.L.	Max. of sea-level anomaly	Maximum pressure fall	Max. of level-heaving wind	
y	m	d	cm	cm	mb		m/s
1926	12	18		67	5.1	WNW	15.9
27	3	9		57	15.6	WNW	9.7
29	4	21		61	23.9	W	19.4
	8	15		68	20.4	W	12.2
31	5	16		67	18.4	W	16.9
	10	13		72	24.7	E	22.8
33	10	20		77	24.4	SW	14.2
34	3	21		63	21.3	SW	13.2
	9	9		59	14.0	SW	14.5
	9	21	— (347)	— (217)	38.3	ESE	22.8
35	8	29	232	64	20.9	E	16.1
	9	24		64	22.5	E	18.5
37	9	11	239	96	28.5	SSW	15.3
38	9	5	228	75	28.7	SW	13.0
41	8	15	231	79	7.6	S	13.2
	10	1		71	26.0	SSW	28.3
42	8	28		61	16.1	SW	17.4
43	9	20		59	25.9	SSW	9.2
44	9	17	252	89	19.2	SW	19.7
45	9	18	274	148	30.7	SSW	27.6
49	4	3		53	10.9	WNW	12.0
	9	23	241				
50	9	3	296 (316)	147 (167)	47.4	W	25.8
	9	14	248				
51	7	2		52	15.5	SSW	10.8
	10	15	275 (286)	115	34.5	WSW	19.6
52	3	19		60	26.1	WSW	12.5
53	5	29		54	20.8	W	7.6
	6	7		61	11.1	SSW	10.7
	9	25	246 (254)				
54	4	12		52	19.0	W	9.6
	8	18	234 (251)	70	23.2	E	7.3
	9	14	260 (285)	92	19.2	S	15.7
	9	26	260 (293)	122 (153)	22.5	SSW	22.6

( ) denotes the value for the peak.

and the table of the χ^2-distribution. The corresponding range of σ^2 or $\frac{x_0}{\sqrt{2}\sigma}$ is easily given from formulas (4) and (5).

Our final object is, undoubtfully, to obtain the frequency of storm surges (sea-level anomalies) exceeding a finite value x_1. We shall denote it by $n(x_1)$. $n(x_1)$ is computed from the corresponding frequency $n(x_0)$, which is easily given from the fundamental table showing the date of x_1-occurence.

If $n(x_0)$ means the frequency in a callendar year, and is considered to be the Poisson's distribution (mean value n_0), $n(x_1)$ is also considered to be the Poisson's distribution, and its mean value is given by

$$n_1 = \frac{n_0\left[1-E\left(\frac{x_1}{\sqrt{2}\sigma}\right)\right]}{\left[1-E\left(\frac{x_0}{\sqrt{2}\sigma}\right)\right]} \quad (9)$$

The fiducial range of n_1 is easily computed from that of s^2, and the unbiased estimate of n_1 is also computed from the distribution curve of s^2.

4. *Numerical computation of surge frequency (including the statistical tests of M's normality and stationariness)*

We must first compute the fiducial range of $\frac{x_0}{\sqrt{2}\sigma}$ from the observed data. From Table 1, we obtain for the period 1926-53

(10) $\bar{x}=75.9$ (cm), $k=28$ and $\Sigma x_i^2=1.908\times10^5$ (cm^2).

Then, we have

(11) $11816>s^2>4758$ (cm^2),

at the significance level of 5%. The corresponding range of is easily read from the $s^2-\frac{x_0}{\sqrt{2}\sigma}$ diagram (Fig. 1), which is computed from (4) and (5) for $x_0=50$(cm). We thus obtain

(12) $0.98>\frac{x_0}{\sqrt{2}\sigma}>0.36$,

at the same significance level. The unbiased estimate of $\frac{x_0}{\sqrt{2}\sigma}$ is also given from the probability distribution of s^2 (cf. Fig. 2), i.e.,

(13) *u.s.* of $\frac{x_0}{\sqrt{2}\sigma}=0.68$.

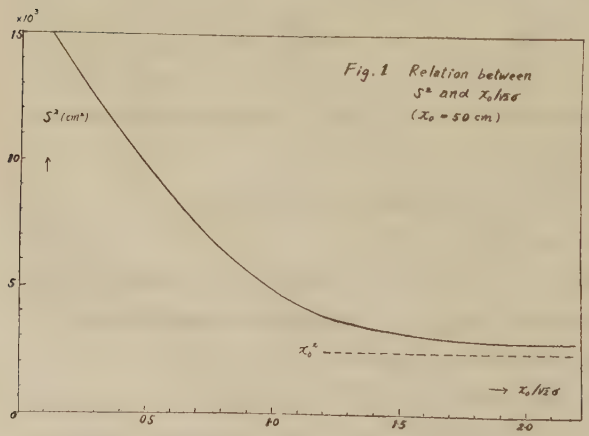

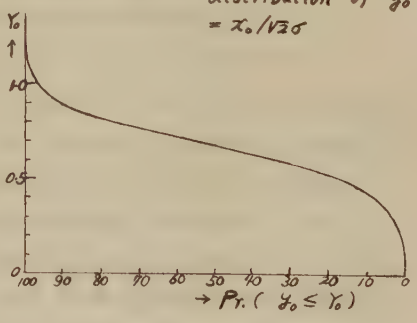

The normality of M is now tested by using (13). We rearrange $\breve{N}$ in order of height, and then divide it into 4 sets. (Table 2). The actual numbers in

Table 2. Normality test of (period 1926-53) total numbers

x_i	Total numbers	
	f_j	f_{j_0}
cm		
~60	8	7.0
61~70	9	5.9
71~80	5	4.7
81~	6	10.3

f_j ·····observed number,
f_{j_0}·····computed number.

these sets are shown in the 1st row, and the corresponding computed numbers are shown in the 2nd row. If M is the normal series as we have assumed, the distribution of

(14) $$\chi_0^2=\Sigma\,(f_j-f_{j_0})^2/f_{j_0},$$

must be that of χ^2. (degree of freedom 2). Computing χ_0^2 from the data of Table 2, we obtain the value 3.59, which is within the significance level of 5%.

The stationariness of M is also tested when we divide $\breve{N}$ into some sets and compute the value

$$s_j^2=\Sigma\,x_i^2,$$

for each set. If M is regarded to be stationary, the distribution of

(15) $$g_j=s_j^2/\Sigma\,s_i^2,$$

will be approximately equal to that of Ogawara's g_i (Ogawara and cooperators 1952). We have 6 sets including 5 elements, and the maximum and minimum values of g_j are 0.39 and 0.092, respectively. Both values are within the significance level of 5%. The assumptions of normality and stationariness in M are thus ascertained.

We must next estimate the annual frequency $n(x_0)$ for the case of $x_0=50$ (cm). The data in the period 1945-46 are not available for this purpose, since we have no continuous tide records in this period. Excepting for these two years, we have

(16) $$n_0=1.00,\quad k=26\quad\text{and}\quad\Sigma\,(n-n_0)^2=18.0.$$

The result of χ^2-test

(17) $$\chi_0^2=\Sigma\,(n-n_0)^2/n_0=18.0,$$

is not negative for the assumption of Poisson's distribution at the significance level of 5%.

Finally, we shall compute the annual frequency $n(x_1)$ from these results.

Their fiducial ranges and unbiased estimates are easily obtained from (9), (12); and Figure 2. For x_1=1.0, 1.5, 2.0 and 3.0 (m), we have the results shown in Table 3. These results represent that the storm surges (measured by the sea-level anomaly) exceeding 1.0 m, 1.5 m, 2.0 m and 3.0 m are expected once per 5, 24, 105 and 455 years, respectively.

Table 3. Annual frequencies of storm surges exceeding finite heights.

x_1	n_{1l}	$\bar{n}_1$	n_{1u}	$1/\bar{n}_1$
m				
1.0	0.505	0.199	0.038	5
1.5	0.207	0.042	—	24
2.0	0.068	0.0095	—	105
3.0	0.0037	0.0022	—	455

n_{1l} ……the maximum frequency at the significance level of 5%,
$\bar{n}_1$ ……unbiased estimate of the annual frequency,
n_{1u} ……the minimum frequency at the significance level of 5%,
$1/\bar{n}_1$……number of years in which the surge is once expected.

5. *Seasonal variations of surge frequency*

The independence of M has been approximately proved in the last paragraph, and the annual frequency of surges $n(x_0)$ is also shown to vary at random. However, there are significant seasonal variations of surge frequency. Total numbers in callendar months are shown in Table 4 for the period 1926–54 (excepting 1945 and 46).

Table 4. Total numbers of surges in callender months (x_0=50 (cm), period 1926–54)

Jan.	0	May	2	Sep.	10
Feb.	0	June	1	Oct.	4
Mar.	3	July	2	Nov.	0
Apr.	3	Aug.	5	Dec.	1

In general, storm surges are most frequent in August to October, next in March and April, and least frequent in winter months. Undoubtfully, they are closely related with the frequency and path of powerful typhoons or extra-tropical cyclones.

We now classificate the storm surges shown in Table 1 by their causes and heights (Table 5). This table clearly shows that the typhoon often causes great storm surges, and the extratropical cyclone causes relatively small surges. The storm surges in July to October are mainly caused by typhoons, and these in other months are mainly caused by extratropical cyclones.

Table 5. Classification of storm surges.

Cause	Total numbers	Sea-level anomalies (cm)			
		50～64	65～79	80～94	95～∞
Tropical low	22	7	7	2	6
Extratropical low	10	8	2	0	0

It is a very important problem to ascertain the relations between surges and storm paths, which are expressed in next paragraph. This contains the problem why the surges caused by extratropical cyclones are most frequent in spring months.

References and notes

Ogawara, M. and cooperators, 1952: Climatic change in Japan and climatological statistics. *Kenkyū Jihō* (**4**), 8, pp. 461-524. (in Japanese with English abstracts)

Yamada, H., 1950: Theoretical estimation of meteorological high water. *Rep. Res. Inst. Fluid Eng.* **6**, pp. 22-33.

Wadati, K., 1938: On tsunami's caused by typhoons in the Osaka Bay. *Umi to Sora.* (**13**), 12, pp. 421-438. (in Japanese)

1) Data are shown in technical reports of the Kobe City.
2) Records are tabulated in the tidal observations published by the Imperial Marine Observatory.

551.465

On the Transport in the Eastern Sea of Honshu

(Part 2. Conditions during 1946–1948)

By

Jiro SUGIURA

(Hakodate Marine Observatory)

§ 1. *Oceanographical observations used for the investigations*

The volume transports were calculated by the same method which had been given in Part 1 of this paper, that is, using the data of nine expeditions for oceanographical observations taken during 1946–48, the quantity Q were computed and the Q charts were drawn. In Figs. 1–7 are illustrated the Q charts.

In the following table are shown oceanographical observations, the results of which are used for the calculations.

period of observations	name of ships	observed area	literatures	Nos. of stations for which Q computed	Q charts
Apr. 17–27, 1946	Ryofu-maru	35.5°–40.5°N 141°–150°E	A	28	Fig. 1
Sept. 9–14, 1946	Kaiyo-maru No. 4	39°–42°N 142°–146°E	B–No. 10	14	Fig. 2
Aug. 10–Sept. 2, 1947	Ryofu-maru	30°–41.5°N 140°–150°E	C–No. 2 D–Vol. 1, No. 2	31	Fig. 3
Oct. 26–Nov. 18, 1947	Oshoro-maru	39.5°–42.5°N 142°–148°E	C–No. 2 E–Vol. 6, No. 2	8	Fig. 4
July. 24–Aug. 14, 1948	Kaiyo-maru No. 5	36.5°–42°N 141°–147°E	B–No. 10 F–No. 10, 11	31	Fig. 5
Aug. 25–27, 1948	Ukuru-maru	38.5°–39°N 142°–153°E	C–No. 4 D–Vol. 1, No. 2	12	Fig. 6
Aug. 31–Sept. 12, 1948	Yushio-maru	39.5°–42.5°N 142°–147.5°E	do.	8	
Oct. 1–17, 1948	Kaiyo-maru No. 4	40.5°–43°N 142°–147°E	B–No. 10 F–No. 11	13	Fig. 7
Oct. 8–11, 1948	Yushio-maru	39.5°–42°N 142°–146°E	C–No. 4 D–Vol. 1, No. 2	7	

In the table the following abbreviations are used for literatures.

A : Kaikyo-gaiho (Gogai), C.M.O.

B : Hydrographic Bulletin, Special Number.

C : The Results of Marine Meteorological and Oceanographical Observations, C.M.O.

D : The Oceanographical Report of the Central Meteorological Observatory.

E : Journal of the Oceanographical Society of Japan.

F : Hydrographic Bulletin.

§ 2. *The transports of the different branches of the currents*

The transports of the different branches of the currents during 1946–48 are shown in following table, and in the table are shown also the values of the transports during 1949–50 for comparison.

character of the currents	localities	transport during 1946–48 (10^6 m^3/sec)	transport during 1949–50 (10^6 m^3/sec)
A. the Kuroshio Extension	34°–37°N 140°–147°E	28–20	44–30
B. current branched from the Kuroshio Extension	35°–38.5°N 146°–151°E	10– 1	23– 3
C. clockwise eddy of the Kuroshio water	38°–40.5°N 143°–144.5°E	13– 2	15– 2
D. clockwise eddy of transmuted Kuroshio water	40.5°–41.5°N 146.5°–149°E	8– 3	6– 4
E. Tsugaru warm current	40°–41.5°N 141.5°–144°E	6– 4	3– 2
F. the branch of the Oyashio current in the offing	39°–42°N 144.5°–147°E	10– 2	6– 2
G. coastal branch of the Oyashio current	39°–40.5°N 143°–144°E	4– 3	6– 2

Alike in Part 1 of this paper, brief explanations for each braches of the currents are given as follows.

A. The Kuroshio Extension

period of observations	localities	direction of currents	max. chlorinity of the centre (‰)	transport (m^3/sec)
Apr. 17–21, 1946	35.5°N, 142°E→36.5°N, 145°E →35°N, 145.5°E	ENE→SSE	19.30	28×10^6
Aug. 10–22, 1947	34°N, 140°E→37°N, 144°E →36.5°N, 145°E→37°N, 147°E →36°N, 147.5°E	NE→SE →ENE→S	19.24	20×10^6

B. Current branched from the Kuroshio Extension

period of observations	localities	direction of currents	max. chlorinity at the centre (‰)	transport (m^3/sec)
Apr. 18–25, 1946	35°N, 148°E→39.5°N, 149.5°E	NNE	19.20	10×10^6
Aug. 25–27, 1948	38.3°N, 148°E	ENE	19.20	1×10^6

C. Clockwise eddy of the Kuroshio water

period of observations	the locality of centre	max. chlorinity at the centre (‰)	transport (m^3/sec)
Apr. 23, 1946	38.3°N, 144.5°E	19.15	13×10^6
Sept. 11–13, 1946	39.5°N, 144.7°E	19.10	10×10^6
Jul. 27, 1948	38°N, 143.7°E	19.05	12×16^6
Aug. 27, 1948	38.5°N, 143°E	19.07	3×10^6
Oct. 10–13, 1948	40.4°N, 144.5°E	19.07	2×10^6

D. Clockwise eddy of transmuted Kuroshio water

period of observations	the locality or centre	max. chlorinity at the centre (‰)	transport (m^3/sec)
Apr. 25, 1946	40.5°N, 149°E	18.90	8×10^6
Aug. 13–14, 1948	41.7°N, 146.5°E	19.05	7×10^6
Sept. 2–12, 1948	41°N, 147°E	18.90	3×10^6

E. Tsugaru warm current

period of observations	localities	direction of currents	max. chlorinity at the centre (‰)	transport (m^3/sec)
Nov. 9, 1947	forming a clockwise eddy with its centre at 41.4°N, 142.8°E		18.89	6×10^6
Aug. 6–12, 1948	41.5°-N, 142°E→40.5N, 143.5°N →40°N, 143°E	SE→SW	18.90	4×10^6
Sept. 3–6, 1948	41.5°N, 142°E→40.5°N, 144°E →40°N, 143°E	ESE→WSW	18.92	4×10^6
Oct. 14, 1948	41.5°N, 142°E→41.5°N, 143°E →40.5°N, 142.5°E	E→SW	18.86	6×10^6

F. The branch of the Oyashio current in the offing

period of observations	localities	pirection of currents	chlorinity for 0 to 150 m (‰)	transport (m^3/sec)
Apr. 26–27, 1946	40.5°N, 146°E→38.5°N, 146.5°E	SSE	18.11–18.51	4×10^6
Sep. 12, 1946	39.5°N, 146°E	SSW	18.24–18.36	10×10^6
Aug. 13–14, 1948	42°N, 144.5°E→40.5°N, 146°E →39°N, 144°E	SE→SSW	18.19–18.48	3×10^6
Sept. 1–12, 1948	41.5°N, 145°E→39.5°N, 146.5°E	SE	18.22–18.50	2×10^6
Oct. 8–13, 1948	42.5°N, 146°E→41.3°N, 144°E →41°N, 145°E	WSW→ESE	18.19–18.49	5×10^6

G. Coastal branch of the Oyashio current

period of observations	localities	direction of currents	chlorinity for 0 to 150 m (‰)	transport (m^3/sec)
Sept. 11, 1946	forming an anticlockwise eddy with its centre at 39.3°N, 143.2°E		18.25–18.60	4×10^6
Aug. 24, 1947	40.7°N, 143.7°E	S	18.01–18.48	4×16^6
Nov. 17–18, 1947	forming an anticlockwise eddy with its centre at 40°N, 144°E		18.41–18.60	3×10^6

§ 3. *The volume transports for each period of observations*

1) April 17th–27th, 1946. (see Fig. 1)

The Kuroshio Extension is running eastward with meander off the Cape Inubozaki and its transport is amounted to 28×10^6 m³/sec; the value is nearly equal to the transport of the Kuroshio Extension in My 1950, 30×10^6 m³/sec.

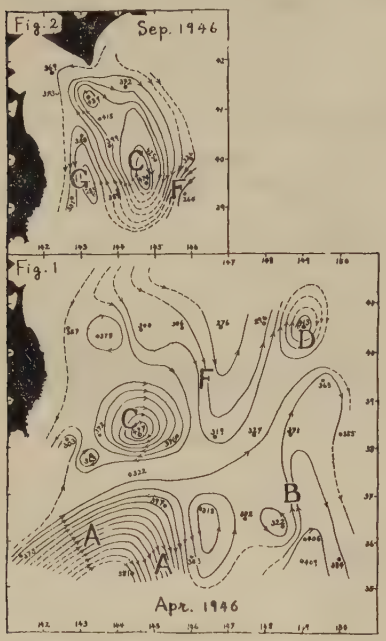

Fig. 1, Fig. 2. *Q*-charts in 1946.
The inserted numbers indicate the *Q*-value (m³/sec²) of each stations, intervals of two parallel *Q*-lines are 20 m³/sec², and the arrows indicate the direction of the transport. Between those two lines the transport above 800 m is about 2.0–2.4 million m³/sec.
The inserted letters indicate the type of currents as follow:

A : the Kuroshio Extension.
B : current branched from the Kuroshio Extension.
C : clockwise eddy of the Kuroshio water.
D : clockwised eddy of transmuted Kuroshi water.
F : the branch of the Oyashio current in the offing.
G : coastal branch of the Oyashio current.

The clockwise eddy of the Kuroshio water with its centre at 38.3°N, 144.5°E off the Cape Kinkazan is rather strong, and its transport is amounted to 13×10^6 m³/sec; the value is equal to the transport of the eddy of the same character observed at 38.3°N, 146°E in August 1950, 13×10^6 m³/sec.

The transport of the branch of the Oyashio current in the offing is amounted to 4×10^6 m³/sec; the value is nearly equal to the transport of the same branch in May 1950, 3×10^6 m³/sec.

It is considered that the coastal branch of the Oyashio current in running southward at 40.5°N, 142.5°E, but it is unable to calculate the transport owing to lack of the stations.

2) September 9–14, 1946. (see Fig. 2)

The clockwise eddy of the Kuroshio water with its centre at 39.5°N, 144.7°E off Miyako is rather strong and its transport is amounted to 10×10^6 m³/sec; the value is nearly equal to the transport of the eddy of the same character observed at 40.5°N, 144.5°E in August 1950, 11×10^6 m³/sec.

The transport of the branch of the Oyashio current in the offing is amounted to 10×10^6 m³/sec and it is the maximum value in the transport of the same branch throughout the period from 1946 to 1950.

The coastal branch of the Oyashio

current is not observed, but an anticlockwise eddy of the Oyashio water is observed at 39.3°N, 143.2°E off Miyako.

3) August 10th–September 2nd, 1947. (see Fig. 3)

The transport of the Kuroshio Extension is amounted to 20×10^6 m³/sec, but the value is not so exact, because no station exists in the area 33°–36.5°N, 141°–146°E. The transport, 20×10^6 m³/sec is nearly half of the same current in July 1949 and August 1950, i.e. 38×10^6 and 44×10^6 m³/sec respectively.

Three vorticies are observed, at the south of the Kuroshio Extension, which are shown in the following table.

kind of vortices	the locality of centre	max. chlorinity at the centre (‰)	transport (m³/sec)
clockwise	31.5°N, 140.5°E	19.39	15×10^6
do.	32°N, 144.5°E	19.22	22×10^6
anticlockwise	34°N, 146.5°E	19.11	24×10^6

The coastal branch of the Oyashio current is observed and its transport is amounted to 4×10^6 m³/sec, this is a remarkable fact because no coastal branch is observed in August, 1948, 1949 and 1950.

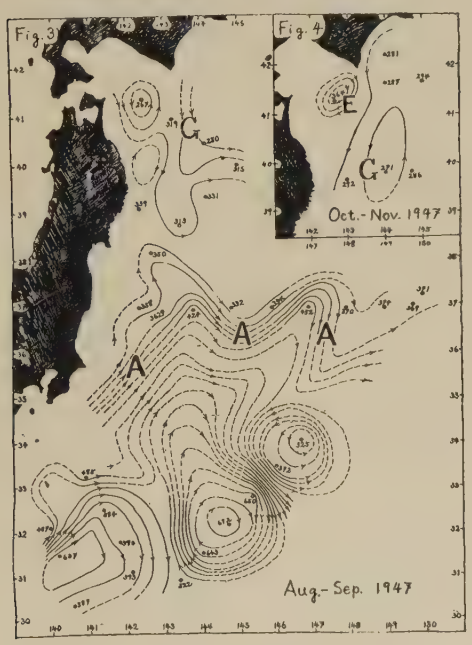

Fig. 3, Fig. 4. *Q*-charts in 1947.

A : the Kuroshio Extension.
E : Tsugaru warm current.
G : coastal branch of the Oyashio current.

4) October 26th–November 18th, 1947. (see Fig. 4)

A clockwise eddy with the transport of 6×10^6 m³/sec is observed at 41.4°N, 142.8°E off the Cape Shiriyazaki. Judging from the chlorinity at the centre, this eddy is considered to be consist of the water originated from the Tsugaru warm current.

Instead of the coastal branch of the Oyashio current, an anticlockwise eddy of the Oyashio water is observed at 40°N, 144°E off Miyako and its transport is amounted to 3×10^6 m³/sec ; the value is nearly equal to the transport of the coastal branch of the Oyashio current calculated in November of 1949 and 1950, that is 5×10^6 and 3×10^6 m³/sec.

5) July 24th–August 14th, 1948. (see Fig. 5)

It is considered that the Kuroshio Extension is running eastward in the south of a boundary between the Oyashio water which is lying from 36°N, 142°E, to 37°N, 147°E.

The transport of the clockwise eddy of the Kuroshio water at 38°N, 143.7°E off the Cape Kinkazan is amounted to 12×10^6 m³/sec and the value is nearly equal to the transport of the eddy of same character which observed at 38.3°N, 146°E in August 1950, 13×10^6 m³/sec.

The transport of another clockwise eddy of the Kuroshio water at 41.7°N, 146.5°E off the Cape Erimomisaki is amounted to 7×10^6 m³/sec and the value is nearly equal to the transport of the clockwise eddy of transmuted Kuroshio water which observed at 41.5°N, 145.5°E in November 1950, 8×10^6 m³/sec.

The Tsugaru warm current is running southeastward from the Cape Shiriya-zaki to the longitude 144°E off Hachinohe and its transport is amounted to 4×10^6 m³/sec.

The transport of the branch of the Oyashio current in the offing is amounted to 3×10^6 m³/sec and the value is equal to the transport of the same branch which calculated in August of 1949 and 1950.

The coastal branch of the Oyashio current is not observed.

6) August 25th–September 12th, 1948. (see Fig. 6)

It is considered that a current branched from the Kuroshio Extension is running eastward in the area 38.5°N, 146°E–152°E off Kinkazan, but it is unable to calculate its transport owing to lack of the stations.

The transport of the clockwise eddy of the Kuroshio water at northeast off Kinkazan is amounted to 3×10^6 m³/sec and the transport has rather decreased from the value calculated in the preceding month.

The transport of the clockwise eddy of transmuted Kuroshio water at 41°N, 147°E off Hachinohe is amounted to 3×10^6 m³/sec and the value also has decreased from the value in the preceding month.

The transports of the Tsugaru warm current and the branch of the Oyashio current in the offing are 4×10^6 and 2×10^6 m³/sec respectively and each values are nearly equal to the values in the preceding month.

7) October 1st–17th, 1948. (see Fig. 7)

The clockwise eddy of the Kuroshio water has moved northeastward from the locality in the preceding month and is observed at 40.4°N, 144.5°E off Hachinohe, but its transport is amounted to be nearly equal to the value in

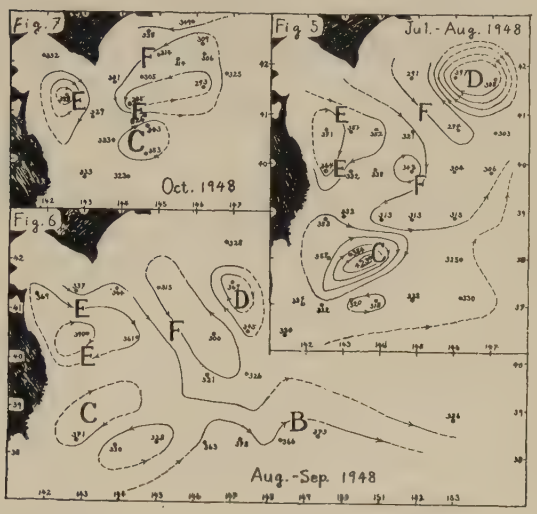

Fig. 5, Fig. 6. Fig. 7. *Q*-charts in 1948.

B : current branched from the Kuroshio Extension.
C : clockwise eddy of the Kuroshio water.
D : clockwise eddy of transmuted Kuroshio water.
E : Tsuruga warm current.
F : the branch of the Oyashio current in the offing.

the preceding month.

The transport of the Tsugaru warm current has increased a little from the value in the preceding month and is amounted to 6×10^6 m^3/sec; the value is nearly equal to the transport of the current calculated in November 1947.

The transport of the branch of the Oyashio current in the offing has increased a little from the value in the preceding month and is amounted to 5×10^6 m^3/sec; the value is a little larger than the value calculated in October 1949, 2×10^6 m^3/sec.

The coastal branch of the Oyashio current is not observed as well as in July, August and September of this year.

§ 4. *Summary*

The transport of the Kuroshio Extension was amounted to $44-30\times10^6$ m^3/sec during 1949-50 but the value was a little small during 1946-48 and amounted to $28-20\times10^6$ m^3/sec.

On the contrary, the transport of the branch of the Oyashio current in the offing was amounted to 6×10^6 m^3/sec in maximum during 1949-50, but the value was a little large during 1946-48 and amounted to 10×10^6 m^3/sec in maximum.

The transport of the Tsugaru warm current was amounted to 3×10^6 m^3/sec in maximum during 1949–50, but was amounted to 6×10^6 m^3/sec in maximum during 1946–48.

§ 5. *Acknowledgement*

In conclusion, the author wishes to express his thanks to Dr. Y. Takenouti for his kind advices.

551.465

An Outline of the Kuroshio in the Eastern Sea of Japan

(Currents and Water Masses of the Kuroshio System IV)

By

Jotaro MASUZAWA

Oceanographical Section, the Central Meteorological Observatory, Tokyo

§ 1. Introduction

The oceanographical observations in the eastern sea of Japan have been carried out systematically since 1910 as a fundamental survey on the fishery ground and promoted for the prediction of the cool summer in Northeast Japan. It may be, however, since the simultaneous observations in August of 1933 on board many research ships of the fishery institutions, that we have become to obtain general knowledges on currents and water masses in the extensive region east off Japan. M. UDA (1935a・b, 1938a・b) showed from the results of these observations that the Kuroshio flows generally eastwards in meandering or sending off one or more branches and the distributions of water masses present various complicated patterns, and suggested that there exist some remarkable seasonal and yearly fluctuations in the location of the boundary (the *Shiozakai* after UDA) between the Kuroshio and the Oyashio (the *Subarctic Water*). For Japanese oceanographers, his interpretations deduced from these investigations have been a fundamental idea on the general oceanographical conditions in this sea. Y. SAITO (1952) analyzed in his investigation on the Oyashio Current several water masses which appears in the western part of the North Pacific, especially discussing the role played by lateral and vertical mixing in this frontal zone.

While these observations were carried out in summer almost simultaneously in the extensive region about 1000 miles east off the coast of Japan, in the other seasons they were neither extensively nor systematically, and so we have hardly any satisfactory knowledges on seasonal fluctuations in the distribution of currents and water masses. From these observations, moreover, we cannot obtain such an actual current pattern as observed in the Gulf Stream System (FUGLISTER & WORTHINGTON 1951), owing to undeveloped instruments for navigation and observation and unsuitable observational networks.

After the World War II, we have been paying attention to synoptic changes

in the distribution of currents and water masses from the continuous observation along the so-called "C-line" (38°15'N, Fig. 1) occupied twice a month in 1948~1953 and several observations persuing the Kuroshio Current (NAN'NITI 1951, HANZAWA 1952, ICHIYE 1953, KAWAI 1954, MASUZAWA 1954, FUKUOKA 1955). In the eastern sea of Japan, the Kuroshio may play a leading role in the synoptic change of oceanographical conditions, thus the present author intends to describe the general features on the current-pattern of the Kuroshio, its sectional profile and its branching from the recent observations in the neighbourhood of the stream axis.

§ 2. Horizontal Current Patterns

As seen in the current pattern (Fig. 1) represented schematically from the former informations (UDA 1938b and KAWAI 1953), the Kuroshio Current leaves the coast of Japan at Cape Inubo-zaki (36°N) and flows generally to the east along the *A*-curve and a northeastward-current (*A'*) branches out from the main stream in the neighbourhood of 37°N, 143°E and comes in contact with the Oyashio Water to the southeast of Hokkaido. These currents form the *multiple currents* (FUGLISTER 1951) or the *double frontal zones* in the distribution of water masses (UDA 1943). The northern zone (*B*) is the southern limit of the Oyashio Water and is called the *Subarctic Convergence*, the oceanic *Polar Front* or the *Oyashio Front*, while the southern zone (*A*) corresponding to the Kuroshio Current itself is the northern limit of the pure warm and haline water mass of the Kuroshio (the *Kuroshio Front*). But the latter could not so exactly be defined owing to inadequency of observational lines almost parallel to the general direction of the Kuroshio Current before the World War II (Fig. 1).

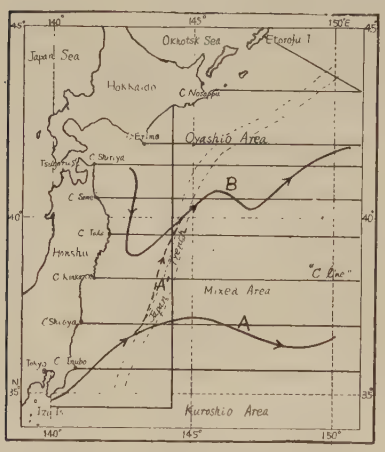

Fig. 1. The schematic current-pattern and the network often occupied before the World War II.

Position of stream-axis

The horizontal distribution of the 10°-isotherm depth is available to see easily an outline of the current pattern, as previously pointed out (MASUZAWA

1955), because it is similar to the chart of dynamic topography. In fact, according to all observational data in 1954 obtained in four cruises of the R.M.S. RYOFU-MARU and the YUSHIO-MARU in the eastern sea of Japan, the relationship between the anomaly of dynamic depth of 1000 d.b. surface (ΔD_{1000} dyn. m) and the 10°-isotherm depth ($d_{10°}$ m) is shown in Fig. 2, which may be approximately expressed by the next linear equation,

$$\Delta D_{1000} = 0.991 + 0.00194\, d_{10°}$$

In Fig. 3 is shown the distribution of the sharp horizontal gradient zones of the 10°-isotherm depth in August from 1933 to 1941. The stream axis of the Kuroshio is located on the average at 36°～37° N, but generally it meanders in the range of 200 miles or more and with the wave-length of 200±50 miles, and the northern bend of its wavy form is located at 144°～145° and 149°～150° E. But, it must be kept in mind that the curve shown in this figure does not always show the main current, but may include some branch currents.

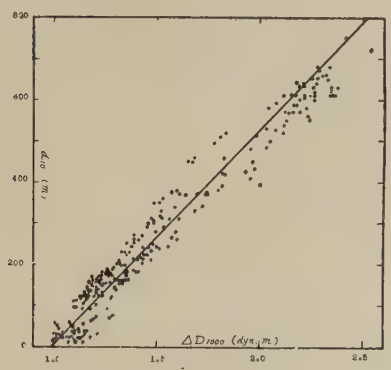

Fig. 2. The relationship between the dynamic depth anomaly of 1000 d.b. surface (ΔD_{1000}) and the 10°-isotherm depth ($d_{10°}$).

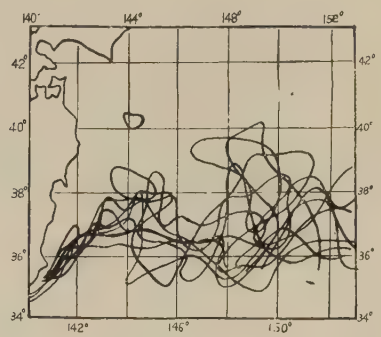

Fig. 3. The distribution of the sharp horizontal gradient zones of the 10°-isotherm depth in August from 1933 to 1941.

Typical current patterns

In August of 1940, the main stream of the Kuroshio flows almost straight eastwards from the coast to 150°E between 36° and 37°N in branching out a weak current to the north at 144°～145°E. On the contrary, in the summer of 1942, the main stream changes its direction to the northwest at the branching position in 1940 and takes a remarkable meandering course. Various current patterns in this sea are generally classified into one of the above typical patterns or their compound one.

As the network in the former observations were not so close in the east from 150°E as in the inshore region from the coast to 150°E, it might be probably misjudged that in the offshore region the Kuroshio Current was not a narrow current but a broad weak current or it was broken into many weak

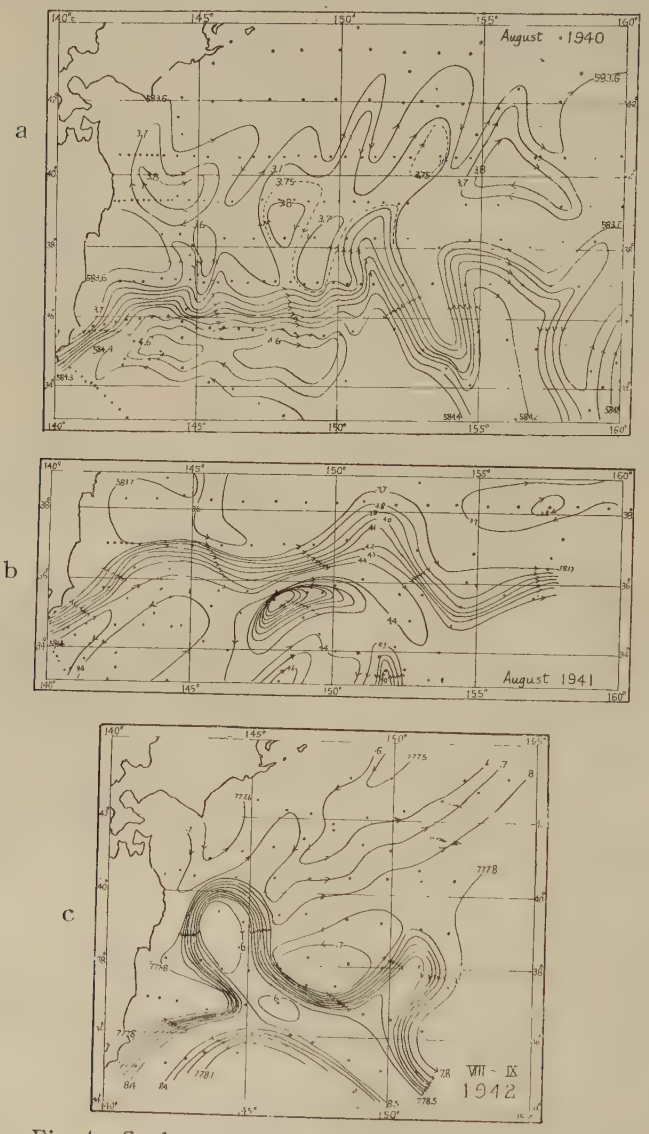

Fig. 4. Surface dynamic topography in the summers of 1940 (a), 1941 (b) and 1942 (c), obtained from the observations under the management of the Hydrographic Department.

branches. As shown in Fig. 4 a, b, however, the relatively systematic observations show that a well-defined current continues as far as 160°E in a remarkable meandering course which is comparable in the wave-length and -amplitude to the meandering in the western inshore region (Fig. 4c). This conspicuous winding course of the main stream at 150°~155°E is found almost in the same area in August of these three years (1940, 1941 and 1942), with decreasing amplitude of meandering and a remarkable variation in the form of the main stream axis.

Branching of the Kuroshio

As seen in the surface dynamic topography in August of 1940 (Fig. 4a), a weak eastward-current continues from 145° to 160°E between 39° and 43°N, following a complicated meandering course. It is originated from the northeast corner of an anticyclonic eddy with the centre at 39°N, 144°E. It is more minutely shown in the surface dynamic topography in the summer of 1954 that such a branch current is originated from the southeast of Hokkaido. The northwestward-current is branched out at 37°N, 144°~145°E from the main stream. Its branching volume transport is about $8\times10^6 m^3$/sec and is only about 20% of the total eastward transport by the main current. In going round a clockwise winding course, it increases to $25\times10^6 m^3$/sec at the Section A (Fig. 5), where about a half of its transport is branching off to the northeastward branching current and the other half is turning back into the clockwise eddy.

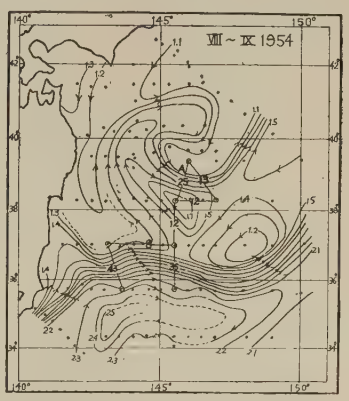

Fig. 5. Surface dynamic topography in the summer of 1954. Thick figures attached to the cross-current section show volume transports ($\times10^6 m^3$/sec).

This branching current and the main stream and a weak countercurrent between these two eastward-flow form the so-called *multiple current* (FUGLISTER 1951) with the Oyashio Current flowing southwestwards. Also in August of 1942 (Fig. 4c), the northward stream generally turns back to the south but a part of it is branched off to the northeast in the neighbourhood of 40°N, 145°E.

§ 3. Sectional Current Profiles

In spite of abundant oceanographical observations, we have had only few knowledges on the exact cross-current structures of the Kuroshio in the

eastern sea of Japan, because most of observational lines were taken almost parallel to the current direction. The Kuroshio in the southern sea of Japan is influenced more or less by the coast, but in the eastern sea it is free from these boundaries in both sides, and so it is expected to show a similarity to the Gulf Stream east off Cape Hatteras (von Arx 1952, Ford and others 1952 a, b and Worthington 1954).

Comparison between calculated and observed velocity profiles

As seen in Fig. 6 showing typically the cross-current distribution of the current-velocity and water mass, the Kuroshio in this sea is such a narrow and stronger current as in the southern sea of Japan or the Gulf Stream,

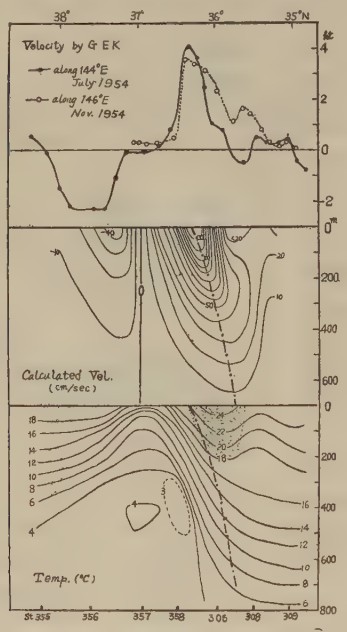

Fig. 6. Cross-current profiles obtained from the observation of the Hydrographic Office in the beginning of July, 1954.

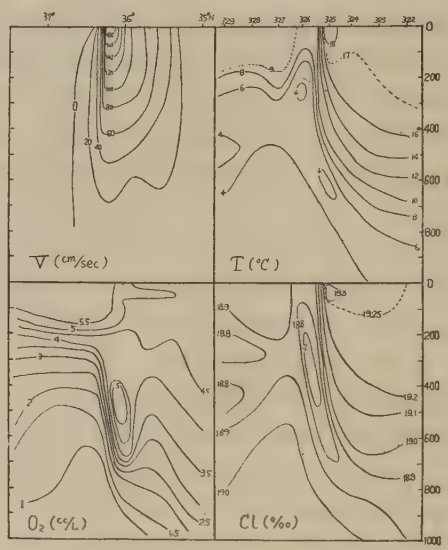

Fig. 7. Vertical distributions of calculated velocity (V), temperature (T), oxygen (O_2) and chlorinity (Cl) in the N-S section along 147°E in February, 1955 (the RYOFU-MARU).

that is, the strongest current (more than 2 knots at the surface) is only about thirty miles wide. The existence of such a narrow, well-defined current is ascertained from the coast to 150°E by recent observations and may be expected to extend even to the east of 150°E. The maximum velocity at the sea surface amounts to 4.2 knots by the Geomagnetic Electrokinetograph (G E K),

but the maximum surface velocity calculated in the interval of about thirty miles is only 2.7 knots relative to the 800 d.b. surface.

In general, such high speeds have not been obtained from the former dynamic calculation based upon the undeep, wide-spaced observations. According to the same data in Fig. 2, we can obtain the following relations among the anomaly of dynamic depth of the 1000, 800 and 600 d.b. surface, and so they mean that the relative velocity to 1000 d.b. is larger, on the average, by about 7% and 16% than those to 800 or 600 d.b. surface respectively.

$$\begin{cases} \Delta D_{1000} = 0.085 + 1.068 \Delta D_{800} \\ \Delta D_{1000} = 0.206 + 1.156 \Delta D_{600} \end{cases}$$

The maximum surface velocity equal to 3.7 knots relative to the 1000 d.b. surface is calculated from the observations obtained in the interval of 20 miles along 147°E in February of 1955 (Fig. 7), but even these observations seem to be too wide to catch an exact peak of the strongest current. As mentioned above, the maximum velocity by the GEK is generally higher than the calculated one, but if the dynamic calculation will be carried out from more deep, close-spaced observations, as shown in three examples of the Gulf Stream (WORTHINGTON 1954), the latter may be almost coincident with the former.

In the vertical distribution of calculated velocity, the stream axis on the sea surface is generally situated at the immediately left (north) (facing downstream) side of the so-called *warm core* in the subsurface layer and it is gradually displaced to the right (south) with the depth as shown in Fig. 6. That is, the warmest (lightest) water mass transported in the upper layer by the Kuroshio Current from the southern region, has an influence upon the density distribution so as to reduce the largest horizontal gradient of density in the deeper layer. It is noteworthy in Fig. 7 that not only this calculated axis on the sea surface coincides with the one obtained by the GEK, but also the surface observed velocity shows a negative (westward) velocity in the right (south) side of the warm core where the upper isentropic surfaces show the inverse inclination to the deeper ones, and so the calculated velocity in the subsurface is smaller than in the mid depth.

It is probably expected from the above comparison of both calculated and observed current velocity that the Kuroshio Current in the eastern sea of Japan is approximately in the geostrophic equilibrium and although the current patterns change considerably rapidly by various external and internal processes, the following geostrophic equilibrium may be soon brought into existence,

so long as the observations are carried out in the interval of several weeks.

Special velocity profiles.

It is often found for the Kuroshio in the southern sea of Japan (MASUZAWA 1954) and the Gulf Stream (HAURWITZ & PANOFSKY 1950, von ARX 1952) that the horizontal shear on either side of the stream axis is such asymmetrical that it is sharper on the left (northern) side of the stream axis than on the right. It seems to be true also in the eastern sea of Japan (Fig. 6, 7) as pointed out in the Gulf Stream by von ARX (1952) that the asymmetry of cross-current velocity distribution is more conspicuous in the section where the curvature of stream axis is cyclonic than in the section where the current-course is convex to the north.

Furthermore, there sometimes exists a narrow cold water zone along the left (north) margin of the Kuroshio Current (Fig. 7, 8). This water mass which is cold, salinity-low and rich in dissolved oxygen, is not the lower

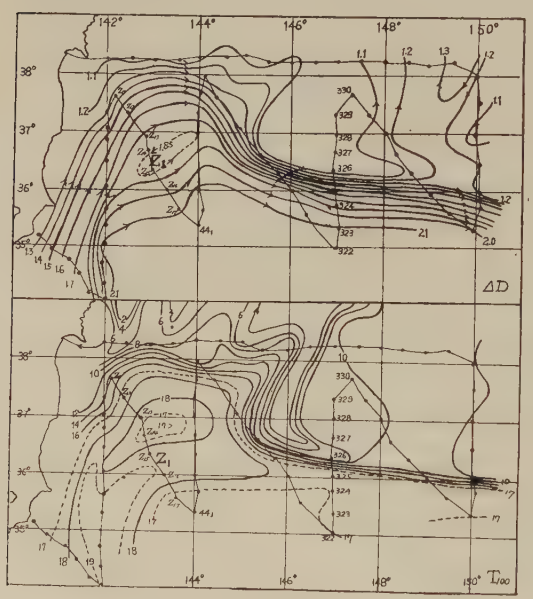

Fig. 8. Surface dynamic topography (ΔD) and water temperature at the 100m layer (T_{100}) in February of 1955 (the RYOFU-MARU)

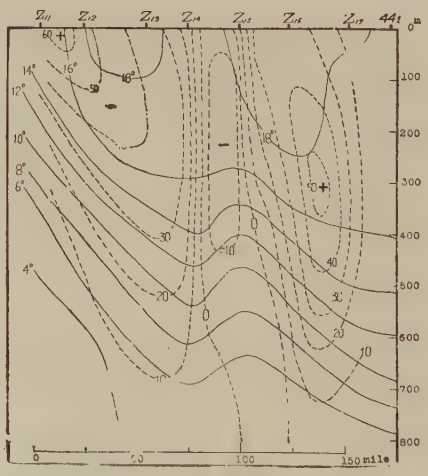

Fig. 9. Vertical distributions of water temperature (full line) and current velocity (broken line) in the section Z_1 in Fig. 8 (the RYOFU-MARU)

water upwelling from the deeper layer of the Kuroshio Water, but the Oyashio or Oyashio undercurrent water draged out by the Kuroshio Current. As pointed

out in the previous papers (MASUZAWA 1952, 1955), those pure subarctic intermediate waters are generally transported with the Kuroshio Current to the east, since such a remarkable salinity-minimum is not found to the south of the Kuroshio main current. Moreover, these cold waters give such an effect as to make the horizontal density gradient sharper in the left (north) edge of the current, and then the Kuroshio Current there becomes more asymmetrical, narrower and higher in velocity.

On the contrary, when the stream axis juts out to the north, especially in the region east off Kwanto District where the Kuroshio leaves the coast of Japan (Fig. 8), the Kuroshio Current is apt to become broader and to be broken into two zones of eastward-flow between which there exists a small cyclonic eddy or a weak current zone (Fig. 8, 9). This branching of the Kuroshio has been unfamiliar to us for the lack of suitable observations, but it may be not so usual phenomena and it may be probably related to the development of a warm eddy to the north of the Kuroshio in the inshore region.

§ 4. Eddies

Warm eddies

As seen in Fig. 4c, 10 and 11a, when the Kuroshio Current takes a remarkable loop-shape course, the region enclosed by this circular current zone is occupied by the warm haline water (K_1) from the surface to the deeper layer. Such a region often becomes an isolated anticyclonic eddy cut off from the main stream. It is pointed out theoretically by ICHIYE (1955) that such a warm eddy isolated in the cold region is to become weak or diffuse rapidly. But most of warm eddies in the inshore region are connected with the main warm water at least in the subsurface layer. For instance, Fig. 12 is such a good example of the warm water mass (K_1) connected with the main warm Kuroshio Water. During this period, however, the connection in the neck of the K_1 water mass is unsettled as seen from the dizzy fluctuations of the water

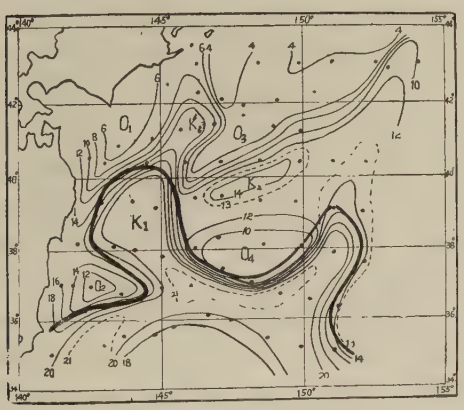

Fig. 10. The mean temperature in the upper 200 m layer in the summer of 1942.

mass distributions in the section east off Cape Kinkazan (38°15′N) and during the period the K_1 water mass changes considerably both its position and form

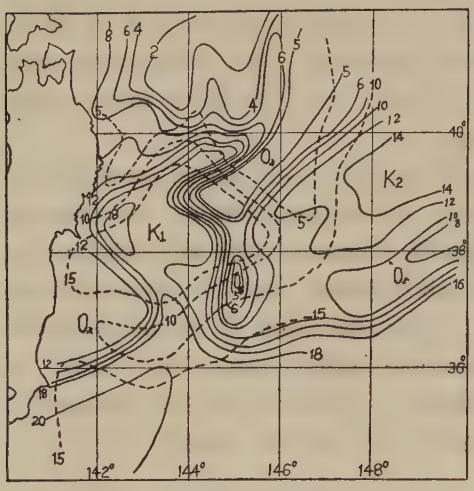

Fig. 11a. The mean temperature in the upper 200 m layer in May~June and February~March (broken line) of 1954.

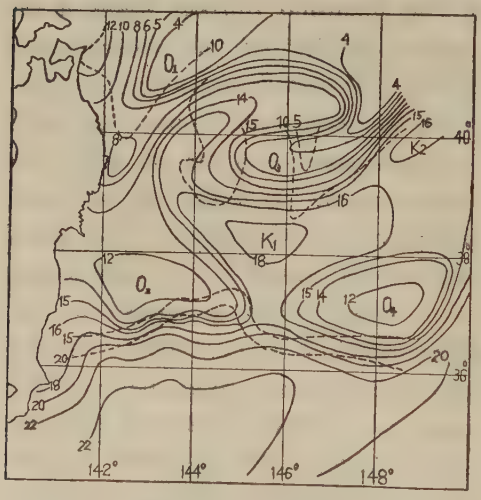

Fig. 11b. The mean temperature in the upper 200 m in August~September (full line) and November (broken line) of 1954.

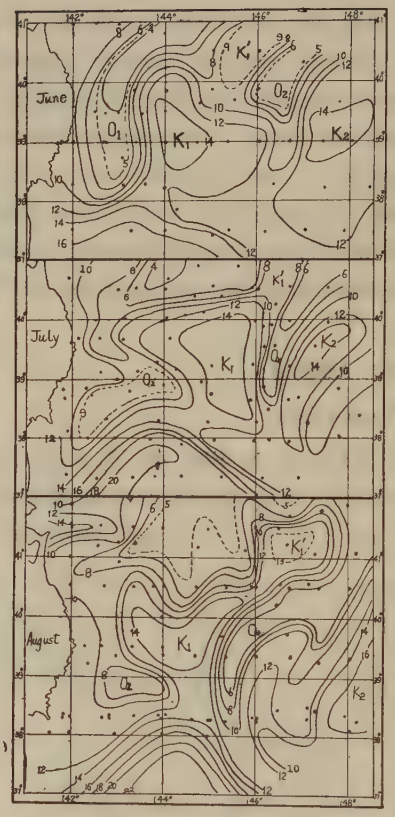

Fig. 12. Mean temperatures in the upper 200 m layer in June, July and August of 1952.

without any significant variations of the mean temperature in the upper 200 m layer. It is sometimes seen in the distribution of water masses in the upper

layer in summer that the K_1 warm water (Fig. 10, 12) spreads more to the northeast (K_1') only in the subsurface layer. In the inshore region of the eastern sea of Japan, the warm eddy with the size of 100 miles or more in diameter seems to be unable to remain completely isolated in the cold region in the period of months. In fact, the remarkable isolated warm eddy (K_1) in March of 1954 connects with the main Kuroshio Current in May and then in summer the connection becomes to be more estranged, and then the warm water mass becomes a complete isolated warm eddy in autumn and furthermore in March of 1955 it is almost vanishing by diffusion.

To the east of the above-mentioned warm water mass exists sometimes a modified warm water mass (K_2 in Fig. 10, 11 and 12). This water mass may be transported principally by the northeastwards-flowing branch of the Kuroshio Current and partly supplied directly from the Kuroshio Water. The boundary between these warm water masses (K_1 or K_1' and K_2) and the cold Oyashio Water corresponds to the Subarctic convergence or Polar front and along this boundary flows a fairly-defined eastward-current which is a member of the so-called multiple currents.

Cold eddies

The cold Oyashio Waters extend to the south usually both along the coast and along the meridian of 145°～146°E at least in the region as far as to 150°E and their terminal portions often end in rather smaller cyclonic cold eddies (0_2, 0_4 in Fig. 10, 11 and 12). Especially, the offshore cyclonic cold eddy along 145°～146°E is colder and lower in salinity, but such a cold water mass is apt to become completely isolated and travell along the northern margin of the Kuroshio Current. The 0_4 water mass in May of 1954 (Fig. 11a) shows the earlier stage of such a cold eddy and the 0_4 water mass in summer may be the modified one in the next stage. Both the 0_4 water mass in the summer of 1942 and the 0_5 water mass in May of 1954 are perhaps more modified ones. By the mixing of these cold water masses (0_4, 0_5) with the warm water masses (K_1, K_2) is produced in the region between the Kuroshio Front and the Oyashio Front, the so-called *mixed water mass* which may be probably correspondent to the *Slope water* in the Gulf Stream System (Ford, 1952).

To the south of the Kuroshio Current exist generally weak anticyclonic warm eddies or countercurrents (Fig. 4a), but sometimes cyclonic cold eddies appear as seen in Fig. 4b. D. Syoji (1951) pointed out that there exists in the late summer of 1933 a similar cyclonic eddy in size and position to the one

shown in Fig. 4b. In the summer of 1939 exist a series of cyclonic eddies far to the south of the Kuroshio Current. These cyclonic cold eddies may be originated from cold trough cut off by the Kuroshio Current as well as the eddy of "Edgar" in the Gulf Stream System on the Operation "Cabot" (FUGLISTER & WORTHINGTON 1951), but we have had hardly any satisfactory observations to see the movement and transformation of the eddy.

§ 5. Seasonal and Other Fluctuations.

(1) *The annual variation of surface water temperature*

The monthly means of surface water temperature are obtained in the mesh of every degree of both latitude and longitude in the region from the coast to 150°E by the Kobe Marine Observatory from observational data of many merchant ships in thirty years from 1911 to 1940. Two zones showing the sharp horizontal gradient of surface temperature can be found in the distributions of both maximum and minimum monthly mean temperature, but the discontinuity at these boundary zones, especially at the southern one, is generally sharper in

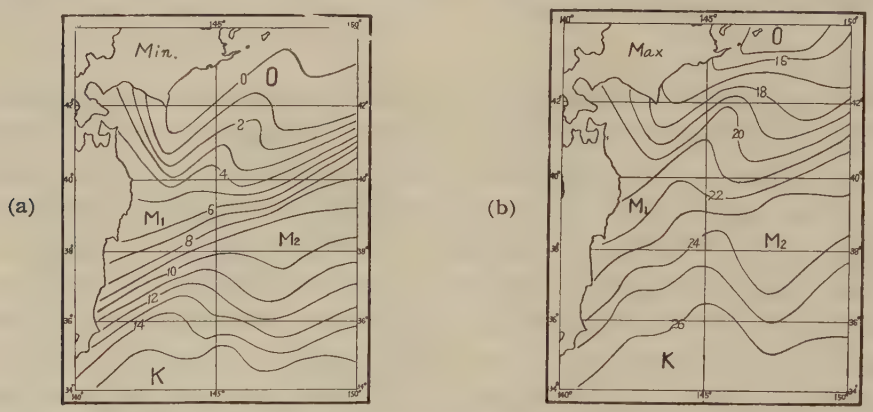

Fig. 13. Distributions of monthly minimum (a) and maximum (b) of surface water temperature

winter than in summer. They divide this sea-region into the Oyashio (O), the Kuroshio (K) and the Mixed (M) Region and furthermore the mixed region is subdivided into the colder western (M_1) and the warmer eastern (M_2) region by another discontinuous zone stretching from Cape Inubo-zaki (36°N, 141°E) to the point of 41°N, 150°E. Furthermore, Fig. 14 shows the seasonal variation of the isotherm of the middle value between the monthly mean temperatures of the representative Kuroshio Water (K) (34°~35°N, 140°~150°E) and

the Oyashio Water (O) (43°～44°N, 145°～150°E) (Table 1, Fig. 14). The middle isotherm in summer is located at the most northern latitude, especially in the western mixed region (M_1). This fact means that so far as the surface temperature is concerned, the western mixed region is more influenced in summer by the Kuroshio Water spreading northwards but less in winter, while the sea surface of the eastern mixed region is more frequently covered by the Kuroshio Water all the year round.

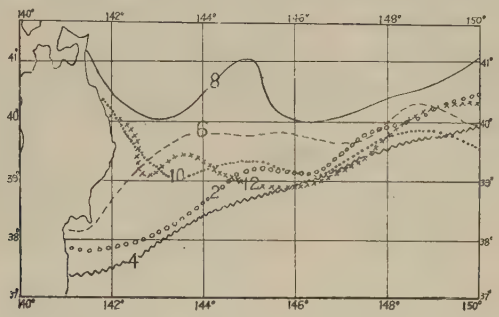

Fig. 14. Seasonal fluctuation of the isotherm of the middle temperature between the Kuroshio and the Oyashio. Figure: Month

Table 1

	Jan.	Feb.	Mar.	Apr.	May	June	July	Aug.	Sep.	Oct.	Nov.	Dec.
Kuroshio (K)	16.0	15.3	15.5	16.8	18.4	21.1	24.4	26.8	25.7	23.2	20.7	18.0
Oyashio (O)	0.5	−0.3	0.6	1.6	3.5	7.2	11.2	14.9	14.8	11.6	7.2	3.3
Mean	8.2	7.5	8.0	9.2	11.0	14.2	17.8	20.8	20.2	17.4	14.0	10.6
Difference	15.5	15.6	14.9	15.2	14.9	13.9	13.2	11.9	10.9	11.6	13.5	14.7

Next, the author intends to account for the seasonal variation of the surface temperature from the results of the harmonic analysis $\theta=\theta_0+\theta_1 \sin(\omega t+\varphi)$. The large horizontal gradient zone of the annual mean (θ_0) stretches from SW to NE across this region, and it is approximately coincident with the 15°—isoline of the annual range ($2\theta_1$). In the northwestern side of this zone, the annual range is more than 15° and shows the maximum (>18°) at the southern edge of the Oyashio Water to the south of Cape Erimo-misaki, Hokkaido, while in the southeastern side it is less than 15° and is only 10°～12° in the Kuroshio water region. And also the distribution of the phase angle (φ) shows characteristically to what direction the Kuroshio Water extends, namely, the

larger values of φ, in other words, the earlier occurence of the maximum and minimum temperature, is found in two zones stretching from Cape Inubo-zaki to the ENE and to the NE.

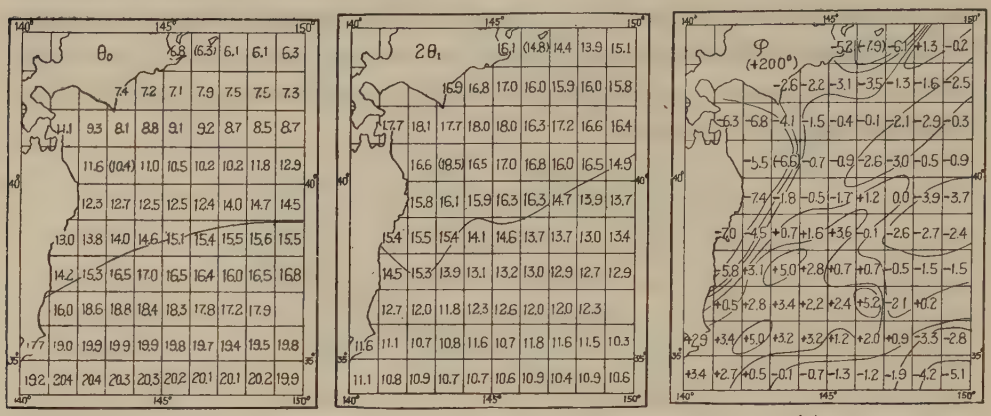

Fig. 15. Distributions of annual mean (θ_0), annual range ($2\theta_1$) and phase angle (φ) of surface water temperature.

Well then, in order to know how much the surface temperature of the Kuroshio Water flowing into this sea region changes by mixing and heat exchange between sea and atmosphere, each term of the right hand of the next equation $d\theta/dt=\partial\theta/\partial t+U\partial\theta/\partial x$ is calculated from the distribution of monthly mean temperature on the line stretching from the point of 35°N, 142°E to the eastnortheast or northeast. The local time change of surface temperature ($\partial\theta/\partial t$) is maximum (about ±0.1° per day) in early summer and later autumn. If the general current speed (U) to ENE or NE (x-direction) is assumed as probable values, as shown in Fig. 16, the Kuroshio Water in this region loses the heat beyond the effective solar radiation by mixing, evaporation and other processes even in summer. But, as expected generally, the net heat loss of the Kuroshio Water is least in summer and most in winter, and the individual time change of surface temperature ($d\theta/dt$) to the NE-direction shows about twofold values of that to the ENE.

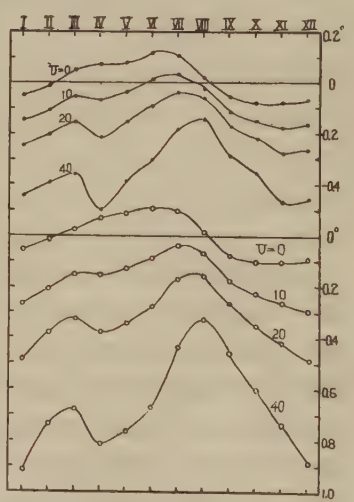

Fig. 16. Seasonal variations of $d\theta/dt$ (°C per day) U: mile per day. ENE: upper. NE: lower.

(2) *Seasonal fluctuations of the warm water east off Cape Kinkazan.*

The present author reported in the previous paper (MASUZAWA 1954) general features on the seasonal variation of the warm water in the section east off Cape Kinkazan from the monthly mean temperature and chlorinity obtained in the period from 1948 to 1953. The warm water masses are apt to appear at two positions of this section and the upper mean temperature of the western warm water shows a remarkable seasonal variation different from the

Table 2. Seasonal variations of the mean temperature (left) in the upper 200 m layer and its varience (right) in the section (C-line) east off Cape Kinkazan (35°15′N). (°C)

Long.	142° ~ 144°	~ 146°	~ 148°	~ 150°	~ 152°	142° ~ 144°	~ 146°	~ 148°	~ 150°	~ 152°E
Jan.	10.30	11.53	11.38	11.12	11.02	10.43	18.74	2.14	2.10	4.35
Feb.	6.61	9.86	10.13	10.66	11.60	4.12	16.15	6.63	5.81	0.50
Mar.	7.16	10.03	10.49	10.96	10.40	11.12	14.24	4.29	1.71	1.47
Apr.	6.68	8.76	9.05	11.33	10.68	8.26	13.58	0.42	8.51	0.60
May	7.66	10.25	9.35	12.05	12.32	9.68	8.43	8.25	6.17	6.08
June	9.28	10.92	11.77	13.14	11.12	3.32	8.73	7.96	4.10	9.36
July	9.90	9.43	12.69	13.98	13.62	10.28	9.43	9.94	4.96	6.50
Aug.	11.25	12.83	12.48	14.38	12.87	8.54	8.86	8.44	4.55	4.11
Sep.	10.08	13.06	14.62	14.15	14.03	6.06	4.30	10.31	5.39	2.25
Oct.	11.67	13.54	14.25	13.75	13.60	6.39	8.12	3.24	2.57	1.35
Nov.	12.25	14.54	13.79	13.69	14.40	4.52	11.19	3.35	1.06	0.11
Dec.	9.75	15.81	13.31	12.26	13.90	4.16	17.96	8.09	2.20	0.97

well-known seasonal variation of the surface water temperature. That is, as shown in Table 2, the upper mean temperature of the western inshore warm water in autumn to early winter is almost equal to or rather higher than the eastern offshore warm water in summer. Furthermore, the western half of this section, especially the western warm region (144°~146°E) shows the maximum varience of the mean upper temperature in a colder half of year (November to April), while in the western warm region (near 148°E) the monthly upper mean temperature is relatively uniform.

The distribution of water masses in this section is complicated and variable owing to the existence of the frontal zone near this section, the sectional area occupied by the warm water in this section, especially in the western half, shows such a fairly regular seasonal variation that it generally increases gradually from February or March to December or January but decreases rapidly from winter to spring. On the other hand, as seen in the seasonal variation of the surface area (A_k in Fig. 17) showing the temperature more than

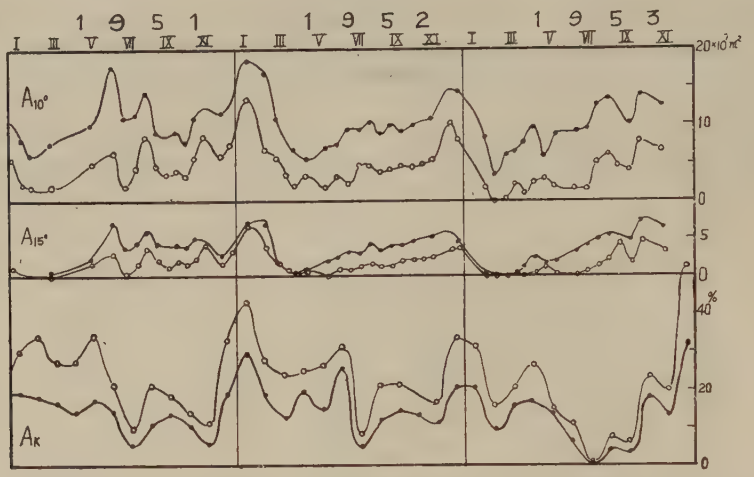

Fig. 17. Seasonal fluctuations of the sectional area more than 10° (A_{10}) and 15° (A_{15}) in the section east off Kinkazan and the ratio of horizontal area (A_k) occupied by the Kuroshio water on the surface of the sea region (35°~43°N, 140°~150°E).

the monthly mean temperature of the representative Kuroshio (Table 1), it is maximum generally also in winter. On the contrary, as shown in Fig. 14, the isotherm of the middle surface temperature between the Kuroshio and the Oyashio moves to the north in summer and to the south in early spring. Therefore, we may obtain a probable idea on the seasonal fluctuation of the distribution of the Kuroshio warm water. That is, the Kuroshio warm water itself extends farthest to the north in the inshore region from the coast to 146°E in winter and so often appears conspicuously in the section east off Cape Kinkazan and forms the sharp boundary with the original Oyashio Water, while in summer it is inclined to extend often to the southeast of Hokkaido only in the upper thin layer of the inshore region.

(3) *Fluctuations of the stream axis.*

The position of the stream axis of the Kuroshio seems to be considerably variable according to a few recent suitable observations.

In 1953, the inshore northern region of the eastern sea of Japan was abnormally covered by the cold Oyashio Water before early summer, and the

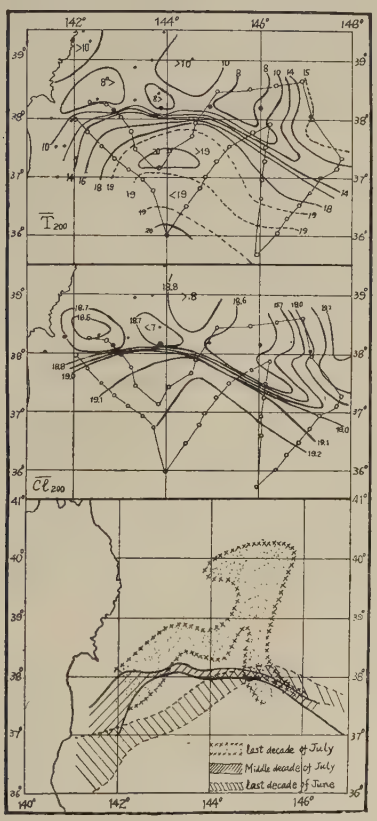

Fig. 18. Distributions of mean temperature ($\overline{T}_{200}$) and chlorinity ($\overline{Cl}_{200}$) in the upper 200 m layer in the middle decade of July of 1953 (the SOYO-MARU) and its fluctuation of the boundary ($\overline{T}_{200}=10°\sim15°$) of water masses (lower).

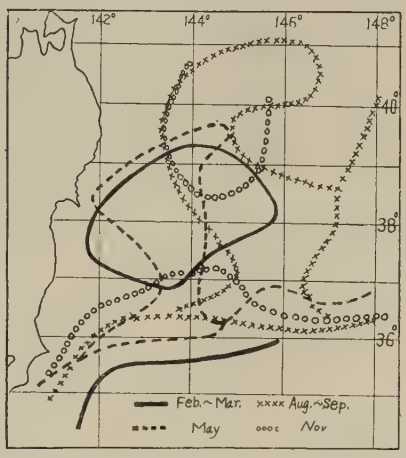

Fig. 19. Fluctuations of the stream axis of the stronger current in 1954.

Kuroshio Water contacted immediately with this cold water in a sharp frontal zone at about 38°N (Fig. 18). This frontal zone seems to move generally northwards at the rate of several miles or more per day from June to July. In the neighbourhood of 38°N, 145°E, the current-direction changed at right

angle from the west-east direction to the north-south direction and the upper warm water extends to the north in 144°~146°E in the period between the middle and last decades of July. These changes are comparable to some results obtained in the Gulf Stream (FUGLISTER & WORTHINGTON 1951, FORD and others 1952 a, b).

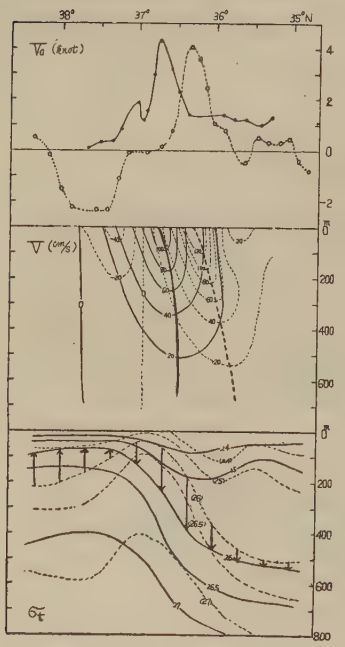

Fig. 20. The variation of cross-current profiles of observed (V_0) and calculated (V) velocity and potential density (σ_t) during the period from the beginning of July to the beginning of August in 1954 (observed by the Hydrographic Office).

In 1954, according to the observations on board the R.M.S. RYOFU-MARU, the main stream of the Kuroshio Current moves gradually to the north in the inshore region from the coast to 146°E, especially at 143°~145°E its change is about a hundred miles during about eight months from March to November (Fig. 19). But if we compare two cross-current sections along the meridian 144°E carried out in the beginning of both July and August, the surface stream-axis observed by the GEK moves northwards by about 25 miles in this period. In accordance with its change, its calculated velocity profile also change in almost parallel from surface to the deeper layer. This horizontal movement of the stream-axis is correspondant to an upwelling equal to about 200 meters or so in a month (on the average the order of 10^{-2} cm/sec) in the mid depth (Fig. 20). These values of the rate of change are only a sort of average values during several weeks. But the actual change of the stream axis may be occurred in the higher speed (ten miles or more per day) as obtained in the Gulf Stream (FUGLISTER & WORTHINGTON 1951). Therefore, such a speedy change may not continue monotonously in several weeks, but occur intermittently or oscilatorily.

Aknowledgements

The author wishes his hearty thanks to Prof. K. HIDAKA for his continuous encouragement and to Mr. Y. FUJII and Dr. T. ICHIYE for their kind advices and suggestions through this investigation and also Messrs. M. YASUI, T. TSUCHIDA, and T. NAKAI for their asistances.

References

FORD, W. L., J. R. LONGARD and R. E. BANKS (1952a): On the Nature, Occurrence and Origin of Cold Low Salinity Water Along the Edge of the Gulf Stream. *Jour. Mar. Res.* **11** (3).

FORD, W. L. and A. R. MILLER (1952b): The Surface Layer of the Gulf Stream and Adjacent Waters. *Jour. Mar. Res.* **11** (3).

FUGLISTER, F. C. (1951): Multiple Currents in the Gulf Stream System. *Tellus* **3** (4).

FUGLISTER, F. C. and L. V. WORTHINGTON (1951): Some Results of a Multiple Ship Survey of the Gulf Stream. *Tellus* **3** (1).

FUKUOKA, J. (1955): The Variation of the Polar Front in the Sea Adjacent to Japan. *Ocean. Mag.* **6** (4).

HANZAWA, M. (1952): On Some Examples of Abrupt Change of Oceanographical Conditions at the Ocean Weather Station 'Extra' Adjacent to the Oceanic Polar Front. *Ocean. Mag.* **4** (3).

HAURWITZ, B. and H. A. PANOFSKY (1950): Stability and Meandering of the Gulf Stream. *Trans. Amer. Geophy. Uni.* **31** (5).

ICHIYE, T. (1953): On the Variation of Oceanic Calculation (IV). *Ocean. Mag.* **5** (1).

ICHIYE, T. (1955): On the Variation of Oceanic Circulation (VIII). (*to be published*).

KAWAI, H. (1953): On the Relation between the Bad Rice-crop in Northeast Japan and the Fluctuation of the Oceanic Polar Front in the Northeastern Sea of Japan. (*not printed*).

KAWAI, H. (1954): Oceanographical Observations Following the Kuroshio in the Eastern Sea of Japan. (*not printed*).

MASUZAWA, J. (1952): On the Intermediate Water in the Northeastern Sea of Japan (II) (in Japanese). *Ocean. Rep. of C. M. O.* **2** (1).

MASUZAWA, J. (1954a): On the Kuroshio South off Shiono-misaki of Japan. *Ocean. Mag.* **6** (1).

MASUZAWA, J. (1954b): On the Seasonal Fluctuation of the Kuroshio East off Kinkazan. (in Japanese). *Ocean. Rep. of C. M. O.* **3** (4).

MASUZAWA, J. (1955): Preliminary Report on the Kuroshio in the Eastern Sea of Japan. *Records Oceanogr. Works Japan.* N. S. **2** (1).

NAN'NITI, T. (1951): On the Fluctuation of the Kuroshio and the Oyashio. *Pap. Met. Geophys.* **2** (1).

SAITO, Y. (1952): On the Oyashio Current. (Part I). *Jour. Inst. Polytechnic Osaka City Univ.* **3** (2).

SHOJI, D. (1951): Variations of Ocean Currents in the Adjacent Sea of Japan. (in Japanese). *Hydrographic Bulletin of Maritime Safety Agency.* **25**.

SUDA, K. (1936): On the Dissipation of Energy in the Density Current (2nd Paper). *Geophys. Mag.* **10** (2).

UDA, M. (1935a): The Results of Simlutaneous Oceanographical Investigations in the North Pacific Ocean Adjacent to Japan Made in August, 1933 (in Japanese). *Jour. Imp. Fish. Expt. St.* No. **6**.

UDA, M. (1935b): On the Distribution, Origin and Movement of the Dichothermal Water in the Neighbouring Sea of Japan (in Japanese). *Umi to Sora* **15** (2).

UDA, M. (1938a): Hydrographical Fluctuation in the Northeastern Sea-region Adjacent to Japan of the North Pacific Ocean (in Japanese). *Jour. Imp. Fish. Expt. St.* No. **9**.

UDA, M. (1938b): Researches on "Siome" or Current Rip in the Seas and Oceans.

Geophys. Mag. **11** (4).

UDA, M. (1h43) : On the Structure of the Boundary Zone of Different Water Masses (in Japanese). *Jour. Oceanogr. Soc. Japan.* **2** (4).

von ARX, W. S. (1952) : Notes on the Surface Velocity Profile and Horizontal Shear Across the Width of the Gulf Stream. *Tellus* **4** (3).

WORTHINGTON, L. V. (1954) : Three Detailed Cross-sections of the Gulf Stream. *Tellus* **6** (2).

551.465

A Short Note on the Vertical Current in the Ocean

By

Takashi ICHIYE

C.M.O. Oceanographical Section

§1. The upwelling in the ocean is the important problem in oceanography, and many researches have been carried out from both theoretical and practical standpoints of view. Here the author presented one approach to this problem, discussing the vertical motion by taking the simple assumption that the ocean currents are maintained only by the effects of wind stress and density stratification under the vertical mixing process. The fundamental equations of motion are given as usual by

$$-\lambda v=-\frac{1}{\rho}\frac{\partial p}{\partial x}+\nu\frac{\partial^2 u}{\partial z^2}, \qquad \lambda u=-\frac{1}{\rho}\frac{\partial p}{\partial y}+\nu\frac{\partial^2 v}{\partial z^2}. \tag{1}$$

In other words we treat the case of the motion in the region far from the coast, since the effect of the horizontal eddy viscosity should predominate above the effects of vertical mixing and wind stress only near the coast.

When we take the boundary conditions as

$$\rho\nu\frac{\partial u}{\partial z}=-T_x, \qquad \rho\nu\frac{\partial v}{\partial z}=-T_y \quad (\text{at } z=0, \text{ surface}),$$

$$\frac{\partial u}{\partial z}=\frac{\partial v}{\partial z}=0 \quad (\text{at } z=\infty),$$

and further we assume that the pressure distribution satisfies the conditions

$$\frac{\partial^2}{\partial x\partial z}p=\frac{\partial^2}{\partial y\partial z}p=0 \quad (\text{at } z=0, \text{ and } z=\infty),$$

we can obtain the solutions of (1) by simple computation. The part of the solutions concerning only to the wind effect is given by the usual theory of Ekman. The current due to the pressure gradient u_g, v_g is also computed formally, but the explicit form is somewhat complicated when we take into account of the eddy viscosity. However, if we assume that the effect of the eddy viscosity is negligible for the components u_g and v_g under the condition $\frac{\partial}{\partial z}\,grad\,p=0$ at $z=0$, then we have $u_g=\frac{1}{\rho\lambda}\frac{\partial p}{\partial y}$, $v_g=-\frac{1}{\rho\lambda}\frac{\partial p}{\partial x}$. The vertical current w_z at any depth z is obtained from the equation of continuity as $-\rho w_z=\int_0^z\left(\frac{\partial\rho u}{\partial x}+\frac{\partial\rho v}{\partial y}\right)dz$, where we put $w=0$ at the surface $z=0$. Then, we have

$$-\rho w_z=-g\frac{\beta}{\lambda^2}\int_0^z\frac{\partial p}{\partial x}\,dz$$
$$+\frac{1}{\lambda}\left\{(1-e^{-mz}\cos mz)\left(\frac{\partial T_y}{\partial x}-\frac{\partial T_x}{\partial y}\right)+e^{-mz}\sin mz\left(\frac{\partial T_x}{\partial x}+\frac{\partial T_y}{\partial y}\right)\right\}$$
$$+\frac{\beta}{\lambda^2}\{T_x(1-e^{-mz}\cos mz)-T_y e^{-mz}\cos mz\}$$
$$+\frac{1}{2}\frac{\beta}{\lambda^2}mz e^{-mz}\{T_y(\cos mz-1)-T_x(\sin mz+1)\}, \qquad (2)$$

where x and y are the east and north coordinates, respectively and $m=\sqrt{\lambda/2\nu}$, $\beta=\partial\lambda/\partial y$. The first term of the equation (2) means the effect of βv_g, the second term the effect of the rotation and divergence of the wind stress, the third term the effect of the north-south component of the wind current corresponding to βv_g and the fourth term the effect of the change of the depth of the frictional influence $D=\pi/m$ with latitude. All these terms are of the same order in the upper layer above D, except the case for the small scale changes of the wind stresses is considered. The estimation of the first term is possible only when the density distribution is known, thus here we estimate only the terms concerned with the wind stress. For simplicity, we take a circular wind system corresponding to the semi-permanent cyclones or anticyclones over the ocean, such as $T_\theta=T_0\left(\frac{r}{a}\right)e^{-r/a}$, then the second term is proportional to $T_\theta(2a/r-1)/a\lambda$, and the third and the fourth terms to $\beta T_\theta/\lambda^2$. Therefore the ratio of these two factors at $r=a$ is given by $\lambda/\beta\alpha$, which has the value as tabulated below :

Lat.	10°	20°	30°	40°	50°	
$\lambda/\beta a$	1.12	1.86	3.68	5.32	7.54	($a=10^3$ km)

Thus, we cannot neglect the effect of the third and the fourth terms, so long as we take the large scale phenomena in low and middle latitudes in question. At great depths the term with a factor e^{-mz} almost vanishes, but the terms $\frac{1}{\lambda}\left(\frac{\partial T_y}{\partial x}-\frac{\partial T_x}{\partial y}\right)+\frac{\beta}{\lambda^2}T_x$ remain finite and the pressure gradient should balance with these terms, which results in the vanishing of the vertical current and the divergence of the mass transport. On the other hand, we can compute the vertical velocity if the wind stresses only are kn wn, with the conditions that the total mass transport is free of divergence and that the density distribution is known.

§ 2. For the practical application of the equation (2), we should know the density distributions besides the wind stresses, but when we assume suitable vertical structures of the density, we can compute the vertical motion by the

equation (2). For this purpose we take the model after R. O. Reid,[1] such as

$$\rho=\rho_0,\ \text{at}\ -\zeta<z<h,\qquad \rho=\rho_a-\Delta\rho e^{1-z/h}\ \text{at}\ z>h\quad(\Delta\rho=\rho_a-\rho_0),\tag{3}$$

then we can estimate the approximation that the current components u_g and v_g are given by the geostrophic current under the effect of the eddy viscosity. First, in the upper homogeneous layer $-\zeta<z<h$ we have exactly

$$u_g=-\frac{1}{\lambda}\frac{\partial p}{\partial y}=-\frac{g}{\lambda}\frac{\partial\zeta}{\partial y},\qquad v_g=\frac{1}{\lambda}\frac{\partial p}{\partial x}=\frac{g}{\lambda}\frac{\partial\zeta}{\partial x}.$$

At the layer below $z=h$ the pressure gradient varies with z, thus we have

$$\begin{aligned}u_g+iv_g&=\frac{h^2g\Delta\rho}{\rho\nu(1-h^2\lambda i/\nu)}\left(1+\frac{2}{1-h^2\lambda i/\nu}+\frac{z}{h}\right)\left(\frac{\partial h}{\partial x}+\frac{\partial h}{\partial y}i\right)\\&=\frac{1}{\lambda}\left(-\frac{\partial p}{\partial y}+\frac{\partial p}{\partial x}i\right)\left\{1+\frac{2}{(1-h^2\lambda i/\nu)(1+z/h)}\right\}\Big/(1+\nu i/h^2\lambda),\end{aligned}\tag{4}$$

under the condition that the eddy viscosity is constant and the value of ρ in the numerator is approximately given by the mean value between ρ_0 and ρ_a. When h or the depth of the homogeneous layer is sufficiently larger than the depth of the frictional influence, we can put $u_g+iv_g=\frac{1}{\lambda}\left(\frac{\partial p}{\partial x}i-\frac{\partial p}{\partial y}\right)$ as in the exact solution within the upper layer. In the practical case the value of eddy viscosity is somewhat fictituous and it is not so unreasonable to assume that the eddy viscosity is only effective above $z>h$. From the condition that the divergence of the mass transport vanishes at $z=\infty$, we have the relation

$$\frac{\beta}{\lambda}\left(g\int_0^\infty\frac{\partial\rho}{\partial x}\,dz-T_x\right)=\frac{\partial T_y}{\partial x}-\frac{\partial T_x}{\partial y},$$

and from the density distribution expressed by (3) and under the condition that $grad\,p=0$ at $z=\infty$, we have relation between the depth h and the wind stress distribution such as

$$h^2=\frac{2}{5g\Delta\rho}\int^x\left\{T_x+\frac{\lambda}{\beta}\left(\frac{\partial T_y}{\partial x}-\frac{\partial T_x}{\partial y}\right)\right\}dx.\tag{5}$$

Further the equation (2) becomes

$$\begin{aligned}-w_z=&\frac{1}{5}\left\{\frac{\beta}{\lambda^2}T_x+\frac{1}{\lambda}\left(\frac{\partial T_y}{\partial x}-\frac{\partial T_x}{\partial y}\right)\right\}\left(2+\frac{z}{h}\right)e^{1-z/h}\\&+\frac{1}{\lambda}e^{-mz}\left\{\sin mz\left(\frac{\partial T_x}{\partial x}+\frac{\partial T_y}{\partial y}\right)-\cos mz\left(\frac{\partial T_y}{\partial x}-\frac{\partial T_x}{\partial y}\right)\right\}\\&-\frac{\beta}{\lambda^2}e^{-mz}(T_x\cos mz+T_y\sin mz)\\&+\frac{1}{2}\frac{\beta}{\lambda^2}mze^{-mz}\{(\cos mz-1)T_y-(1+\sin mz)T_x\},\end{aligned}\tag{6}$$

for $z>h$, under the above conditions. On the other hand, the equation (2)

can be used for the depth range $-\zeta<z<h$, only by substituting $\rho g\frac{\partial\zeta}{\partial x}$ and $\rho g\frac{\partial\zeta}{\partial y}$ in $\frac{\partial p}{\partial x}$ and $\frac{\partial p}{\partial y}$, respectively, where the relation between h and ζ is given by $\zeta=2\Delta\rho\cdot h/\rho_0$. In short, we can compute the vertical current $-w_z$ for $-\zeta<z<h$ from the equation (2), and for $z>h$ from (6), if only T_x and T_y are known and the values of h are obtained from the equation (5) with given values of h along any meridian.

§ 3. As an example of such calculation, we apply the above relations to obtain the vertical motion in the equatorial region, by use of the analytic results of R. O. Ried. His empirical relations of the wind stresses in this region are given by[1]

$$T_x=T_0+b\sin\omega(\phi-\phi_0),\qquad T_y=0,$$

where

$$T_0=-0.3,\qquad b=0.3\ \text{(c.g.s.)},\qquad \omega=13.85,$$
$$\phi_0=1^\circ\ (\phi\ \text{in degrees of latitude}).$$

Further the equation of h in (5) is also given by[1]

$$h^2=\frac{(x-x_0)^2}{5g\Delta\rho}\{T_0+b\sin\omega(\phi-\phi)$$
$$-\omega b\tan\phi\cos\omega(\phi-\phi_0)\},$$

with

$$\Delta\rho=4.4\times10^{-3},\qquad K=3.8\times10^8\ \text{(c.g.s.)}$$

Then we compute $-w_z$ along the meridian W. 150°, which corresponds to the Carnegie Section approximately, by the procedure discussed in the last section. For the values of ν we take three cases of $\nu=0$, 100 and 1000 (c.g.s.), where the first case corresponds to the current only of the gradient components, in which the wind stresses are effective for the redistribution of the density structures, and the third value of ν seems to be somewhat larger than the usual estimation, thus the results of the calculation are shown only for the purpose of the comparison with the other cases. The meridional distributions of $-w_z$ at several depths are shown in Fig. 1, with the boundaries of the equatorial counter currents in this area determined theoretically by Reid.[2] From these curves we can see that below the depth of 100 m the vertical currents

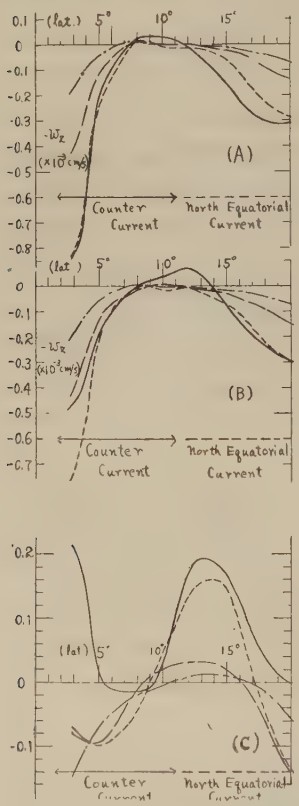

Fig. 1. The distributions of vertical velocity ($\times10^{-3}$ cm/sec) at different depths. (Positive values mean upwards motion. —— 50 m. - - - - 100 m. – – – 200 m. -·-·- 300 m.) (A) $\nu=0$. (B) $\nu=10^2$ c.g.s. (C) $\nu=10^3$ c.g.s.

are similar for the eddy viscosity 0 and 100 (c.g.s.), except near the equator, indicating that the vertical currents are determined simply from the pressure gradient term in the equations (2) and (6) for the reasonable values of the eddy viscosity. The curves for $\nu=1000$ show the large disagreement with others, especially at 50 m and 100 m layers, with deviation to the positive values. When we consider that the cases for $\nu<100$ correspond to the practical conditions in the ocean, we can see that the strong sinking motion occurs near the southern boundary of the Counter Current and in the northern section of the North Equatorial Current from these curves, which corresponds to the generally accepted convergence zone in the region.[3] As for the divergence zone at the northern boundary of the Counter Current, the computed velocity indicates weak upwelling, though limited only above 50 m ($\nu<100$) or 100 m layer ($\nu<1000$). In Fig. 2, we plot the vertical distributions of $-w_z$ at several latitudes. Generally speaking, the absolute values $|w_z|$ are maximum at the

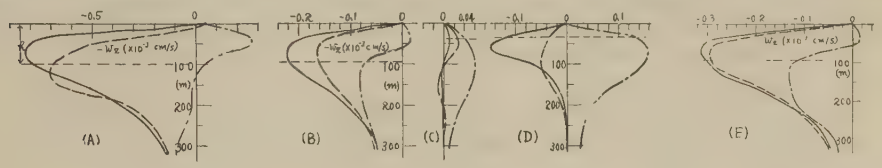

Fig. 2. Vertical distributions of vertical velocity ($\times 10^3$ cm/sec) at different latituds.
(—— $\nu=0$ - - - $\nu=10^2$ c.g.s. -·-·- $\nu=10^3$ c.g.s.
The depth of h is indicated by the broken line.)
A=3° B=5° C=10° D=15° E=20° (lat.)

depth between 50 m and 100 m, corresponding approximately to h or D, and further the increasing values of ν are apt to cause the upwelling motion, or to increase $-w_z$ algebraically, that is a matter of course, since the contributions of the drift current in the equation (6) become

$$\frac{1}{\lambda R}e^{-mz}\left\{b\omega\cos mz\cos\omega(\phi-\phi_0)-\tan\phi\cdot T_x\left(\cos mz+\frac{1}{2}mz+\frac{1}{2}mz\sin mz\right)\right\},$$

where R=radius of the earth
and $\cos\omega(\phi-\phi_0)>0$ for $\phi<13°$ and $T_x<0$ for all latitudes under consideration, and the above term increases with the increasing value of ν for the given depth above the layer of the frictional influence.

The present estimation is only tentative, because the values of the eddy viscosity are not determined definitely and the wind stress distribution is also given by rough estimation. However, the order of the vertical velocity and the domains of the sinking and upwelling motion agree well with the general

conception, which suggests that the present methods is useful for the computation of the vertical velocity simply from the wind data, and its usefulness may be promoted with the more adequate and exact estimation of the eddy viscosity and the wind stresses.

In other words, it seems to suggest that the current system in the large scale is only governed by the wind effect and the density stratification induced by the wind, and the effect of the lateral mixing and other complicated process are negligible in the open ocean.

In the last the author expresses his hearty thanks to Mr. Y. Fujii and Dr. K. Yoshida for many useful suggestions and discussions. Further he is indebted to Dr. K. Hidaka for the constant encouragements.

Literatures

(1) R. O. Reid: A model of the vertical structure of mass in equatorial wind driven currents of a baroclinic ocean. *Journ. Mar. Res.* Vol. VII, No. 3, 1949.
(2) R. O. Reid: The equatorial currents of the eastern Pacific as maintained by the stress of the wind. *Journ. Mar. Res.* Vol. VII, No. 2, 1948.
(3) Sverdrup *et al*: The Oceans.
(4) K. Yoshida, H-L. Mao and P. L. Horrer: Circulation in the upper mixed layer of the equatorial north Pacific. *Journ. Mar. Res.* Vol. XII, No. 1, 1953.

On the Friction in the Tidal Current

By

Takashi ICHIYE

C. M. O. Oceanographical Section

§1. The friction of the tidal currents has been determined by the various authors since 1918[1][2][3], and the results have been applied to the several problems. Here the present author has discussed the problem by use of the

Table 1. Harmonic Components of Tidal Currents at Each Station (Time origin of analysis is taken at the upper transit of the moon, $u=\Sigma U_n \cos(n\sigma t-\mu_n)$, $v=\Sigma V_n \cdot \cos(n\sigma t-\nu_n)$ U, V in cm/sec, μ, ν in degrees. $n=1$, Diurnal, $n=2$, Semi-diurnal)

Moon Age	Up. Transit	Obs. Depth (m)	N—Comp.					E—Comp.					Interval of Obs.
			U_0	U_1	μ_1	U_2	μ_2	V_0	V_1	ν_1	V_2	ν_2	
1.	III. 1.	0	3.6	16.5	257.3	5.1	249.7	2.2	12.4	267.0	2.3	230.4	II. 28.
15. 1	0h 03m	2	−0.1	8.3	251.5	4.0	241.3	3.4	9.2	251.0	4.5	134.6	12h
		4	−1.7	2.7	261.1	5.3	234.3	1.6	7.1	264.1	7.1	198.0	～
		5	−0.5	0.8	275.1	4.0	221.8	0.5	4.1	269.9	9.4	192.8	III. 1.
		6	−1.4	2.2	60.1	4.2	202.3	−0.2	3.1	242.6	7.9	181.2	13h
2.	III. 2.	0	−1.8	9.3	134.3	15.4	206.3	−4.6	13.0	142.6	17.7	199.4	III. 1.
16. 1	0h 42m	2	−3.7	6.2	150.6	16.0	211.1	−0.9	8.2	132.1	16.4	218.2	13h 40m
		4	−3.3	5.9	121.9	9.1	230.4	−2.5	8.8	112.7	11.3	216.7	～
		5	−0.1	1.6	199.4	12.0	221.6	0.3	2.7	122.3	14.5	215.5	III. 2.
		6.5	−1.1	1.0	166.2	8.4	210.3	0.3	1.6	110.6	12.1	209.4	15h
3.	III. 4.	0	−9.8	10.5	128.4	13.9	188.4	8.8	11.2	202.1	11.3	222.6	III. 3. 8h
18. 1	2h 02m	2	−5.9	5.7	125.5	17.6	210.8	2.9	5.4	155.5	13.0	205.3	～
		4	−0.7	4.7	130.1	20.2	199.5	−1.2	3.1	95.2	12.8	200.3	III. 4. 9h
		5	2.1	2.8	173.4	16.1	209.5	−1.1	0.3	203.3	10.1	203.2	
4.	III. 5.	0	2.5	10.6	329.2	5.3	324.5	−13.2	8.5	54.7	18.3	186.2	III. 4.
19. 1	2h 44m	2	4.2	7.6	354.7	7.4	307.3	−11.0	7.5	39.7	21.0	180.2	9h 40m
		4	2.6	1.7	279.8	3.8	319.6	−6.5	2.4	105.5	20.6	170.0	～
		6	0.9	2.1	271.7	2.7	341.7	−3.1	1.9	256.1	20.6	164.1	III. 5.
		7.5	−0.3	1.3	332.0	3.9	340.6	−3.2	2.7	280.7	18.1	158.4	11h
5.	III. 7.	0	−7.3	0.3	120.3	12.1	217.5	−13.5	9.8	56.3	10.4	237.8	III. 5. 11h
21. 1	4h 18m	3	−5.3	8.1	20.7	8.5	217.3	−3.0	5.4	48.3	3.6	259.5	～
		5	1.4	5.6	334.9	7.7	190.5	0.0	5.5	354.0	7.5	203.6	III. 6. 12h
		10	−0.8	4.3	343.2	5.5	196.1	1.2	2.4	339.6	5.6	196.5	
6.	III. 8.	0	4.0	13.9	224.4	11.4	272.8	5.0	12.9	275.5	8.0	305.4	III. 7.
22. 1	5h 11m	3	−1.4	12.3	267.2	11.8	231.3	1.2	12.5	291.5	9.6	230.9	12h 30m
		5	3.5	7.9	307.5	7.6	227.6	2.9	8.7	291.9	10.8	220.1	～
		10	−1.9	8.3	317.7	6.8	174.3	0.2	8.0	299.9	10.8	203.8	III. 4.
		12	−3.1	7.4	309.8	5.6	170.2	1.0	8.9	296.7	10.2	196.7	13h 30m
7.	III. 9.	0	−12.7	13.9	337.7	16.3	217.1	−19.6	7.4	4.5	18.3	248.3	III. 4. 14h
23. 1	6h 07m	3	−11.6	11.4	345.2	18.5	214.0	−12.0	10.3	345.5	16.8	228.5	～
		5	−7.3	4.8	331.5	12.4	214.0	−9.1	8.7	341.4	17.1	223.2	III. 9. 15h
		10	−4.3	4.0	292.7	6.6	201.4	−2.7	10.5	279.8	12.4	201.0	

observed data in Osaka Bay[4], which were obtained from Feb. 28th to Mar. 9th in 1953, and he has determined various coefficients relating to the friction, including the vertical and horizontal eddy viscosity.

§2. The stations of the current observation during one lunar day are shown in Fig. 1 and the harmonic components of the tidal current at each station are tabulated in Table 1 up to the second harmonics.

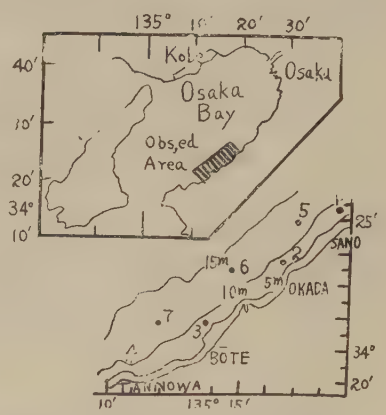

Fig. 1. Locations of observation stations

First, the mean currents at each station indicates the decrease of velocity with the depth and they seem to be related with the mean wind stress during the observation. In fact, we compute the mean wind stress from the observed wind data by Rossby's formula[5]

$$u/\sqrt{\tau/\rho} = 5.5 + 5.75 \log (z/\nu)\sqrt{\tau/\rho} \quad \text{(Below wind vel. 4 m/sec)}$$

$$\tau = 0.0302\, \rho u^2 / \left(ln \frac{z+z_0}{z_0} \right)^2 \quad \text{(Above wind vel. 4 m/sec)}$$

since the wind observation was carried out at 5m layer above the sea level, and the mean wind stress over one lunar day at each station are shown in Table 2. Comparing them with the mean currents, we can see that the latter

Table 2. Mean wind stress computed from wind observations at each st. (c.g.s.)

St.	1	2	3	4	5	6	7
N—Comp.	0.57	−0.07	−0.72	−0.12	−0.11	0.92	−0.63
E—Comp.	0.50	−0.07	1.39	−0.10	−0.10	0.45	−0.45

is due to the wind during the observation, since the mean surface current flows almost in the same direction as the wind blows, and the current velocity decreases with the depth, sometimes accompanying the back flow at the bottom of the shallow stations. On the other hand, the velocity of the mean surface current is not always proportional to the wind stress, which is probably due to the variability of the wind, since the wind velocity and direction were much variable, except at St. 3 and 7. Thus we make use of the data of St. 3 and 7 to determine the vertical eddy viscosity of the mean current, where the former station is the example of the onshore wind and the latter is that of the longshore wind. In Fig. 2 the vertical distributions of the component of

the mean current perpendicular (St. 3) and parallel (St. 7) to the coast are shown, which indicate the return flow at St. 3, and this is explained only by taking account of the surface elevation acting against the effect of wind stress, which is also reasonable since the wind blew onshore at this station. First we consider the current at St. 3, which is governed by the wind stress and the surface slope. Then the equation of motion is given simply by $\nu d^2u/dz^2=\gamma$, where γ and ν are the surface slope and the vertical eddy viscosity assumed as constant. Then, the vertical distribution of the velocity is easily obtained as

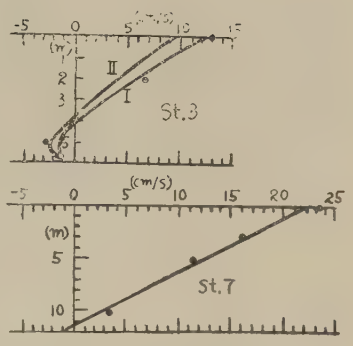

Fig. 2. The stationary currents normal to the coast (St. 3) and parallel to it (St. 7). ● Observed. Curve =Theoretical (I. for const. ν II. for const. mixing length)

$$u=\frac{1}{\nu}\left\{\frac{1}{2}(T-B)\frac{z^2}{h}-Bz\right\}+u_0$$

where $\nu du/dz=T$ at the surface ($z=h$) with taking $z=0$ at the bottom and T, B and u_0 are the surface wind stress, bottom stress, and the bottom current, respectively. By taking $h=6$ (m) and $T=1.41$ (c.g.s.) (the stress perpendicular to the coast) and making use of the observed values of u at $z=6$, 4, 2 and 1 (m), we have four linear equations for three unknown constants B, ν, and $u_0\nu$, thus they can be determined by the method of least squares. The results are shown in Table 3 and the theoretical current distribution is shown in Fig. 2 with the curve I. When we consider the friction term is expressed by the mixing length theory, the above equation of motion is replaced by

$$l^2\frac{d}{dz}\left(\left|\frac{du}{dz}\right|\frac{du}{dz}\right)=\gamma \qquad \cdots\cdots(1)$$

or

$$l^2\left|\frac{du}{dz}\right|\frac{du}{dz}=\gamma z-B=(T+B)\left(\frac{z}{h}\right)-B \qquad \cdots\cdots(2)$$

where l is the mixing length assumed to be constant, considering the water depth is shallow. By substituting the difference of u at $z=6$, 4, 2 and 1 (m) for the differential of the left hand side of (2), we have three linear equations for the unknown constants B and $(l/h)^2$ of the following type

$$\left(\frac{l}{h}\right)^2\frac{u_1-u_2}{(z_1-z_2)^2/h^2}\frac{(u_1-u_2)}{}=T\left(\frac{z}{h}\right)-B\left(1-\frac{z}{h}\right) \qquad \cdots\cdots(3)$$

where u_1, u_2 are the velocity at $z=z_1$, z_2, respectively. The results of com-

putation of B and l/h by the least squares are also shown in Table 3, which indicates almost the same value of B as the above method. The theoretical distribution indicated by the curve II is also shown in Fig. 2 by computing from the following relations.

$$\left.\begin{aligned} u&=\frac{4}{3}\frac{B}{Al}\left\{B^{\frac{3}{2}}-\left(B-A\frac{z}{h}\right)^{\frac{3}{2}}\right\}+u_0 \quad \text{for} \quad B>Az/h, \\ u&=\frac{4}{3}\frac{B}{Al}\left\{\left(A\frac{z}{h}-B\right)^{\frac{3}{2}}+B^{\frac{3}{2}}\right\}+u_0 \quad \text{for} \quad B<Az/h, \end{aligned}\right\} \qquad \ldots\ldots(4)$$

where $A=T-B$.

The agreement with the observed data is better for the curve I, but taking into consideration the fact that the constants are determined from the velocity itself for the curve I, while from the vertical gradient of the velocity for II, we cannot conclude whether the eddy viscosity is constant or the mixing length is constant. In any case the order of these quantities seems to be reasonable comparing with those obtained heretofore. Next, for St. 7 both the current and wind stress are longshore and we can assume that there was no surface slope, and the assumption of constant eddy viscosity gives the vertical distribution of the velocity such as

$$u=Tz/\nu+u_0 \qquad \ldots\ldots(5)$$

As before we can determine T/ν and u_0 by the least squares from the current data of the longshore components and further the value of ν is obtained from the computed value of T. The results is shown in Table 3 and the theoretical curve of vertical distribution of the velocity with these constants is also indicated in Fig. 2. In this case the assumption of the constant mixing length leads to the similar linear relation between the current and the depth such as

Table 3. Some physical constants obtained from the mean wind stress and the stationary currents

	St. 3	St. 7	(All in c.g.s. units)
T	1.41	1.26	(Mean wind stress)
ν	23.6	60.2	(Eddy viscosity)
B	$\left\{\begin{matrix}0.12\\0.14\,(*)\end{matrix}\right.$	1.26	(Bottom stress)
l/h	0.15	0.53	(l=mixing length, h=depth)
u_0	−0.7	−0.6	(Bottom current)

Remark: At St. 3 the wind stress and currents are of the normal component to the coast; At St. 7 they are parallel to it. (*) Determined from constant mixing length assumption.

$$u=T^{\frac{1}{2}}z/l+u_0 \qquad \ldots\ldots(6)$$

and we can obtain l/h by use of the value of $T/\nu=T^{\frac{1}{2}}/l$ determined from the

mean gradient of the current as above, which gives somewhat larger value of the mixing length than at St. 3. Summarizing these results,

(1) The onshore wind causes the surface elevation towards the coast and the reverse bottom stress, whereas the longshore wind seems to have no effect on the surface slope along the shore and it gives the constant stress from surface to bottom.

(2) The bottom current is reverse to the wind stress and the surface current in both cases, though it is slight.

§3. The harmonic components also indicates the decrease in amplitude with the depth and this seems to be attributed to the vertical eddy viscosity. However, the change of the phase lag with the depth is not so regular, as given by the simple theory of the constant eddy viscosity. Therefore we should determine the values of eddy viscosity at each depth from the observed vertical change in these harmonic components by the adequate relation. For this purpose we start from the equations of motion such as

$$\frac{\partial u}{\partial t}-\lambda v=-g\frac{\partial \zeta}{\partial x}+\frac{\partial}{\partial z}\left(\nu\frac{\partial u}{\partial z}\right) \qquad \cdots\cdots(7\cdot 1)$$

$$\frac{\partial v}{\partial t}+\lambda u=-g\frac{\partial \zeta}{\partial y}+\frac{\partial}{\partial z}\left(\mu\frac{\partial v}{\partial z}\right) \qquad \cdots\cdots(7\cdot 2)$$

By integrating them between $z=z_1$ and z_2, we have

$$\partial\bar{u}/\partial t-\lambda\bar{v}=-g\partial\zeta/\partial x+[(\nu\partial u/\partial z)_{z=z_2}-(\nu\partial u/\partial z)_{z=z_1}]/h_1$$

$$\partial\bar{v}/\partial t+\lambda\bar{u}=-g\partial\zeta/\partial z+[(\mu\partial v/\partial z)_{z=z_2}-(\mu\partial v/\partial z)_{z=z_1}]/h_1$$

for the layer between $z=z_1$ and $z=z_2$, where $\bar{u}$, $\bar{v}$ are the mean of u, v and $h_1=z_2-z_1$. Further, we take the difference of each equation for successive layers in order to eliminate the surface slope, and we have

$$\frac{\partial}{\partial t}[u(2)-u(1)]-\lambda[\bar{v}(2)-\bar{v}(1)]=\frac{1}{h_2}\nu_3u'(z_3)-\left(\frac{1}{h_1}+\frac{1}{h_2}\right)\nu_2u'(z_2)+\frac{1}{h_1}\nu_1u'(z_1) \qquad \cdots\cdots(8)$$

and similar equation from $(7\cdot 2)$, where $\bar{u}(1)$, $\bar{v}(1)$ and $\bar{u}(2)$, $\bar{v}(2)$ are the mean values of u and v in the layer $z_1\leq z\leq z_2$ and $z_2\leq z\leq z_3$, respectively and $h_2=z_3-z_2$. When we put $u=u_1\cos\sigma t+u_2\sin\sigma t$, $v=v_1\cos\sigma t+v_2\sin\sigma t$, then we obtain

$$\left.\begin{aligned}-\sigma[u_1(2)-\bar{u}_1(1)]-\lambda[\bar{v}_2(2)-\bar{v}_2(1)]&=\frac{1}{h_2}\nu_3u'_2(z_3)-\left(\frac{1}{h_1}+\frac{1}{h_2}\right)\nu_2u'_2(z_2)+\frac{1}{h_1}\nu_1u'_2(z_1)\\ \sigma[\bar{u}_2(2)-u_2(1)]-\lambda[\bar{v}_1(2)-v_1(1)]&=\frac{1}{h_2}\nu_3u'_1(z_3)-\left(\frac{1}{h_1}+\frac{1}{h_2}\right)\nu_2u'_1(z_2)+\frac{1}{h_1}\nu_1u'_1(z_1)\end{aligned}\right\} \qquad \cdots\cdots(9)$$

and similar two equations from (7・2).

Here the values of $\bar{u}_1$, $\bar{u}_2$, $\bar{v}_1$, $\bar{v}_2$ are given from the harmonic components and the vertical gradients of velocity components such as u'_1, u'_2 etc. can be replaced by their difference, thus we have four equations for two layers and eight linearly independent equations for three successive layers for eight unknown constant ν_i, μ_i $(i=1\sim4)$. These constants can be determined twice for each depth, except the surface and bottom layer. Thus we take mean values of them and the results are shown in Table 4, where μ is the eddy viscosity for N—components and ν for E—components. Some of their values are negative, which is of course unreasonable. However, we can see that the order of eddy viscosity is about 1~10 cm²/sec and it tends to decraese from the large value at the surface to the minimum at the mid-depth, then again increase near the bottom. Such changes seem to be inconsistent with the results obtained for the atmospheric turbulence over the ground, and should be studied in detail. The difference between the values of eddy viscosity for diurnal and semi-diurnal components is not so obvious, though those for the latter indicate somewhat larger values.

Table 4. Vertical eddy viscosity computed from the harmonic components of tidal currents. (μ is for N—Comp. ν is for E—Comp. of currents in c.g.s.)

St.	Depth (m)	Diurnal		Semi-diurnal	
		ν	μ	ν	μ
1	0	12.1	8.3	32.6	10.2
	2	5.4	5.4	24.5	6.9
	4	6.2	(−3.2)	10.1	4.5
	5	4.8	6.4	8.9	1.3
	6	9.2	3.5	7.1	4.4
2	0	1.6	3.8	6.7	3.6
	2	(−0.2)	(−0.3)	2.5	2.5
	4	2.2	4.9	1.8	1.7
	5	0.2	3.7	3.8	2.8
	6.5	3.4	4.8	7.4	5.4
3	0	2.6	3.0	5.0	10.5
	2	7.5	8.5	0.7	1.3
	4	1.7	2.0	3.8	3.2
	5	4.3	(−3.2)	4.1	6.3
4	0	8.5	1.2	4.2	5.1
	2	2.4	1.9	10.5	4.1
	4	2.1	2.9	(−1.1)	2.7
	6	2.7	2.1	3.5	3.8
	7.5	3.0	8.9	4.2	1.6

The eddy viscosity at the surface layer can be determined also by use of the surface stress condition $[\nu(\partial u/\partial z)]_{z=h}=T$, where T is the wind stress. For this purpose, we compute the harmonic components of the wind stress at St. 1, 3 and 6, where the wind variation with time was relatively conspicuous. To compute the shear of the surface current $\partial u/\partial z$ in practice, we take the difference of harmonic components of the current at the surface and 2 m depth (3 m depth at St. 6). Practically the surface shear and the wind stress have not the same phase with time and we should express the eddy viscosity as

$\nu = \nu_n e^{ik_n}$, where n means each harmonic component of the current. The results of the computation of the harmonic components of the wind stress and ν are shown in Table 5, which indicates somewhat larger values of eddy viscosity

Table 5. Harmonic components of wind stress and computed surface eddy viscosity from the current shear and the wind stress. Wind stress$=\Sigma T_n e^{i(n\sigma t-\varphi_n)}$. Eddy viscosity$=\nu_n e^{ik_n}$. Amplitudes T_n and ν_n are in c.g.s. Units and phase lags φ_n and ν_n in degrees

	N—Comp.				E—Comp.			
	Diurnal		Semi-diurnal		Diurnal		Semi-diurnal	
St.	T_1	φ_1	T_2	φ_2	T_1	φ_1	T_2	φ_2
1	1.16	251	0.49	53	1.09	242	0.24	74
3	1.18	112	0.48	58	1.68	236	0.56	164
6	2.08	181	1.64	328	0.65	171	0.97	318
	ν_1	k_1	ν_2	k_2	ν_1	k_1	ν_2	k_2
1	27.3	349	45.1	(82)	41.7	348	9.1	(45)
3	47.6	338	13.5	339	39.2	6	28.8	(73)
6	76.5	15	59.0	313	54.6	330	52.1	315

than determined by the above method. Such discrepancy seems to be due to the uncertainty in the values of the current shear, the error in the computed wind stress and especially the neglect of the effect of Coriolis' force in the latter method. Limiting only to the present case, we may note the following points :

(1) The values of ν_n are larger at St. 6 for each components than at other stations, which seems to be due to the larger depth of that station.

(2) Generally the values of ν_n are larger with increasing amplitude of the wind stress, though no definite relations between the eddy viscosity and the wind stress are obtained owing to the insufficient numbers of the data.

(3) The phase lag is limited almost within $\pm 45°$ and has negative values, except several cases. This means that the current shear changes with time somewhat retarded from the change of the wind stress, which seems to be reasonable, since the wind disturbs the sea surface in the form of wave initially and it takes some time to set the current in motion. However, the several cases with positive values of k_n cannot be explained only from the present data.

§ 4. When we take the friction term such as proportional to the velocity or its square, we have the difference of the friction force at two depths, by eliminat-

ing the gradient terms from the equations of type of (7) and thus[8]

$$\left.\begin{aligned}
&\sigma\{u_2(1)-u_2(2)\}-\lambda\{v_1(1)-v_1(2)\}=f_1(2)-f_1(1)\\
&\sigma\{u_1(2)-u_1(1)\}+\lambda\{v_2(2)-v_2(1)\}=f_2(2)-f_1(1)\\
&\sigma\{v_2(1)-v_2(2)\}+\lambda\{u_1(1)-u_1(2)\}=g_1(2)-g_1(1)\\
&\sigma\{v_1(2)-v_1(1)\}+\lambda\{u_2(1)-u_2(2)\}=g_2(2)-g_2(1)
\end{aligned}\right\} \quad \cdots\cdots (10)$$

where we put $F=f_1\cos\sigma t+f_2\sin\sigma t$ and $G=g_1\cos\sigma t+g_2\sin\sigma t$ as the friction term in x-and y-direction, respectively. $u_1(1)$, $u_2(1)$ etc. have the similar meaning as in (9). From these relations, we can determine the friction terms if we know those of one layer. This can be done for the bottom layer by computing the bottom stress with the relations similar to the wind stress equation given in §2, but for this purpose it is necessary to obtain the more accurate knowledge about the hydraulic properties of the bottom and the bottom current,[9] thus here we consider the case with no surface friction. The current with almost no wind stress at the surface may correspond approximately to the case. For this purpose we compute the various constants for St. 2 and 4, which seem to satisfy such conditions, where we put approximately

$$\left.\begin{aligned}
&F=kU^2\cos(\sigma t-\varphi-p) \quad \text{or} \quad \alpha U\cos(\sigma t-\varphi-p)\\
&G=jV^2\cos(\sigma t-\psi-q) \quad \text{or} \quad \beta V\cos(\sigma t-\psi-q)
\end{aligned}\right\} \quad \cdots\cdots (11)$$

where U, V and φ, ψ are the amplitude and phase lag of u and v, respectively. Then the friction constants k, j; α, β and the phase lag of the friction from the current p, q are determined from the four equations by use of the harmonic components of the velocity. The results are shown in Table 6 (1) A, which indicate the general increase of the friction coefficients k, j; α, β towards the bottom and the larger values of them for the diurnal tide. However the dispersion of absolute values of the friction coefficients and the phase lag is relatively conspicuous and the order of k, j ranges from 10^{-6} to 10^{-3}, and that of α, β from 10^{-5} to 10^{-3} (c.g.s.), thus only from these results it seems to be more appropriate to take the friction term proportional to the velocity itself for the dynamical equation of the tidal wave than that proportional to its square. The phase lag is also almost dispersed in all quadrant, though most of them are within $\pm 90°$ and further the values of the deeper layers show less phase lag of the friction to the current. This seems to be due to the fact that in the present computation the friction of the surface layer is put to zero, but practically the surface friction has some finite value, thus the absolute values of the friction coefficients at the layers near the surface show the decrease and the phase lag indicates larger values than the deeper layers as expected from the

Table 6 (1). Friction coefficients and time lags of frictional force to the current. k, α and p are for E—components of the current and j, β and q are for N—components. k, j in $10^{-6}\,cm^{-1}$, α, β in $10^{-5}\,sec^{-1}$, and p, q in degrees.

(A) St.	Depth (m)	Diurnal Comp.						Semi-diurnal Comp.					
		k	α	j	β	p	q	k	α	j	β	p	q
2	2	16.9	10.5	9.5	7.8	210	317	2.3	3.3	2.9	4.8	109	170
	4	18.7	11.0	8.2	7.2	258	2	13.8	12.5	9.6	10.8	96	268
	5	457	73.0	183	44.0	257	315	7.0	6.5	3.9	5.6	214	235
	6.5	833	83.3	490	73.6	288	327	15.2	12.8	5.4	6.5	270	220
4	2	6.7	5.1	7.7	5.8	231	232	10.7	7.9	4.3	3.0	331	232
	4	448	76.0	220	33.0	256	221	23.5	8.9	0.7	1.5	341	285
	6	387	81.6	417	79.0	303	77	24.0	6.5	1.4	2.7	285	312
	7.5	755	98.2	206	55 8	284	51	19.7	7.5	3.3	6.0	35	329
(B)													
2	0—2	3.2	2.6	6.9	4.5	240	337	2.7	4.5	1.5	2.4	80	264
	2—4	5.1	4.5	12.4	7.3	295	359	9.9	11.6	8.3	7.6	205	262
	4—5	111	30.0	238	38.0	244	306	4.5	6.5	6.6	7.9	203	261
	5—6.5	250	46.1	411	56.2	260	304	12.3	14.9	18.1	15.2	213	294
4	0—2	8.0	6.0	7.1	5.3	30	326	1.0	2.1	6.4	4.8	88	82
	2—4	85.5	21.5	106	18.1	76	29	2.1	4.4	57.8	21.1	25	321
	4—6	43.2	8.2	53.7	11.3	331	312	2.9	5.9	121	32.8	16	272
	6—7.5	12.2	3.3	213	27.9	121	2	4.0	7.3	60.3	17.5	7	256

Case A=No friction at the surface.

Case B=Constant coefficients within the layer in the depth range shown on the 2nd collum.

eqs. (10), though the increase of the former towards the bottom is partly due to the bottom friction. Anyhow, the scattering of the constants seems to be too large to be considered as reasonable, thus we should take another relations for the friction and the velocity. For this purpose, we abondon the assumption that these friction constants is variable at each depth, and in place we assume that they are constant within each layer between the depths where the current observations are carried out. In other words we put

$$F(i) = \alpha U(i) \cos(\sigma t - \varphi i - p), \quad i = 1, 2 \text{ etc.}$$

where $i=1, 2$ means the two succesive depths, between which the absolute value α and the phase lag p of the frictional coefficient is assumed constant. Then we have a simple relation between the difference of the friction term and the velocity for these two depths such as

$$F(2) - F(1) = \alpha\{U(2) \cos(\sigma t - \varphi_2 - p) - U(1) \cos(\sigma t - \varphi_1 - p)\}$$

or when we put

$$u(2)-u(1)=[u_1(2)-u_1(1)]\cos\sigma t+[u_2(2)-u_2(1)]\sin\sigma t=U_0\cos(\sigma t-\varphi_0) \quad \ldots\ldots (12)$$

we have

$$F(2)-F(1)=\alpha U_0\cos(\sigma t-\varphi_0-p) \quad \ldots\ldots (13)$$

or

$$\left.\begin{aligned} f_1(2)-f_1(1)&=\alpha U_0\cos(p+\varphi_0)\\ f_2(2)-f_1(1)&=\alpha U_0\sin(p+\varphi_0)\end{aligned}\right\} \quad \ldots\ldots (14)$$

The left hand sides of these equations can be computed from the relations (10) and the value of U_0 and φ_0 are also determined from (12), so that we obtain the absolute value α and the phase lag p of the frictional coefficient can be determined. When the frictional force is given by

$$F(i)=kU^2(i)\cos(\sigma t-\varphi_i-p')\ ;\ i=1,2$$

we can determine k and p' similarly, where we put

$$F(2)-F(1)=kU_a^2\cos(\sigma t-\varphi_a-p') \quad \ldots\ldots (15)$$

then the amplitude U_a^2 and phase lag φ_a are defined as

$$\left.\begin{aligned} U_a\cos(\sigma t-\varphi_a)&=[U(2)u_1(2)-U(1)u_1(1)]\cos\sigma t\\ &\quad+[U(2)u_2(2)-U(1)u_2(1)]\sin\sigma t\\ &=U_2u(2)-U(1)u(1)\end{aligned}\right\} \quad \ldots\ldots (16)$$

instead of U_0 and φ_0 in the equation (12). Thus in this method the phase lag p' is not equal to p. The friction coefficient for G can be similarly obtained and the trouble of the computation somewhat increases from the previous method, since we should compute two sets of the amplitude and phase lag of velocity for the case of friction force proportional to the linear and square velocity, but more reasonable results may be expected comparing with the previous method. Theoretically this method leads to the abrupt change of the coefficients at the boundary between two layers, but such condition would be inevitable for the numerical method as the present treatment. The results of the computation by use of the same current data of St. 2 and 4 are shown in Table 6 (2),

Table 6 (2). Friction coefficients and time lags of frictional force to the current

(B) St.	Depth (m)	Diurnal Comp.		Semi-diurnal Comp.	
		p'	q'	p'	q'
2	0—2	262	327	28	298
	2—4	301	346	224	255
	4—5	276	352	252	343
	5—6.5	258	319	226	372
4	0—2	291	297	29	277
	2—4	34	315	83	306
	4—6	356	46	51	331
	6—7.5	253	18	22	293

p' and q' are the phase lag determined from the eq. (15).

which indicates less scattering of the numerical values of k, j and α, β, comparing with those obtained by the previous method. The order of the former is about $10^{-6}\sim10^{-4}$ (c.g.s.) and that of the latter is about $10^{-5}\sim10^{-4}$ (c.g.s.), and the increase of these values towards the bottom layer is also observed, but the phase lag becomes closer to 0 near the surface than in the previous case, though they indicate the retardness of the frictional force to the current only at half of all cases at the surface layer.

Next, we assume that the above relation for the frictional force is valid only for the mean current between two successive depths, then we should take the mean values of u and v with the depth for the equations (10) instead of u and v. Then we have similar relations for the friction constants, and we compute these constants by the same method with the same data, but by use of the mean values of the harmonic components of the currents within the successive depths of the current observation instead of those of the observed current and the results are shown in Table 7 (1) and (2), where the same symbols are used as before and (A) and (B) corresponds to two assumptions for the friction force as stated above. Comparing these with those in Table 6 (1), (2) we can see that the dispersion of the order of k, j, α, β is diminish-

Table 7 (1). Friction coefficients and time lags determined from the mean velocity. (Symbols are the same as in Table 6)

(A) St.	Depth (m)	Diurnal Comp.						Semi-diurnal Comp.					
		k	α	j	β	p	q	k	α	j	β	p	q
2	3	3.1	2.6	7.1	4.3	290	77	3.4	4.7	4.4	5.4	205	258
	4.5	11.6	6.7	30.2	9.6	266	20	4.6	5.9	8.4	8.8	207	248
	5.8	127	33.2	141	17.6	242	331	3.2	4.4	8.5	8.7	237	268
4	3	10.9	4.1	9.2	3.9	50	71	0.7	1.5	1.9	1.1	60	6
	5	66.1	53.5	123	22.8	95	65	2.2	4.6	85.5	25.4	4	271
	6.3	40.5	11.0	155	23.0	355	87	3.3	6.4	47.8	20.4	14	285
(B)													
2	1—3	18.5	6.4	68.0	13.0	51	56	30.4	13.8	41.0	16.5	60	62
	3—4.5	16.8	4.7	45.9	12.5	41	320	12.7	12.7	45.5	10.9	350	104
	4.5—5.8	32.6	11.7	10.8	3.0	47	17	10.2	12.8	53.5	8.9	63	108
4	1—3	8.5	3.6	7.5	3.5	328	310	81.1	10.5	94.5	7.5	29	341
	3—5	21.6	8.2	23.4	10.7	16	279	21.3	14.2	92.1	25.1	294	232
	5—6.3	29.4	8.4	265	37.7	57	60	54.6	12.6	206	25.3	270	264

Case A=No friction at the surface.
Case B=Constant coefficients within the layer.

ed more conspiucously than the previous case, especially for the case (A). In short, we may conclude that the order of the friction coefficients k, j and α, β is $10^{-6}\sim 10^{-4}$ and $10^{-5}\sim 10^{-4}$, respectively, which show the increase towards the bottom and the phase lags are within the range of $\pm 90°$, which indicate closer values to zero than those obtained by the previous method.

Table 7 (2). Friction coefficients and time lags determined from the mean velocity

(B) St.	Depth (m)	Diurnal Comp.		Semi-diurnal Comp.	
		p'	q'	p'	q'
2	1—3	69	47	115	43
	3—4.5	37	21	326	89
	4.5—4.8	28	351	54	295
4	1—3	321	332	43	351
	3—5	48	256	327	265
	5—6.3	23	79	306	278

p' and q' are the phase lag determined from the eq. (15).

Summarizing the results of computation of the frictional constants by four method, we have the following table, where I and II indicate the value of Table 6 and 7, respectively.

(1) The order of k, j (cm^{-2}) and α, β (cm^{-1}).

	IA	IB	IIA	IIB
k, j	$10^{-6}\sim 8\times 10^{-4}$	$10^{-6}\sim 4\times 10^{-5}$	$10^{-6}\sim 2\times 10^{-4}$	$10^{-5}\sim 2\times 10^{-4}$
α, β	$10^{-5}\sim 10^{-3}$	$10^{-5}\sim 6\times 10^{-4}$	$10^{-5}\sim 8\times 10^{-4}$	$10^{-5}\sim 2\times 10^{-4}$

(2) The percentage of the numbers of the phase lag within the range $-90° < p, q < 90°$ to the total of each case.

	IA	IB	IB′	IIA	IIB	IIB′
(%)	56	66	78	66	78	87

(3) The percentage of the numbers of the phase lag within the range $0 < p, q < 180°$, which corresponds to the retardness of the frictional force to the current.

(%)	25	31	25	46	58	50

(4) The percentage of the cases which have larger phase lag at the bottom than the surface, corresponding to the cases where the bottom friction retards to the surface friction.

(%)	50	50	34	34	50	50

(IB′ and IIB′ are concerened to the phase lag p', q'.)

As a result, we can see that the scattering of the absolute values of frictional coefficients and the time lag of the friction to the current are reduced in the method II more than in I′ and also in (B) than in (B). On the other hand the bottom friction does not always show the retardness to the surface

friction and also the friction at all depths does not always retard from the current, as indicated in the above percentage, which should be remarkable and is inconsistent with the conventional concept, though the definition of the frictional force is different in two cases.

The present frictional force can be given by the ordinary definition[10] $F=\partial Fz/\partial z$, and when we put the bottom friction F_b, then the frictional force for the mean current from the surface to the bottom is given by F_b/h, (h, the depth) or when we take $F_b=2\times10^{-3}\rho Cu_b/h$, where u_b is the periodic bottom current and C its amplitude, then we have the relation for the mean frictional coefficient $\bar{\alpha}$ corresponding to the present definition as $\bar{\alpha}=2\times10^{-3}\rho C/h$ ($\sec^{-1}$). However, this relation gives much small value of α, since it gives 6.7×10^{-5}, even when we take the upper limit $h=6$ m, $C=20$ cm/sec (roughly corresponding to the N—component of semi-diurnal tide of St. 3). Such discrepancy seems to be due to the hydraulic conditions of the bottom, the effect of the Coriolis' force and the horizontal eddy viscosity, neglect of the surface friction, etc. On the other hand, this relation indicates that the mean frictional force has no time lag to the bottom current, whereas the present determination also shows the less phase lag at the bottom, especially those computed by the method (A), which corresponds to no surface friction. The more detailed discussion about the effect of Coriolis' force and the horizontal eddy viscosity are shown in § 5 and § 6.

§ 5. Here we determine the theoretical relations of the eddy viscosity and the friction coefficient, where the latter has been used widely for the theoretical discussion of the tidal wave. For this purpose we should start from the equations of motion such as (7・1) and (7・2), but their solutions are too complicated to give the clear conclusion, and further for the constant and equal value of μ and ν the detailed discussions have been already given by the extensive work of H. U. SVERDRUP[14], as to the effect of eddy viscosity to the propagation of the tidal waves. On the other hand, the present object is to know the relation between the eddy viscosity and the frictional force, it should be sufficient to obtain the vertical change of the current velocity in the tidal current, and we take the equations of motion such as

$$\left.\begin{aligned}\partial u/\partial t-\lambda v&=-\gamma+\mu\partial^2u/\partial z^2\\ \partial v/\partial t+\lambda u&=\nu\partial^2u/\partial z^2\end{aligned}\right\}\qquad(17)$$

as the basic equations. When we put $\gamma=F\cos\sigma t$, then the velocity components under the following boundary conditions $\partial u/\partial z=\partial v/\partial z=0$ at the surface ($z=h$)

and $u=v=0$ at the bottom $(z=0)$ are given as

$$\left.\begin{aligned} u&=\Re\left\{\frac{i\sigma Fe^{i\sigma t}}{\sigma^2-\lambda^2}\Big[1-(1-m/n)\,(1-m/m_0-n/m_0)\,\frac{\cosh p(h-z)}{2\cosh ph}\right.\\ &\qquad\left.-(1+m/n)\,(1-m/m_0+n/m_0)\,\frac{\cosh q(h-z)}{2\cosh qh}\Big]\right\}\\ v&=\Re\left\{\frac{\lambda Fe^{i\sigma t}}{\sigma^2-\lambda^2}\Big[(1-m/n)\,\frac{\cosh p(h-z)}{2\cosh ph}+(1+m/n)\frac{\cosh q(h-z)}{2\cosh qh}-1\Big]\right\}\end{aligned}\right\}\quad\cdots\cdots(18)$$

where $m=\sigma(1/\mu+1/\nu)$, $m_0=2\sigma/\nu$, $n=[\sigma^2(1/\mu-1/\nu)^2+4\lambda^2/\mu\nu]^{\frac{1}{2}}$

$$p^2=\frac{1}{2}(m+n),\quad q^2=\frac{i}{2}(m-n)$$

When we put the friction term for the mean current from the surface to the bottom as $-\alpha\bar{u}$, $-\beta\bar{v}$ where $\bar{u}$, $\bar{v}$ are the mean velocity and α, β are frictional coefficient in x and y direction, respectively, then the relations between α, β and other dynamical constants are given by[11]

$$\left.\begin{aligned}\alpha&=\frac{\left(\nu\dfrac{\partial u}{\partial z}\right)_{z=0}}{\bar{u}h}=\frac{-l(\lambda+\sigma)\,i\,\{(\lambda-\sigma)\tanh ph-l(\lambda+\sigma)\tanh qh\}}{2\sigma qh+l(\lambda-\sigma)\,\tanh ph-(\lambda+\sigma)\,\tanh qh}\\ \beta&=\frac{\left(\nu\dfrac{\partial v}{\partial z}\right)_{z=0}}{\bar{v}h}=\frac{-l(\lambda+\sigma)\,i\,\{(\lambda-\sigma)\tanh ph+l(\lambda+\sigma)\tanh qh\}}{-2\lambda qh+l(\lambda-\sigma)\,\tanh ph+(\lambda+\sigma)\,\tanh qh}\end{aligned}\right\}\quad\cdots\cdots(19)$$

where we put $\mu=\nu$ for simplicity, therefore $p^2=i(\sigma+\lambda)/\nu$, $q^2=i(\sigma-\lambda)/\nu$, $m=m_0=2\sigma/\nu$, $n=2\lambda/\nu$, $l=q/p$. These equations give the complex expression of α and β, and their absolute values $|\alpha|$ and $|\beta|$ correspond to α and β determined in § 4, the arguments Arg. α and Arg. β are represented by $-p$, $-q$, where p and q are the phase lag defined there. In other words, when we put the mean velocity as $\bar{u}=\bar{U}\cos(\sigma t-\bar{\varphi})$, $\bar{v}=\bar{V}\cos(\sigma t-\bar{\psi})$ then the friction term in x and y direction is given by

$$-|\alpha|\,\bar{U}\cos(\sigma t-\bar{\varphi}+\text{Arg. }\alpha),\quad -|\beta|\,\bar{V}\cos(\sigma t-\bar{\psi}+\text{Arg. }\alpha)\qquad\cdots\cdots(20)$$

respectively. The eqs. (19) can be reduced to the next form, when $|q|h\gg 1$ (since $|p|>|q|$).

$$\left.\begin{aligned}\alpha&=il(\sigma+\lambda)\,[l(\lambda+\sigma)-(\lambda-\sigma)]/2\sigma qh=\sqrt{\nu(\sigma+\lambda)}[l(\lambda+\sigma)-(\lambda-\sigma)]e^{i\pi/4}/2\sigma h\\ \beta&=il(\sigma+\lambda)\,[l(\lambda+\sigma)+\lambda-\sigma]/2\lambda qh=\sqrt{\nu(\sigma+\lambda)}[l(\lambda+\sigma)+\lambda-\sigma]e^{i\pi/4}/2\lambda h\end{aligned}\right\}$$

$$\cdots\cdots(21)$$

Further for the case $\sigma>\lambda$

$$\left.\begin{aligned}\alpha&=\frac{\sqrt{\nu}\,(\sigma^2-\lambda^2)}{2h\sigma}\Big[\frac{1}{\sqrt{\sigma+\lambda}}+\frac{1}{\sqrt{\sigma-\lambda}}\Big]e^{i\pi/4}\\ \beta&=\frac{\sqrt{\nu}\,(\sigma^2-\lambda^2)}{2h\lambda}\Big[\frac{1}{\sqrt{\sigma+\lambda}}-\frac{1}{\sqrt{\sigma+\lambda}}\Big]e^{i\pi/4}\end{aligned}\right\}\quad\cdots\cdots(22)$$

and for the case $\lambda > \sigma$

$$\left.\begin{aligned}\alpha &= \frac{\sqrt{\nu}\,(\lambda^2-\sigma^2)}{2h\sigma}\left[\frac{1}{\sqrt{\sigma+\lambda}}+\frac{i}{\sqrt{\lambda-\sigma}}\right]e^{-i3\pi/4}\\ \beta &= \frac{\sqrt{\nu}\,(\lambda^2-\sigma^2)}{2h\lambda}\left[\frac{1}{\sqrt{\sigma+\lambda}}-\frac{i}{\sqrt{\lambda-\sigma}}\right]e^{i\pi/4}\end{aligned}\right\} \quad \cdots\cdots (23)$$

therefore the phase lag of the friction to the mean current is different for the diurnal and semi-diurnal tide, since the former corresponds to the eqs. (23) and thus the phase lag has different values for α and β, with the retardness of the friction to the mean current (Arg. $\alpha = -60°$, Arg. $\beta = -30°$), whereas the latter has the equal value of $\pi/4$ for Arg. α and Arg. β, and it indicates the advance of the phase of the friction. (Comp. eq. (20)) On the other hand, the frictional coefficient corresponding to α is always less than $|\beta|$, which suggests that the current in the direction of surface gradient is more influenced by the frictional force. Further these equations indicate that α and β vanishes in proportion to $\sqrt{\nu}$ with the decreasing value of ν, since $\nu \ll h^2/|\lambda-\sigma|$ as $|q|h \gg 1$. When $|p|h \ll 1$, we have simple relations

$$\alpha = 3\nu/h^2, \quad \beta = 5\nu/2h^2 \qquad \cdots\cdots (24)$$

by taking the 3rd order term (for α) and the fifth order (for β) of the power series of $\tanh ph$, $\tanh qh$, which indicate that the friction coefficient becomes independent with σ and λ, while it increases with the decreasing depth and increasing value of ν and that the friction terms have the same phase as the mean current, where $|p\ h \ll 1$ corresponds to the case of small depth or large value of ν.[12]

The practical application of these simplified relations (21), (24) are restricted in the present case, since the order of ν is within $1 \sim 10^2$ (c.g.s.) as determined in § 3, and the critical values of ν for the condition $|q|h=1$, $|p|h=1$ or $\nu_q = h^2/|\lambda-\sigma|$, $\nu_p = h^2/(\lambda+\sigma)$ are as follows for the depth $h=10$(m), $\nu_p=153$, $\nu_q=12$ (diurnal), $\nu_p=234$, $\nu_q=59$ (semi-diurnal) (in c.g.s.), therefore only for the values of ν within $0 \sim 10$ the above relations (20) are valid. The amplitude and the argument of α and β computed from the original relation (19) are shown as a function of ν in Fig. 3, for the range of ν from 0 to 100, with $h=10$(m). The numerical values of the absolute values and the argument are much different for the diurnal and semi-diurnal tide, and the order of α and β of the diurnal tide is about 1/10 of that of the semi-diurnal one, in the given range of ν. The argument also fluctuates in both cases and that of the diurnal tide shows the general increase with increasing value of ν, especially abruptly for Arg. β, whereas Arg. α and Arg. β are diminished for the semi-diurnal tide,

though the decrease of Arg. α is more rapid. Further both cases show the positive and negative values of arguments within this range of ν, or in other words the friction shows both advance and retard to the mean current for the conditions, which correspond approximately to the present observation as refered to the depth and the value of ν, and such state of the change in arguments seems to be one reason for the scattering of the phase lag p and q determined in § 4, where almost the equal numbers of the computed phase lags indicates both the retard and advance of the friction to the current, though the friction constants are determined there only for each layer. The absolute values of α, β here determined theoretically seem to be less than those obtained in § 4, especially for diurnal tide, and such discrepancy is also due to the difference in the definition of α and β in this theory and the previous computation, but partly it seems to suggest that the eddy viscosity is different in the diurnal and the semi-diurnal tide, though the satisfactory data for the basis of such discussion are not obtained and also the present theory is not adequate enough for the discussion of this problem.

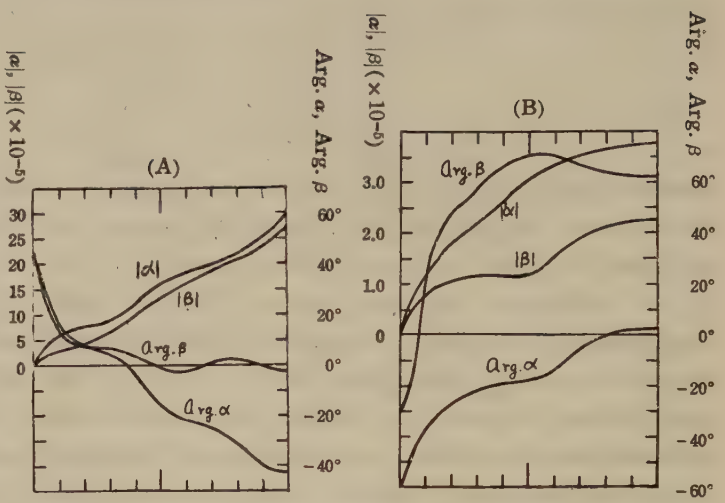

Fig. 3. Theoretical curves for frictional constantsd α and β ($|\alpha|$, $|\beta|$ =absolue value, Arg. α, Arg. β=argument, h=10(m), (A) Semi-diurnal tide, (B) Diurnal tide)

§ 6. The effect of horizontal eddy viscosity on the ocean current has been attached great importance to, and the order has been also determined by various methods, but for the tidal current it seems to be neglected heretofore. However, in the present case the decrease of the amplitude of the harmonic components near the coast should be explained from the effect of the horizontal viscosity at the boundary layer adjacent to the coast. On the other hand, the present observation was not carried out for the determination of this effect, thus the exact values cannot be obtained only from this data, and here only

the approximate consideration is given.

For simplification, we start from the basic equations of motion such as

$$\frac{\partial u}{\partial t}-\lambda v=-\gamma-ku+B\frac{\partial^2 u}{\partial y^2},\quad \frac{\partial v}{\partial t}+\lambda u=-kv+B\frac{\partial^2 v}{\partial y^2} \qquad \text{..... (25)}$$

where γ is the surface slope equal to $\gamma=F\cos\sigma t$ and $-ku$, $-kv$ are the frictional term caused by the bottom friction and B is the coefficient of horizontal eddy viscosity. These equations are valid by taking u and v as the mean current velocity with the depth, when the wind stress does not act on the surface. However, we apply them to the present data, neglecting the effect of the wind stress. Putting $u=u_1\cos\sigma t+u_2\sin\sigma t$ etc. as before, we have

$$-\sigma w_1+i\lambda w_2=-kw_2+B\frac{d^2w_2}{dz^2},\quad \sigma w_2+i\lambda w_1=-F-kw_1+B\frac{d^2w_1}{dz_2}$$

where $w_1=u_1+iv_1,\quad w_2=u_2+iv_2$

The solutions are given by

$$\left.\begin{aligned} w_1&=\frac{F}{2}\{(e^{-\sqrt{\alpha/B}y}-1)/\alpha+(e^{-\sqrt{\beta/B}y}-1)/\beta\}\\ w_2&=\frac{iF}{2}\{(e^{-\sqrt{\alpha/B}y}-1)/\alpha-(e^{-\sqrt{\beta/B}y}-1)/\beta\}\end{aligned}\right\} \qquad \text{..... (26)}$$

under the boundary condition that $w_1=w_2=0$ at the coast $y=0$ and finite at $y=\infty$, where

$$\alpha=k+i(\lambda+\sigma),\quad \beta=k+i(\lambda-\sigma)$$

Separating the real and imaginary parts, we have

$$\left.\begin{aligned} u_1&=\frac{F}{2}[(P-P_0)/r+(R-R_0)/s]\\ v_1&=-\frac{F}{2}[(Q-Q_0)/r+(S-S_0)/s]\\ u_2&=\frac{F}{2}[(Q-Q_0)/r-(S-S_0)/s]\\ v_2&=\frac{F}{2}[(P-P_0)/r-(R-R_0)/s]\end{aligned}\right\} \qquad \text{..... (27)}$$

where

$$\begin{aligned} P&=e^{-\sqrt{r/B}\cos\varphi\cdot y}\cos(2\varphi+\sqrt{r/B}\sin\varphi\cdot y)\\ Q&=e^{-\sqrt{r/B}\cos\varphi\cdot y}\sin(2\varphi+\sqrt{r/B}\sin\varphi\cdot y)\\ R&=e^{-\sqrt{s/B}\cos\psi\cdot y}\cos(2\psi+\sqrt{s/B}\sin\psi\cdot y)\\ S&=e^{-\sqrt{s/B}\cos\psi\cdot y}\sin(2\psi+\sqrt{s/B}\sin\psi\cdot y)\end{aligned}$$

and P_0, Q_0 are the values of P, Q, when we put $y=0$ at P, Q. Or

$$P_0=\cos 2\varphi,\quad Q_0=\sin 2\varphi,\quad R_0=\cos 2\psi,\quad S_0=\sin 2\psi$$

Further we take the angle φ, ψ, so as to give the positive value of $\cos\varphi$ and $\cos\psi$, and

$$p^2=(\lambda+\sigma)^2+k^2, \quad q^2=(\lambda-\sigma)^2+k^2$$
$$\tan 2\varphi=(\lambda+\sigma)/k, \quad \tan 2\psi=(\lambda-\sigma)/k$$

The difficulty in determining B from the observed data of tidal currents is that simultaneous observation of the current is not so easy. However, we have approximate harmonic components for the same tidal age by taking account of the astronomical constants of the period of the observation, when the current at one station is observed during a suitable period. In the present case, we correct only the semi-diurnal component according to the lunar age by use of the result of the seperation of lunar and solar tide obtained from the observations carried out in 1950, 1951 and 1952 at the St. 1, 2, 3 and 4 and apply them also to the offshore stations. The detailed discussion for the method of such correction is not given here.[13]

For the practical computation by use of these harmonic components of each station, we should derive more convenient relations for the computation from the above solutions (27). In other words we should have the equations including only one term such as $P-P_0$ by combining the suitable relations for u_1, u_2, v_1 and v_2, and we obtain

$$\left.\begin{aligned} u_1+v_2&=F(P-P_0)/r, \quad u_2-v_1=F(Q-Q_0)/r \\ u_1-v_2&=F(R-R_0)/s, \quad v_1+u_2=-F(S-S_0)/s \end{aligned}\right\} \qquad \cdots\cdots(28)$$

Further, the eddy viscosity B is included only in P, Q, R and S, and we cannot determine the surface slope F, so we eliminate it by taking the ratio of the above relations at two stations located at the different distances from the coast. Then we have

$$\left.\begin{aligned} \frac{u_1(1)+v_2(1)}{u_1(2)+v_2(2)}&=\frac{P(1)-P_0}{P(2)-P_0} \\ \frac{u_1(1)-v_2(1)}{u_1(2)-v_2(2)}&=\frac{R(1)-R_0}{R(2)-R_0} \quad \text{etc.} \end{aligned}\right\} \qquad \cdots\cdots(29)$$

where $u_1(1)$, $u_1(2)$ etc. mean the values of u_1 at $y=y_1$ and $y=y_2$, respectively. For the application to the present case we can put $y_1=1.0$ (km) for near shore station 1, 2, 3 and 4 and $y_2=2.5$ (km) for St. 5, 6 and 7, by taking the mean distances of each set of the stations from the coast. Therefore when we compute the ratios for the diurnal and semi-diurnal components with these constants, we can express them as a relation such as

$$\frac{u_1(1)+v_2(1)}{u_1(2)+v_2(2)}=\frac{e^{-aX}\cos(2\varphi+aX\tan\varphi)-\cos 2\varphi}{e^{-X}\cos(2\varphi+X\tan\varphi)-\cos 2\varphi} \quad \text{etc.} \qquad \cdots\cdots(30)$$

where $X=\sqrt{r/B}\,y_2\cos\varphi$, $a=y_1/y_2$ and we replace X by $Y=\sqrt{s/B}\,y_2\cos\psi$ for the relations including R and S. Then we can determine the argument X and Y by comparing these relations with the ratios of the left hand side computed from the harmonic components of the current corrected for nearly equal tidal age as stated above. The curves of the right hand side of above relations for the range of X and Y between 0 and 5 are shown in Fig. 4, for diurnal and semi-diurnal tides with the constants such as

$\lambda=8.25\times10^{-5}$, $k=10^{-4}$ (c.g.s.),

where the friction coefficient k is taken from the approximate mean value of those determined in § 4 and it seems to be somewhat over-estimated, comparing with the value heretofore used for the dynamics of tidal waves, since the coefficient k given by the ordinary theory is about equal to 1.5×10^{-5} for the semi-diurnal tide and 2.2×10^{-5} for the diurnal tide with the mean depth of 9.5 m and the mean bottom current for the corrected harmonic components, from the relation $k=2\times10^{-3}\,U_b/h$. (§ 4). However, we take the above value of k, partly due to attach the importance to the present calculation of § 4 derived from the direct data and partly owing to the simplicity of numerical computation. These curves indicate the lower limit 0.4 at $X=0$, $Y=0$, since the ratios are equal to a there, as seen from the equation (30). For the purpose of the computation of the eddy viscosity B, we should compute the ratio of the left hand side of the equations (30) from the harmonic components of the current and determine the values of X or Y corresponding to this ratio from these curves, from which we can determine B, since the relations between B and X or Y include only the known constants. However, some of these curves have the maximum

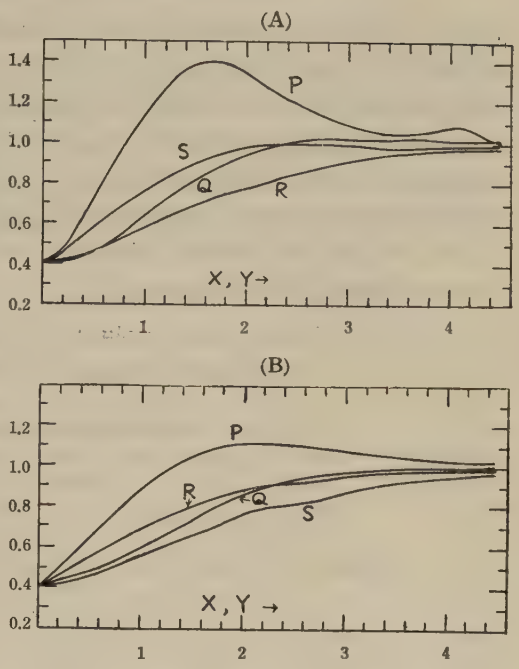

Fig. 4. The curves for the ratios of eqs. (29.). ($X=\sqrt{r/B}y_2\cos\varphi$, $Y=\sqrt{s/B}\cos\psi$, P, Q etc. mean $[P(1)-P_0]/[P(2)-P_0]$, $[Q(1)-Q_0]/[Q(2)-Q_0]$ etc.) (A) Semi-diurnal tide, (B) Diurnal tide.

value at the finite value of X or Y and others also becomes asymptotic much gradually to the limiting value as X or Y increases. Therefore, the corresponding value of X or Y to the given ratio of the left hand side is not always able to be determined uniquely, or at least it is much difficult to find it for the part of the curves almost parallel to the abscissa. Thus we should cut off the values beyond a certain limiting value, say X_c, for each curve and make use of the part of the curves, where we can easily find the value of X or Y for the given value of the ordinate.

In Table 8 the numerical values of horizontal eddy viscosity determined from the data of each pair of stations by use of the relations are shown, where

Table 8. Horizontal eddy viscosity ($\times 10^5$ cm^2/sec)

y_1	y_2	Diurnal				Semi-diurnal			
		P	Q	R	S	P	Q	R	S
St. 1	St. 5	193	25.2	2.0	0.9	**	2.8	0.6	3.6
St. 1～2	St. 5	*	102	15.3	10.8	65.8	3.9	2.2	2.2
St. 2	St. 5	*	**	112	***	7.6	***	0.8	2.0
St. 2	St. 6	*	46.3	27.8	1.9	14.6	3.0	***	1.8
St. 2～3	St. 6	*	21.5	**	1.3	12.3	3.6	***	0.5
St. 3	St. 6	*	33.5	**	1.5	10.5	3.4	***	0.8
St. 3	St. 7	*	20.1	**	0.9	61.2	3.0	***	4.5
St. 3～4	St. 7	402	41.2	8.3	1.3	42.8	6.8	***	13.9
St. 4	St. 7	99	21.5	1.1	1.5	**	***	***	102

* unable to determine due to the negative ratio
** 〃 〃 〃 the value below 0.4
*** 〃 〃 〃 the value above the upper limit
St. 1～St. 2 etc. indicates that the mean values of St. 1 and St. 2 are taken for the harmonic components.
P, Q, etc. indicates that the eddy viscosity is calculated from the relation including P, Q etc., respectively.

the stations for y_1 are taken not only as one station but also as the mean values of two adjacent stations and the kind of the equations (30) for each determination is also indicated. Further, we imply the case unable to determine the eddy viscosity due to the negative value, above the upper limit or below the minimum value of the ratio derived from the observed data. The range of these values is limited between 10^5 and 10^7 (c.g.s.), and they are widely scattered, even though we cut off the argument X above X_c which means that we neglect the smaller value of B corresponding to X_c. However, notwith-

standing the simple model for the effect of horizontal eddy viscosity and the many sources of errors accompanying with the left hand side of the equation (30) derived from the observed data, we can determine these values in most cases and the order is also not so unreasonable, compared with those heretofore obtained, thus we may conclude that the assumption on which the present method to computate eddy viscosity has not so much discrepancy to the actual conditions.

The changes of the amplitude and the phase lag of the theoretical current with Z are shown in Fig. 5, where we put $Z=\sqrt{r/B}y$ and $U=\sqrt{u_1^2+u_2^2}$, $V=\sqrt{v_1^2+v_2^2}$ (amplitudes), then the amplitude is shown by $2U/F$ and $2V/F$ and the phase lag by degrees.

The equations for u_1, u_2 etc. become

$$
\left.\begin{aligned}
u_1 &= -\frac{F}{2}\frac{y}{\sqrt{B}} \times\left(\frac{1}{\sqrt{r}}\cos\varphi+\frac{1}{\sqrt{s}}\cos\psi\right)\\
u_2 &= \frac{F}{2}\frac{y}{\sqrt{B}} \times\left(-\frac{1}{\sqrt{r}}\sin\varphi+\frac{1}{\sqrt{s}}\sin\psi\right)\\
v_1 &= \frac{F}{2}\frac{y}{\sqrt{B}} \times\left(\frac{1}{\sqrt{r}}\sin\varphi+\frac{1}{\sqrt{s}}\sin\psi\right)\\
v_2 &= \frac{F}{2}\frac{y}{\sqrt{B}} \times\left(-\frac{1}{\sqrt{r}}\cos\varphi+\frac{1}{\sqrt{s}}\cos\psi\right)
\end{aligned}\right\} \quad \cdots\cdots (31)
$$

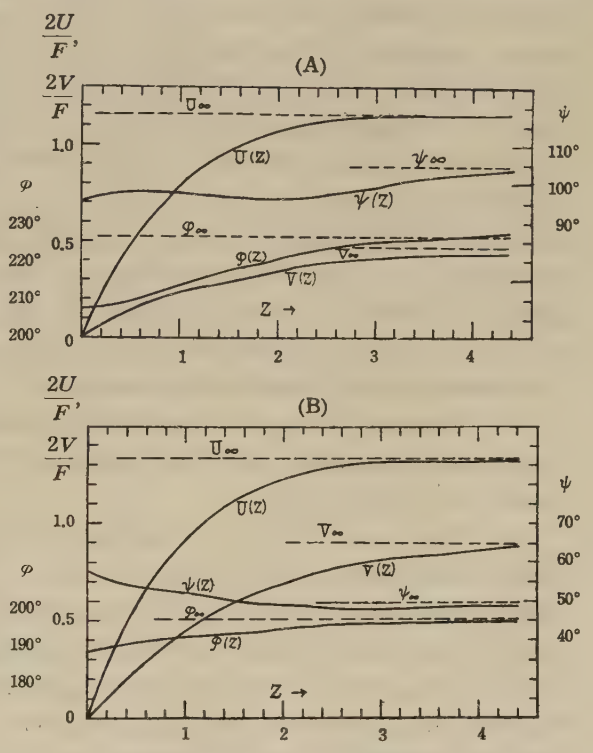

Fig. 5. The change of the amplitude and phase lag of tidal currents with the distance from the coast. ($u=U(Z)\cos(\sigma t-\varphi)$, $v=V(Z)\cos(\sigma t-\psi)$, U_∞, V_∞ etc. correspond to the values at $Z=\infty$, $Z=\sqrt{r/B}y$). (A) Semi-diurnal tide, (B) Diurnal tide.

for the small value of y. These curves indicate that the amplitudes of the semi-diurnal tide almost approach to those of the offshore currents or for $Z=\infty$ near the value of $Z=2.5$ and those of the diurnal tide assymptote to the offshore value more gradually than those of semi-diurnal tide. The change of

the phase lag is slight in all cases, which seems to be due to the large value of k. When we put $D_1=\pi\sqrt{B}/r\cos\varphi$, $D_2=\pi\sqrt{B}/s\cos\psi$, then Max ($D_1$, D_2) is the distance of the frictional resistance, so called, with analogy to the depth of the frictional resistance. Only in this case, it depends not only with the values of the horizontal eddy viscosity and the friction coefficient k but also with the period of the current. In Table 9 the values of the coefficient of $\sqrt{B}$ in D_1 and D_2 are tabulated for the diurnal and semi-diurnal component as to the range of $0<k<2\times10^{-4}$ (sec^{-1}), which indicates that these distances become shorter for the semi-diurnal component, and further that the effect of k is predominate for $k>10^{-4}$, thus the difference between the values for each component diminishes. It should be notable that the increase of k diminishes these distances, with contrast to the horizontal eddy viscosity B.

Table 9. Distances of frictional influence

k ($\times10^{-4}$)	Diurnal		Semi-diurnal	
	$D_1/\sqrt{B}$	$D_2/\sqrt{B}$	$D_1/\sqrt{B}$	$D_2/\sqrt{B}$ ($\times10^{-2}$ c.g.s.)
0	3.58	12.81	2.70	5.78
0.5	3.04	4.40	2.66	3.95
1.0	2.63	3.13	2.39	3.01
1.5	2.32	2.56	2.17	2.52
2.0	2.09	2.22	1.99	2.19

Summarizing the results of this section:

(1) The eddy viscosity of the horizontal direction is estimated as $10^5\sim10^7$ (c.g.s.), when we assume that the decrease of the tidal current near the coast is due to its effect.

(2) Theoretical decrease in the amplitude of tidal currents near the coast is more remarkable for shorter period current. The phase lag is variable only within a small range, and sometimes it tends to decrease towards the coast, when we take account of the bottom friction estimated in § 4.

(3) The distance of frictional resistance has also smaller value for shorter period and it decreases with increasing bottom friction.

In the last the author expresses his hearty thanks to Mr. Y. FUJII, the Chief of Oceanographical Section for many useful suggestions and encouragements. Further he is indebted to Dr. M. NAKANO and to the Special Committee on Marine Resources in the UNESCO Committee of Japan for the constant support.

References

(1) G. I. TAYLOR: Tidal friction in the Irish Sea. Phil. Trans. Roy. Soc. (A), v. 220, 1918.

(2) S. F. GRACE: Friction in the tidal currents of the Bristol Channel. Geophys. Supp. M.N.R. Astron. Soc. v. 3, 1936.
(3) K. BOWDEN and L. A. FAIRBAIRN: A determination of the frictional forces in a tidal current. Proc. Roy. Soc. (A), v. 214, 1952.
(4) T. ICHIYE: On the tidal currents and waves on the south-eastern coast of the Osaka Bay. (V) Reports of Committee of Investigation for Beach Erosion on SE coast of the Osaka Bay. v. 3, 1953. (In Japanese)
(5) H. U. SVERDRUP *et al*: The Oceans, p. 491.
(6) T. ICHIYE: A short note on the wind factor determined by the slope of sea surface. Mem. Kobe Mar. Obs. v. 10, 1952.
(7) C. G. ROSSBY and R. B. MONTGOMERY: The layers of frictional influence etc. Pap. Phys. Oceano. and Met. 1935.
(8) T. ICHIYE: On the tidal currents near Ushi-Shima in Bisan-Seto. Oceanographical Report. Cent. Met. Obs. Tokyo, v. 3, no. 1～2, 1953. (In Japanese)
(9) T. ICHIYE: On the tidal currents and waves along the north-eastern coast of the Harima-Nada. Oceanographical Report. Cent. Met. Obs. Tokyo, v. 2, no. 2, 1951.
(10) J. PROUDMAN: Dynamical Oceanography, Chap. XIV, pp. 302～322, 1953.
(11) T. ICHIYE: A note on the friction terms in the equation of ocean currents. Oceano. Mag, v. 2, no. 2, 1950.
(12) Y. YAMADA: On the high water induced by a travelling pressure disturbance. (III) Reports of Res. Inst. for Fluid Eng. (Kyushu Univ.) v. 4, no. 19, 1947. (In Japanese)
(13) T. ICHIYE: On the tidal currents and the waves in the south-eastern coast of the Osaka Bay. (III) and (IV). Rep. Comm. Beach Erosion of SE Coast of the Osaka Bay. v. 2, 1952. (In Japanese)
(14) H. U. SVERDRUP: Dynamics of tides on the North Siberien Shelf. Geofys. Publik. v. 4, 1927.

551.463

A Note on the Coagulation of Small Particles in the Electrolytes

By

Takashi ICHIYE

C.M.O. Oceanographical Section

1. *Introduction*

It has been well known that the sedimentation volume of mineral powders increases with the increasing concentration of cations in the liquid, and this effect is important in two problems, one of which is the mechanical analysis of sediments by usual pipette's method, and the other is the sedimentation of suspended materials transported by land waters into the sea. The present author gives some information on the first problem deduced from the dispersion experiments carried out by the standard method of mechanical analysis, and also he shows some discussions on the mechanism of coagulation of sediment particles, which seem to give some contributions to the second problem.

2. *Description of the experiments*

Samples of sediments used in the dispersion experiments were obtained at the station near the mouth of the Yamato River, which flows into Osaka Bay. First, the sediment was sieved by wet method and only the particles with diameter less than 1/16 mm* were retained. Next, this sample was dried at about 110°C, and then it was divided into several portions of 10 gr. and 20 gr. weight, which were dispersed in the water of 1 *l*, separately. Then the salinity of the solvent was determined for each dispersed samples by usual titration, the values being distributed between 0.06 and 0.17 ‰.** Heretofore, the experiment on effect of electrolytes on the dispersion of the sediment particles had been made only by adding various kinds of electrolytes individually to the normal solution of the particles,[1][2] but for the practical application it is more adequate to determine the relation between the salinity of the natural sea water and the effect of coagulation, both for the purposes of the contributions to the two

* When expressed by ϕ-scale, this corresponds to $\phi=4$, where $\phi=-\log_2 \xi$ and ξ is the diameter in mm.

** Mean values are 0.081 ‰ (for 10 gr.) and 0.129 ‰ (for 20 gr.), respectively.

problems above stated. Therefore the salinity of each sample was controled by the decantation of the solvent or by adding the sea water. Further two samples of 20 gr. sediments were washed by the water in order to purify the salts of the sediment, and they were diluted as the other samples, where the $N/100$ solution of Sodium Oxyalate was added to one of them, for the purpose of estimating the effect of this peptizer. Thus we analyzed the grain size distributions of each sample by the usual pipette's method, taking the settling time determined by the Stokes' law for each round number of ϕ from 5 to 9. The results of percentage compositions for different salinities are shown in Table 1, where the median values, $M_d\phi$ quartile mean values $Q_1\phi$, $Q_3\phi$ and quartile deviations $Q_d\phi=(Q_3\phi-Q_1\phi)/2$[3] determined graphically are also tabulated.

Table 1. Grain size distributions for different salinities.
(Distributions are expressed in percentages, diameters in ϕ-scale, and salinities in ‰)

Case I. 10 gr. sediment (dry weight) in 1 *l* solvent.

Sal. (‰) / ϕ	0.050	0.075	0.100	0.200	0.300	0.50	1.00	2.00
4~5	11	9	8	11	10	13	16	17
5~6	32	31	30	30	31	28	26	21
6~7	20	20	21	22	22	19	21	23
7~8	11	13	14	15	13	24	28	31
8~9	10	7	7	6	11	7	2	7
>9	15	19	19	15	12	9	6	
$M_d\phi$	6.2	6.4	6.5	6.3	6.3	6.4	6.3	6.5
$Q_1\phi$	5.5	5.8	5.7	5.5	5.6	5.5	5.4	5.5
$Q_3\phi$	8.0	8.1	8.3	7.8	7.9	7.6	7.4	7.5
$Q_d\phi$	1.3	1.3	1.3	1.2	1.2	1.1	1.0	1.0

Case II. 20 gr. sediment (dry weight) in 1 *l* solvent.

Sal. (‰) / ϕ	SO	0.000	0.025	0.050	0.075	(0.10)	0.15	0.20	(0.30)
4~5	11	20	20	14	22	15	14	9	8
5~6	19.5	18	25	31	22	23	25	31	30
6~7	15.5	16.5	18	19	21	19	23	21	21
7~8	13.5	13.5	14	14	17	28	20	22	33
8~9	4.5	32	8	6	9	5	9	5	3
>9	35		15	16	9	9	9	11	5
$M_d\phi$	7.3	6.7	6.2	6.1	6.3	6.6	6.5	6.4	6.5
$Q_1\phi$	5.7	5.3	5.3	5.3	5.2	5.5	5.5	5.6	5.6
$Q_3\phi$	(12.5)	(8.8)	7.8	7.8	7.6	7.7	7.6	7.6	7.5
$Q_d\phi$	3.4	1.8	1.3	1.3	1.2	1.1	1.1	1.0	1.0

SO Adding Sodium Oxalate.

The experiments for sal. 0.10 and 0.30 ‰ are somewhat doubtful, due to the bad condition of the pippette.

3. General features of the grain size distributions

We plot the histograms for the particles larger than $\phi=9$ in Fig. 1, displaying more clearly the changes of the distributions with the concentration of salts. From these curves we can see the following characteristics;

(1) Case 1 (10 gr. sediment) The distribution curves are almost similar for the salinity 0.05~0.30 ‰, or the dispersion seems to be stable for such ranges of the salinity. When it increases to 0.50 ‰, the percentages of the particles for $\phi>8$ decrease and on the other hand those for $8>\phi>7$ increase rapidly with the increase of the salinity, therefore the distribution curves have

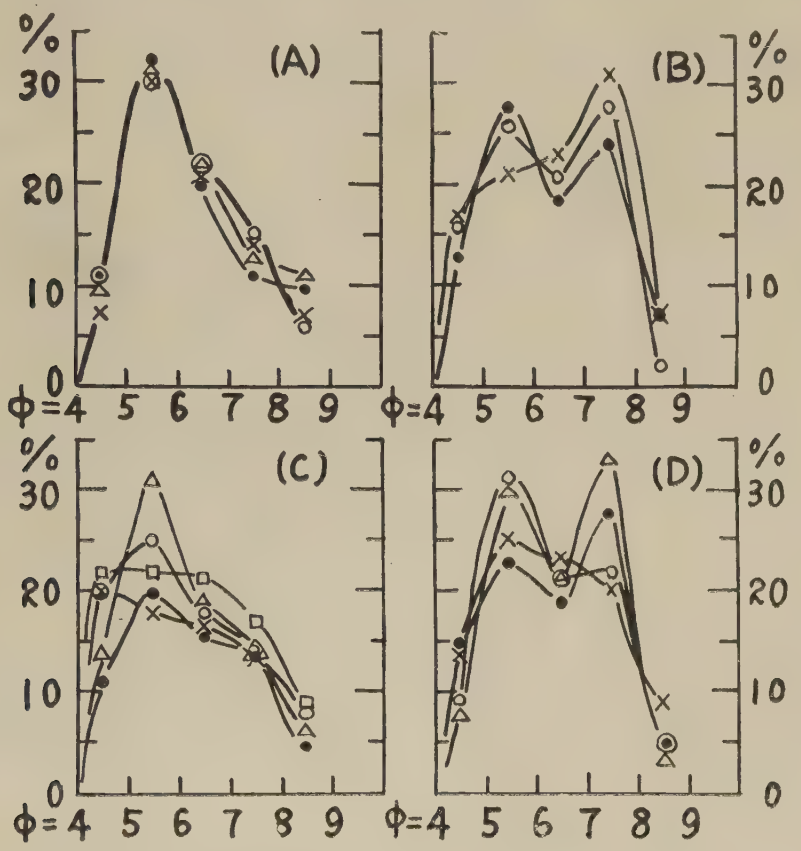

Fig. 1. Distribution curves of grain size for different salinities.

Case I. (A) ● 0.05 × 0.10 ○ 0.20 △ 0.30 (‰)
(B) ● 0.50 × 1.00 ○ 2.00 (‰)
Case II. (A) ● SO × 0.00 ○ 0.025 △ 0.05 □ 0.075 (‰)
(B) ● 0.10 × 0.15 ○ 0.20 △ 0.30 (‰)

two extreme values. Such condition suggests that the coagulation of the particles does not occur at the equal rate for all ranges of the diameter. The particles smaller than $\phi=8$ are most conspicuously adhered with each other with increasing salinity and form the particles of $7<\phi<8$, thus increasing the percentage for this range. The percentage of particles larger than those corresponding to $\phi=8$ seems to be controled by the balance of the increase of the particle number due to the coagulation of smaller particles and the decrease due to the coagulation to larger ones,[4] therefore the percentages of the particles for $7<\phi<8$ are almost constant for the increase of salinity.

(2) Case 2 (20 gr. sediment) The effect of the peptizer is most predominant for the dispersion of the particles with $4<\phi<5$, and in this case the similar distributions for the stable dispersion in case 1 are found only in the range of the salinity $0.05\sim0.075\,‰$, and for the salinity above $0.10\,‰$ we can see the occurence of the coagulation of small particles, judging from the double maximums in the distribution curves.

In short, the coagulation is apt to occur for the lower concentration of the salts as the initial weight of the dispersed sediment is the larger, and the resultant distribution after the occurence of the coagulation has the second maximum value as a result of the aggregation of colloidal particles.

The changes of statistical values such as $Q_3\phi$ and $Q_a\phi$ reflect similar tendency as the distribution curves, indicating the gradual decrease as increasing salinity, though such decrease is extremely abrupt between the case of no salinity and the slight concentration of the salts. The effect of the coagulation produces the good sorting, notwithstanding the double maximums in the distribution curves, since the percentages of smaller particles are diminished. The values of $M_a\phi$ and $Q_1\phi$ have not so regular tendency as $Q_3\phi$ and $Q_a\phi$, though their variations are also slight as compared with the latter, which suggest that the coagulation diminishes only smaller particles. Further the singularity of the grain size distributions for the samples of no salinity seems to be due to the change of the surface conditions of the particles by washing rather than to the direct effect of the coagulation.

4. The coagulation of small particles with $\phi>8$

As shown in the previous section, the effects of salinity on the coagulation is more obvious for the small particles, which include the colloidal ones. We plot the relation between the total percentages of the particles $\phi>8$ and salinity in Fig. 1, which indicates more rapid decrease for the case 2.

The theory of the colloidal particles has been treated by many authors since Smouluchowski,[5] but for the explanation of the present experiments the classical theory seems to be somewhat inadequate. For example, it gives the rate of the decrease of the particle number ν with time as

$$d\nu/dt=-8\pi\sigma D\nu^2 \quad \text{or} \quad 1/\nu=1/\nu_0+8\pi\sigma Dt, \tag{1}$$

where σ is the effective radius of coagulation, D the molecular diffusion coefficient, which is given by $kT/6\pi\eta d$ (η the viscosity, d the radius of the particles, k Boltzmann's constant, and T the absolute temperatures), ν_0 the initial value of ν. Then the half value duration $\Theta=\frac{1}{8}\pi\sigma\nu_0 D$ is about equal to 3.1×10^2 (sec) for for the various numerical values of case 1, since

$$d=10^{-4}, \quad T=288^\circ\text{K}, \quad D=2.1\times10^{-9},$$

$$\nu_0=(\text{total weight for } \phi>8)\Big/\left(\frac{4}{3}\pi\rho d^3\right)\fallingdotseq3\times10^8 \quad \text{(c.g.s.)}.$$

Therefore, if the relation (1) is valid for the present experiment, the particles under consideration should be almost eliminated to nil by the coagulation, since the time for the determination of the particle size distribution is far longer than this half value time. Thus the term compensating $-8\pi\sigma D\nu^2$ is necessary in the right hand side of the first equation of (1), since we have the finite value of ν even after the satisfactorily long time.

The complete discussion about the increase of coagulation with increasing concentration of electrolytes should be carried out by taking account of the molecular theory of charged particles, but here only the phenomenological explanation is proposed. As usually accepted, mineral particles have generally negative charges in the liquid and the repulsive force acts between them. When electrolytes exist in the liquid, this repulsion is diminished, since the cations are attached around the surface of each particle. In other words the effective radius σ increases with increasing salinity of the solvent, which in turn has an effect of adhering more particles to each one. Therefore the particle number of the definite range of diameter decreases with the increasing length of the effective radius, due to the coagulation. On the other hand, the particle number penetrating into the radius σ is given by $4\pi DC\sigma$ for the steady state from the diffusion theory, where $C=\nu/V$ is the particle concentration with ν, the particle number per unit volume, and V, the total volume. Then the increase of this quantity with the increase of σ from σ to $\sigma+d\sigma$ is equal to $4\pi DCd\sigma$. Therefore, when we put $d\nu$ the increase of ν accompanying with the increase $d\sigma$, then $-d\nu$ is proportional to the total number ν multiplied

by $4\pi DCd\sigma$, since the latter is the change of ν only about one particle. Consequently we can put $d\nu \propto -\nu^2 d\sigma$, or $d\nu \propto -\nu^2 dS$, when we assume $d\sigma \propto dS$, where S means the salinity of the solvent. In the presente experiments it is more convenient to express ν in terms of the percentage P and the total weight N, where $P=\nu V/N$. Thus we have

$$dP=-aNP^2dS \quad \text{or} \quad 1/P=1/P_0+aNS, \tag{2}$$

where P_0 is the percentage for $S=0$ and a is the proportional constant. In order to ascertain the relation (2) from the experimental data, we plot $1/P$ against S in Fig. 2 (B), which indicates the linear relation between $1/P$ and S

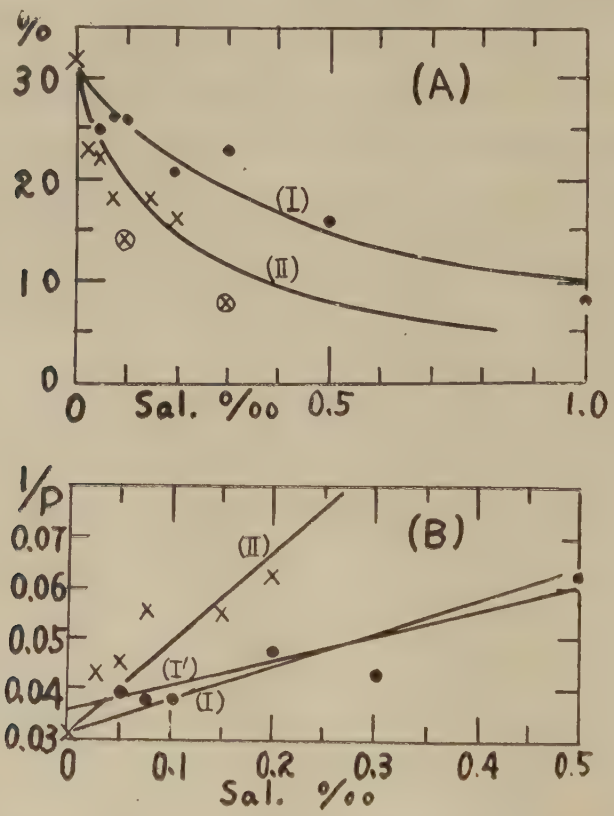

Fig. 2. Relations between the percentage of particles witn $\phi>8$ and the salinity.
Experimental data (● case 1, × case 2).
Curves obtained by least squares (I, I′; case 1, II; case 2).
(A) Percentage against salinity (⊗ indicates the value omitted for the least squares).
(B) Reciprocals of percentage against salinity.

approximately, with steeper slope for a set of data of the case 2, corresponding to the increase of aN. When we determine aN by the method of least squares from the experimental data, we have $aN=0.063$ (curve I, for $N=10$ gr.) $=0.179$ (curve II, for $N=20$ gr.) by fixing $P_0=32\%$, and $aN=0.050$, $P_0=28\%$ (curve I', for $N=10$ gr.) without the fixed value of P_0. The value of aN for the case 2 should be twice for the case 1 theoretically, but the disagreement of such order seems to be permissible considering the accuracy of the present experiments.

For more detailed discussion, we should obtain the relation between σ and S by taking account of the cohesion between two particles, which is generally expressed by

$$V_r=C_1/r^2-C_2/r^5,$$

where V_r is the relative velocity of two particles with the distance r and the first term with $C_1=a_1q^2+b_1$ means the sum of Coulomb's force and the molecular force, in which q is the charge and a_1 is positive only for the same sign of the charges, though b_1 is always positive, and the second term with $c_2=a_2q^2+b_2$ is the repulsion due to the induced dipoles. Thus, when we assume that the effective radius corresponds to the value of r giving $V_r=0$, which is not so unreasonable assumption, then we have

$$\sigma^3=c_1/c_2=\sigma_0^3/\{m(1-S/S_0)^2+1\},$$

where we consider that the charge q is expressed by $q\propto(1-S/S_0)$ and further $b_2\gg a_2q^2$ from the slight effect of the induced dipoles, with S_0 the saturation salinity, for which the resultant charge of each particle vanishes, and σ_0 the value of σ for $S=0$. The more detailed discussion seems to be insignificant only from the present experimental data, though it should be given in the future. However, we can explain empirically the decrease of the percentage of smaller particles with increasing salinity without much contradiction by the above rough estimation.

5. *Concluding remarks*

The experimental result on the dispersion of the sediment particles in the haline water is discussed and some empirical relations between the coagulation and the salinity of the solvent are proposed. For more complete explanation of the changes of distribution curves, it is necessary to treat the mechanism of the cohesion of larger particles than colloidal ones, which is perhaps quite difficult, since the interactive force between such particles has not be definitely obtained in the present stage.

In the last, the author expresses his hearty thanks to Mr. Y. Fujii, the Chief of the Oceanographical Section for the useful suggestions and the kind encouragement. Further he is indebted to Mr. M. Ichihara, the Osaka City University for the cooperation of the present experiment and to Dr. Y. Miyake and Mr. A. Okubo for the kind advices.

Literatures

(1) A.N. Puri and B.A. Keen: The dispersion of soil in water under various conditions. *Journ. of Agric. Sci.* XV, 1925.

(2) T. Nomitsu and T. Takegami: On the actions of sea salts upon the sedimentation of fine mud. *Rec. Oceano. Works in Japan.* 1st series, vol. XI, no. 1, 1937.

(3) Trask: Recent marine sediments. 1939.

(4) In other words, we should replace the equation (2) with the relation such as

$$d_i = -k_i \nu_i^2 dS + \sum_{n>i}^{n} k_n \nu_n^2 dS$$

where ν_i means the particle number belonging to $i < \phi < i+1$. The estimation of the coefficients k_n is more complicated in the above relation, since we should take account of the errors produced by shape factors in Stokes' law estimates of particle radius for the aggregation of small particles, as demonstrated by W. B. Kunkel (*J. Apply. Phys.* 18. 1948).

(5) M. v. Smoluchowski: *Phys. Zeit.* 17, 1916.

(6) W. Kunkel: Growth of charged particles in clouds. *J. Apply. Phys.* 18, 1948.

(7) R. S. Bradley: The cohesion between smoke particles. *Trans. Farad. Soc.* 32, 1936.

昭和30年10月15日印刷
昭和30年10月20日発行

編集兼
発行人　中央気象台
東京都千代田区大手町一ノ七

印刷人　花崎実
東京都中央区新富町二ノ十九

印刷所　大東印刷工芸株式会社
東京都中央区新富町二ノ十九